Physics Department

Research Area
Strongly Correlated Electron Systems

Annual Report 2009 / 2010

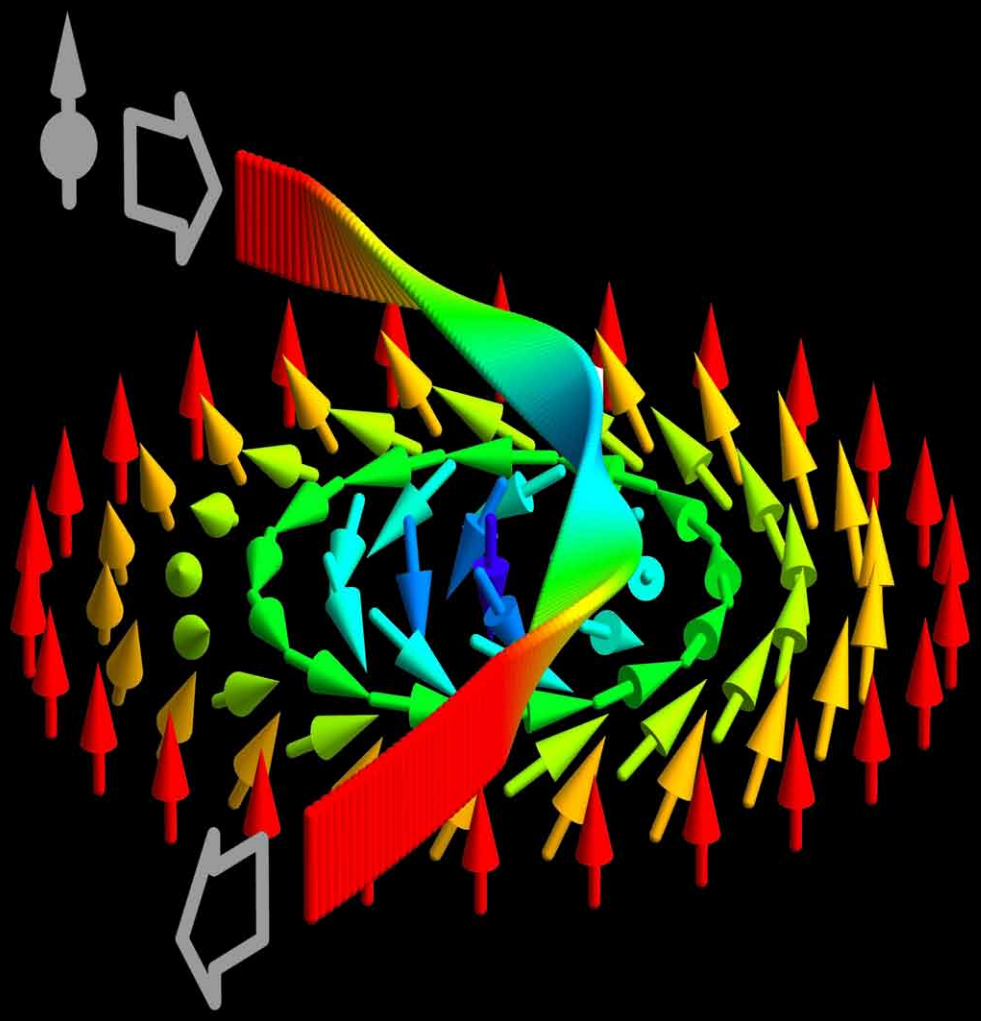

Cover page

Movement of an electron through a skyrmion lattice, twisting its spin and thereby changing its direction of travel.

Illustrations on the title page and the top right corners of all pages by courtesy of Prof. Achim Rosch, Universität zu Köln.

Annual Report 2009/2010

of the Research Area Strongly Correlated Electron Systems
(formerly Institute for Experimental Physics E21)

Chair for Neutron Scattering – Prof. Dr. P. Böni
Group for Magnetic Materials – Prof. Dr. C. Pfleiderer

Technische Universität München

Annual Report 2009/2010
of the Research Area Strongly Correlated
Electron Systems
published: February 2011
Layout by Georg Brandl
Edited by Georg Brandl
http://www.e21.ph.tum.de/

Technische Universität München
James-Franck-Straße 1
85748 Garching, Germany

Secretary: Astrid Mühlberg
Phone: +49-89-289-14712
Fax: +49-89-289-14713

Contents

Preface

We are pleased to present the Annual Report 2009/10 of the research area Strongly Correlated Electron Systems (formerly institute E21) at the Physik-Department of the Technische Universität München.

Both years were very successful for our institute with major advances in numerous research projects. For instance, combining neutron scattering with bulk measurements we established that skyrmion lattices form in a large class of B20 compounds. Interestingly, the skyrmion lattice exhibits a pronounced spin torque effect when ultra-low currents are applied. In inelastic neutron scattering studies we identified intense helimagnon bands as a universal characteristic of chiral magnets. Using x-ray synchrotron radiation, we succeeded to identify strong electron phonon correlations along the N-H zone boundary line of chromium in a very small regime of wavevector space. Combining longitudinal polarization analysis with neutron imaging we used neutron radio- and tomography for studies of the magnetization distribution in ferromagnets close to quantum criticality. By means of Larmor diffraction we even proved the parasitic nature of the small moment antiferromagnetism in the enigmatic hidden order phase of URu_2Si_2.

These and further advances became possible through new developments and major upgrades of instrumentation. In our low temperature laboratory a vibrating coil magnetometer was taken into operation for studies down to milli-Kelvin temperatures. At FRM II, the neutron resonance spin-echo spectrometer RESEDA is developing into a workhorse for the investigation of diffusive processes in magnetic and soft matter materials. At the diffractometer MIRA, the MIEZE technique for experiments at sub-μeV resolution in large magnetic fields was successfully installed for normal user operation. The design of the triple-axis spectrometer KOMPASS is progressing very well and advances in neutron optical devices promise major improvements concerning intensity and resolution. Improvements of the optics of the positron source NEPOMUC allowed decreasing the measurement time of positron induced Auger electron spectroscopy (PAES) rather dramatically thus establishing PAES as a unique tool for studies of the upper most surface of materials.

As in previous years the members of our institute carried out a heavy teaching load covering all areas from magnetism and materials preparation over positron physics to reactor physics. In addition, numerous tours of FRM II were guided by the members of our institute.

We were very pleased about the decision of DFG to fund our application for a joint Transregional Research Center (TRR 80) “From Electronic Correlations to Functionality”, in collaboration with the University of Augsburg, the Walter Meissner Institut and the Ludwig Maximilian University. Also, the DFG Forschergruppe on quantum phase transitions (FOR 960) was reviewed positively and approved for a second funding period. At this place we wish to thank again all other funding agencies and neutron scattering centers for their ongoing support of our activities.

Finally, several important changes of the staff of our institute took place. Perhaps most importantly, Prof. Dr. Klaus Schreckenbach retired on March 31, 2009. Fortunately he continues to contribute to the research at E21 and in the organization of seminars.

Garching, January 2011

Peter Böni Christian Pfleiderer Klaus Schreckenbach

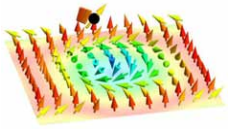

Chapter 1

Magnetism and Superconductivity

Spin Transfer Torques in MnSi at Ultra-low Current Densities

F. Jonietz[1], S. Mühlbauer[1], C. Pfleiderer[1], A. Neubauer[1], W. Münzer[1], A. Bauer[1], T. Adams[1], R. Georgii[2,1], P. Böni[1], R. A. Duine[3], K. Everschor[4], M. Garst[4], and A. Rosch[4]

[1] *Physik Department E21, Technische Universität München, D-85748 Garching, Germany*
[2] *Forschungsneutronenquelle Heinz Maier-Leibnitz (FRM II), Technische Universität München, D-85748 Garching, Germany*
[3] *Institute for Theoretical Physics, Utrecht University, 3584 CE Utrecht, The Netherlands*
[4] *Institut für Theoretische Physik, Universität zu Köln, D-50937 Köln, Germany*

Spin manipulation using electric currents is one of the most promising directions in the field of spintronics. We used neutron scattering to observe the influence of an electric current on the magnetic structure in a bulk material. In the skyrmion lattice of MnSi we observe the rotation of the diffraction pattern in response to currents which are over five orders of magnitude smaller than those typically applied in experimental studies on current-driven magnetization dynamics in nanostructures [1]. We attribute our observations to an extremely efficient coupling of inhomogeneous spin currents to topologically stable knots in spin structures.

The skyrmion lattice in chiral magnets, like MnSi and related B20 compounds, was only recently discovered in neutron scattering studies [2, 3] and confirmed to exist in Lorentz force microscopy for $Fe_{1-x}Co_xSi$ (x = 0.5) [4]. It represents a new form of magnetic order that shares remarkable similarities with the mixed state in type II superconductors.

To understand the effect of an electric current, the skyrmion lattice may be viewed as an array of circulating dissipationless spin currents, because the skyrmions are characterized by gradients in the spin-orientation related to their quantized winding number. This is analogous to superconductors, where dissipationless charge currents flow around quantized vortices due to gradients of the phase. When an extra spin current is induced by driving an electric current through the magnetic metal, the spin currents on one side of the skyrmion are enhanced while they are reduced on the other side. As for a spinning tennis ball, this velocity difference gives rise to a Magnus force acting on the skyrmions. Note, however, that spin (due to spin-orbit coupling) is in contrast to charge not conserved and therefore this intuitive picture is incomplete. Most importantly, also further dissipative forces arise which drag the skyrmions parallel to the current.

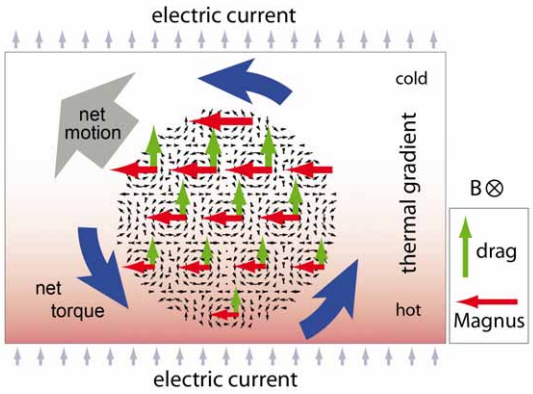

Figure 1: Schematic view of the interplay of an electric current flowing transverse to the skyrmion lattice where Magnus and drag forces arise that vary with the size if the spin polarization.

Above a clear threshold of 10^6 A m^{-2} an increasingly strong rotation is observed of the sixfold diffraction pattern of the skyrmion lattice. The rotation is antisymmetric under inversion of the current direction and field direction. Moreover, the rotation arises only in the presence of a small temperature gradient along the current direction (the sense of rotation is also antisymmetric under inversion of the temperature gradient). A detailed theoretical account suggests that this rotation is accompanied by a sliding motion of the skyrmion lattice [1].

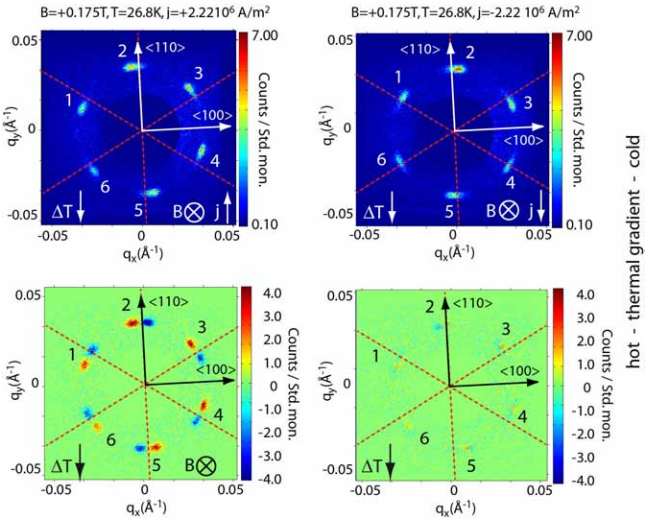

Figure 2: Antisymmetric rotation of the diffraction pattern under current reversal. Reversal of the applied magnetic compensates the change of rotation under current reversal.

Our observations identify chiral magnets and systems with nontrivial topological properties as ideal systems to advance the general understanding of the effects of spin transfer torques. For instance, spin transfer torques may even be used to manipulate individual skyrmions, recently observed directly in thin samples [4]. In fact, even complex magnetic structures at surfaces and interfaces may be expected to exhibit the spin torque effects we report here [5].

We gratefully acknowledge financial support through SFB608 and TRR80, SFB/TR12 of the German Science Foundation (DFG), the Deutsche Telekom Stiftung (KE), the NSF grant PHY05-51164 (AR) and by FOM, NWO and the ERC (RD).

References

[1] F. Jonietz et al. *Science*, 326:1348, 2010.
[2] S. Mühlbauer et al. *Science*, 323:915, 2009.
[3] W. Münzer et al. *Phys. Rev. B (R)*, 81:041203, 2010.
[4] X. Z. Yu et al. *Nature*, 465:901, 2010.
[5] M. Bode et al. *Nature*, 447:190, 2007.

Neutron resonance spin-echo studies of $Mn_{1-x}Fe_xSi$

Alexander Tischendorf[1,2], Wolfgang Häußler[2], Julia Repper[2], Christian Pfleiderer[1], and Peter Böni[1]

[1] *Physik Department E21, Technische Universität München, D-85748 Garching, Germany*
[2] *Forschungsneutronenquelle Heinz Maier-Leibnitz (FRM II), Technische Universität München, D-85748 Garching, Germany*

One of the major puzzles in the search for novel electronic phases of correlated matter concerns the putative formation of a genuine non-Fermi liquid phase in the B20 transition metal helimagnet MnSi under pressure [1]. The observation of partial magnetic order in MnSi at high pressures indicates that the non-Fermi liquid behavior is related to the spin dynamics of unusual spin textures [2]. However, since these phenomena occur at high pressures it has not been possible so far to measure the spin dynamics directly.

In a comprehensive study of the magnetization, specific heat, AC susceptibility and electric transport properties we have recently established, that the helimagnetic order in MnSi may be suppressed by substitutional Fe- or Co-doping at the Mn-sites [3]. In turn the resulting quantum phase transitions offer an alternative route to determine the nature of the spin dynamics of itinerant electron systems in the presence of Dzyaloshinsky-Moriya interactions and complex spin textures.

We have performed elastic and quasi elastic neutron scattering experiments on $Mn_{1-x}Fe_xSi$, where the quantum phase transition may be reached for $x \approx 0.19$. In our study we focussed on the lifetime of the paramagnetic fluctuations using the spin echo spectrometer RESEDA at FRM II. Neutron spin echo measures the time-Fourier transform of the scattering function $S(\mathbf{Q}, \omega)$, which is essentially proportional to the generalized susceptibility $\chi(\mathbf{Q}, \omega)$.

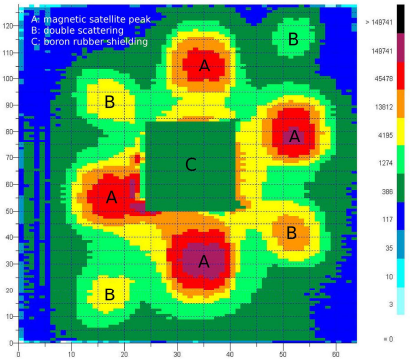

Figure 1: Diffraction pattern in pure MnSi, characterized by four helimagnetic satellite peaks (A) along the ⟨111⟩ directions. The four peaks with reduced intensity (B) arise from to double scattering. The direct beam in the center of the detector (C) was shielded with boron rubber.

In order to study the spin dynamics at small scattering angles (NRSE-SANS), we use an appropriate beam collimation to reduce the background scattering of the direct beam. The incident mean wavelength is $\lambda = 5.5\,\text{Å}$ providing the best compromise between neutron flux and resolution available at RESEDA. This instrument set up is well suited for the investigation of magnetic phase transitions. We used a closed circle cryostat to investigate both crystals near their phase transition temperature. The samples show a high scattering intensity around the magnetic satellite peaks. In our measurements we varied both the temperature around the phase transition temperature and the momentum transfer around satellite peak. The typical lifetime of the magnetic fluctuations matches the spin-echo times available at RESEDA well.

We studied two different single crystals, notably $x = 0$ and $x = 0.12$. In pure MnSi and Fe-doped MnSi ($x = 0.12$) the magnetic transition temperatures are $T_c = 28.85\,\text{K}$ and 6.5 K, and the pitches of the helix are $\lambda_h \simeq 180\,\text{Å}$ and $\simeq 88\,\text{Å}$, respectively. Fig. 1 shows a typical diffraction pattern measured in pure MnSi with a CASCADE detector [4]. Between the four magnetic satellite peaks at an ordering vector of $Q = 0.039\,\text{Å}^{-1}$ additional peaks are observed which arise from double scattering.

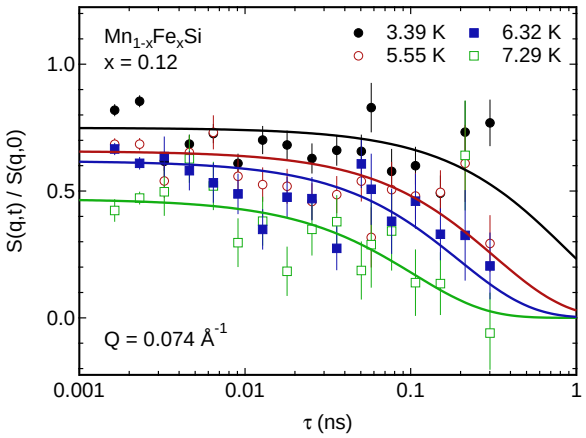

Figure 2: Intermediate scattering function of $Mn_{0.88}Fe_{0.12}Si$ as measured by means of neutron spin echo at $Q = 0.074\,\text{Å}^{-1}$. The fluctuations speed up with increasing temperature.

Fig. 2 illustrates the intermediate scattering function of $Mn_{0.88}Fe_{0.12}Si$. The linewidth Γ increases due to the thermal excitation of the fluctuations with increasing temperature. In contrast, below T_c, the linewidth remains finite. This result differs from pure MnSi, where the linewidth is zero for temperatures well below T_c [5]. Moreover, for both compositions $\Gamma(\mathbf{q} = 0)$ is finite above T_c (here: $\mathbf{q} = \mathbf{Q} - \mathbf{k}$, where $\mathbf{k}$ describes the magnetic ordering vector). This is in contrast to isotropic ferromagnets, where the linewidth vanishes for $\mathbf{q} = \mathbf{Q} = 0$. The linewidth Γ in pure MnSi is small and increases with temperature, whereas in $Mn_{0.88}Fe_{0.12}Si$ it is larger due to additional damping. Further measurements for different concentrations x are planned for the future to determine the evolution of the linewidth when approaching quantum criticality.

References

[1] C. Pfleiderer et al. *Nature*, 414:427, 2001.
[2] C. Pfleiderer et al. *Nature*, 427:227, 2004.
[3] A. Bauer et al. *Phys. Rev. B*, 82:064404, 2010.
[4] C. Schmidt and M. Klein. *Neutron News*, 17:12–15, 2006.
[5] A. Tischendorf. Spin echo measurements of magnetic fluctuations in helical $Mn_{1-x}Fe_xSi$. Diploma thesis, Technische Universität München, 2010.

High Resolution Rocking Scans of the Skyrmion Lattice in MnSi

Sebastian Mühlbauer[1], Tim Adams[1], Florian Jonietz[1], Robert Georgii[1,2], Achim Rosch[3], Christian Pfleiderer[1], and Peter Böni[1]

[1] *Physik Department E21, Technische Universität München, D-85748 Garching, Germany*
[2] *Forschungsneutronenquelle Heinz Maier-Leibnitz (FRM II), Technische Universität München, D-85748 Garching, Germany*
[3] *Institut für Theoretische Physik, Universität zu Köln, D-50937 Köln, Germany*

Recent SANS experiments have proved the existence of a skyrmion lattice in the A-phase of the helical magnet MnSi. The skyrmion lattice is characteristic of a hexagonal magnetic spin crystal whose entities are topological knots of the magnetization characterized by a topological charge = −1 per unit cell. A Ginzburg-Landau ansatz including Gaussian fluctuations, based on the superposition of three single **k** helices, inclined at an angle of 120° with respect to each other and perpendicular to the applied magnetic field indicates that the spin crystal represents a stable ground state [1].

Neutron scattering has established [2] that the propagation vector **k** of the helical order is locked by cubic crystal field anisotropy to the crystalline ⟨111⟩ directions in the helical phase of MnSi. A gaussian mosaic spread with ∼ 3° FWHM was obtained for several samples with excellent purity. In contrast to the helical phase, recent rocking scans performed in the A-phase revealed (i) a strictly perpendicular alignment of the **k**-vectors of the spin crystal with respect to the applied magnetic field, (ii) a peculiar exponential shape of the rocking curve with 1.85° FWHM and (iii) a slight distortion of the hexagonal symmetry to an ellipsoidal shape was observed for a particular sample. The measurements also showed that the magnetic structure of the spin crystal is extremely sensitive to demagnetizing fields inside the sample.

To quantize the influence of demagnetizing fields on the structure and the rocking curve of the A-phase we have performed scans using a high resolution setup on MIRA, FRM II. The sample used for this study consists of an irregular shaped thin plate with a length of ∼ 14 mm, a width of ∼ 9 mm and a thickness of ∼ 1.4 mm. The normal vector of the sample is aligned in the crystalline ⟨110⟩ direction. With a sample aperture of 4×4 mm^2, only the central part of the sample is exposed to the neutron beam. Edge effects can be neglected. The sample can thus be regarded as flat, thin plate, oriented perpendicular to the applied magnetic field and the neutron beam. A demagnetizing factor $N = 1$ applies.

Rocking scans with respect to a vertical axis with a step-size of $\eta = 0.075°$ have been performed in the helical phase at a temperature $T = 10$ K and at zero magnetic field as well as in the A-phase ($T = 32$ K, $\mu_0 H = 0.16$ T). Typical SANS data is shown in Fig. 1, panel (i) for the helical phase and panel (iii) for the A-phase. The horizontal axis corresponds to a ⟨110⟩ crystalline direction.

Consistent with previous work [2, 3], a mosaic of $\eta_m = 3.0 \pm 0.3°$ has been obtained for the helical phase, well described by a Gaussian line shape, taking the Lorentz factor into account, shown in Fig. 1, panel (ii). However, the rocking width obtained for the A-phase (panel (iv)) yields a value of $\eta_A = 0.4°$ which represents the instrumental resolution limit $\Delta\beta_{\mathbf{kf}} = 0.35°$. The line shape is characteristic of a Gaussian function. The small value of $\eta_A = 0.4°$ indicates an surprisingly well ordered state exhibiting long range order over several 10 000 Å and underscores the influence of demagnetizing effects on the shape of the rocking scans.

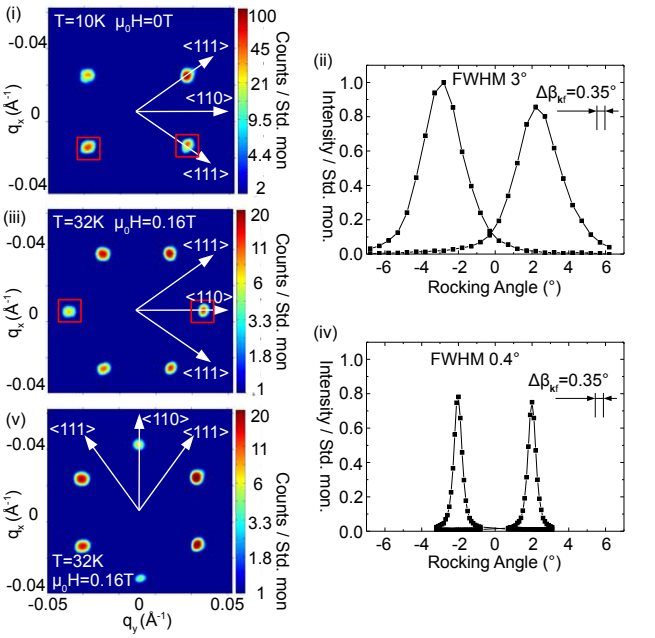

Figure 1: High resolution rocking scans of the helical phase (panels (i) and (ii)) and the spin crystal (panels (iii) to (v)) of MnSi. The direct beam has been masked in panels (i), (iii) and (v). For details see text.

To check whether the distortion of the hexagonal scattering pattern of the A-phase to an ellipsoidal shape is an intrinsic feature, rocking scans have been recorded in the high resolution setup with both a crystalline ⟨110⟩ direction aligned vertical as well as horizontal. The data is shown in Fig. 1: Panel (iii) depicts the typical hexagonal scattering pattern of the A-phase at a temperature $T = 32$ K and a magnetic field $\mu_0 H = 0.16$ T where the ⟨110⟩ crystalline direction is aligned horizontal. Panel (v) depicts the typical hexagonal scattering pattern of the A-phase at identical temperature and magnetic field where the ⟨110⟩ crystalline direction is aligned vertical. A regular hexagonal shape with diffraction spots aligned under $\Delta\psi = 60 \pm 0.4°$ was obtained for the crystalline ⟨110⟩ direction aligned horizontal whereas $\Delta\psi = 60 \pm 0.7°$ was obtained for the crystalline ⟨110⟩ direction aligned vertical. This strongly indicates that the elliptical distortion, observed for other sample is a result of demagnetizing effects due to the sample geometry or caused by instrumental artifacts.

References

[1] S. Mühlbauer et al. *Science*, 323:915–919, 2009.
[2] B. Lebech et al. *J. Magn. Magn. Mater.*, 140-144:119–120, 1995.
[3] C. Pfleiderer et al. *Phys. Rev. Lett.*, 99(15):156406, 2007.

Phonon Softening in Cr without Fermi Surface Nesting

D. Lamago[1,2], M. Hoesch[3], M. Krisch[3], R. Heid[1], K.-P. Bohnen[1], P. Böni[4], and D. Reznik[1,5]

[1] *Karlsruher Institut für Technologie, Institut für Festkörperphysik, P.O. Box 3640, D-76021 Karlsruhe, Germany*
[2] *Laboratoire Léon Brillouin, CEA Saclay, F-91191 Gif-sur Yvette, France*
[3] *European Synchrotron Radiation Facility, F-38043 Grenoble Cedex, France*
[4] *Physik Department E21, Technische Universität München, D-85748 Garching, Germany*
[5] *Department of Physics, University of Colorado-Boulder, Boulder, Colorado 80309, USA*

Nesting of the Fermi surface can soften and broaden phonons at the nesting wavevectors. Unexpectedly, huge electron-phonon anomalies have been reported in copper oxide superconductors and their origin remains enigmatic. Here we present results of inelastic x-ray scattering measurements that uncovered similarly pronounced softening of certain phonons in chromium that occur far from the Fermi surface nesting wavevectors.

In metals with Fermi surfaces, phonons may couple to singularities in the electronic density of states, which appear at so-called nesting wavevectors $\mathbf{Q}_n$, which connect parallel (nested) sheets of the Fermi surface [1]. This nesting greatly enhances the number of possible electronic transitions at wavevectors $\mathbf{Q} = \mathbf{Q}_n$ compared to other wavevectors, which results in softer and broader phonons. A density functional calculation of the lattice dynamics using the mixed basis pseudopotential method and the linear response technique yields the joint density of states for electron-hole excitations at the Fermi surface shown in Fig. 1. The bright spots near the H- and N-points reproduce the nesting features that are held responsible for the phonon softening near H and N. Of particular interest is the H-point, where a spin density wave is observed below $T_N = 311$ K at $\mathbf{Q}^{\pm}$ [2].

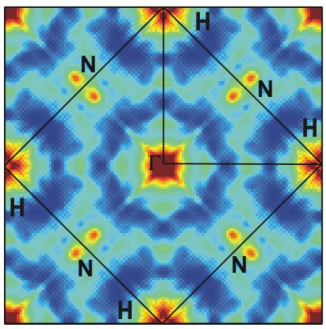

Figure 1: Joint density of states for electron-hole excitations, whose hotspots (in red) correspond to potential phonon anomalies.

Our goal was to determine whether or not there is a correspondence between phonon anomalies and the FS nesting in Cr. To improve the Q-resolution over the previous INS study [3], which covered only the high symmetry directions, we used inelastic x-ray scattering (IXS). We investigated the phonon dispersion near the H-point and extended the measurements along the zone boundary to the N-point. This region around the line connecting the H-point and the N-point (Fig. 1) has not been investigated experimentally before.

Fig. 2 shows an example of a phonon at $\mathbf{Q} = (0.5, 3.5, 0)$ corresponding to the acoustic [110] T2 branch. The solid line is a fit assuming a Lorentzian. Following this result, we have determined the dispersion of the phonons in detail for $\mathbf{Q}$ along [100] as well as along the N-H line [4].

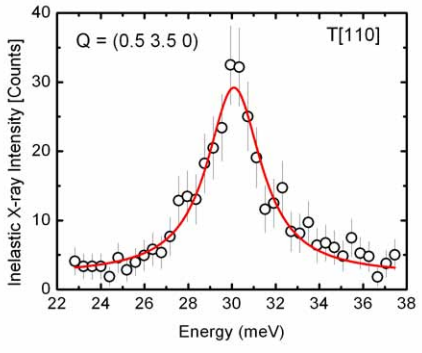

Figure 2: Raw data from inelastic X-ray scattering as function of energy transfer at $T = 320\,K$ and $\mathbf{Q} = (0.5, 3.5, 0)$. The solid line corresponds to a fit to the data using a Lorentzian.

Fig. 3 shows the difference between a Born-von-Karman model for Cr and the experimental values along the [100] direction (red) and along the zone boundary N-H (blue). Along the [100] direction, the phonon softening has a distinct maximum at the nesting wavevectors $\mathbf{Q}^{\pm} = (0.95, 0, 0)$. Surprisingly, a strong anomaly also appears along the entire zone boundary line between the N- and P-point, indicating that strong electron phonon coupling limited to a small range of wavevectors alone can also result in strong phonon anomalies.

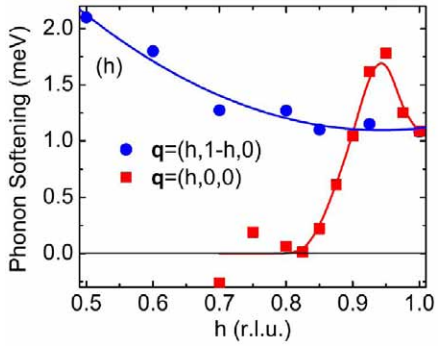

Figure 3: Difference $E_{calc} - E_{exp}$ between the calculated and experimental phonon dispersion along the zone boundary N-H (blue) and along the high symmetry direction Γ-H (red).

Our results imply that the phonon anomalies in copper oxide superconductors may be explained by an enhanced electron-phonon coupling without invoking novel collective modes or some hidden nesting of the Fermi surface.

References

[1] W. Kohn. *Phys. Rev. Lett.*, 2:393, 1959.
[2] C. R. Fincher, G. Shirane, and S. A. Werner. *Phys. Rev. B*, 24:1312, 1981.
[3] W. M. Shaw and L. D. Muhlestein. *Phys. Rev. B*, 4:969, 1971.
[4] D. Lamago, M. Hoesch, M. Krisch, R. Heid, K.-P. Bohnen, P. Böni, and D. Reznik. *Phys. Rev. B*, 82:195121, 2010.

Phason Modes in Incommensurate Chromium

P. Böni[1], E. Clementyev[1,2], T. G. Perring[3], Hyungje Woo[3,4], M. Fujita[5], and S. Hayden[6]

[1] *Physik Department E21, Technische Universität München, D-85748 Garching, Germany*
[2] *Department of Exp. Physics, Russian Federal Nuclear Center, Snezhinsk, 456770 Chelyabinsk Region, Russia*
[3] *ISIS Facility, Rutherford Appleton Laboratory, Chilton, Didcot, Oxon, OX11 0QX, UK*
[4] *Department of Physics & Astronomy, University of Tennessee, Knoxville, TN 37996-1200*
[5] *Institute for Materials Research, Tohoku University, Sendai, 980-8577, Japan*
[6] *H. H. Wills Physics Laboratory, University of Bristol, Tyndall Avenue, Bristol BS8 1TL*

With the discovery of high-temperature superconductivity the interest in the role of antiferromagnetic fluctuations in incommensurate magnetic systems has risen because of their possible relevance for pairing. A common feature of the cuprates, in particular LSCO is the presence of parallel 2-dimensional copper oxide planes containing stripes of charge carriers and magnetic moments [1] leading to incommensurate spin ordering and incommensurate magnetic fluctuations exhibiting a so-called 'hourglass' dispersion.

Because of the striking similarities with incommensurate antiferromagnetic Cr, we have measured the excitation spectrum of Cr using the time-of-flight spectrometer MAPS at ISIS (Fig. 1). Two cones of inelastic scattering around the allowed satellites are clearly visible at E = 25 meV evolving into a single blob of scattering at (100) at high E in qualitative agreement with triple-axis data [2].

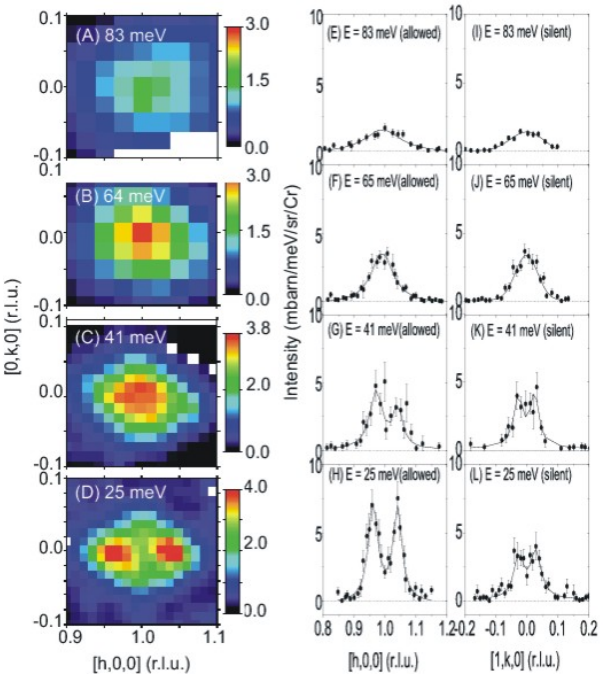

Figure 1: Constant-E slices (A)-(D) at E = 25, 41, 64, and 83 meV as measured near (100)*. Corresponding cuts through the allowed (along* [100]*) and the silent peaks (along* [010]*) are displayed in ((E)-(H)) and ((I)-(L)), respectively.*

Fig. 2 shows the dispersion of the excitations along [100] and [010]. The data points are extracted from the cuts through the allowed and silent peaks in Fig. 1. The shape of the dispersion curve is very similar to the low-energy part of the 'hour glass' dispersion observed in the cuprates [1]. The dispersion branches meet at the commensurate position (100) near E = 62 meV, where the long sought phason mode was predicted [3] and possibly observed [4].

We have interpreted the MAPS-data in terms of the 3-band model of Fishman and Liu [3]. A calculated contour map in the $E - Q_x$ plane is shown in Fig. 3. The spectral weight of the magnetic fluctuations shifts with increasing E towards (100). This shift is caused by the inner phason mode whose spectral weight increases with increasing E when compared with the conventional spin wave scattering.

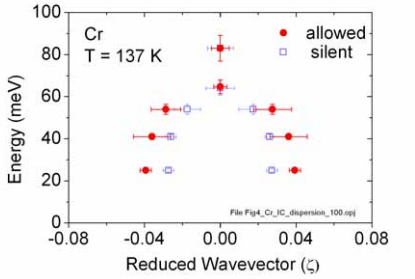

Figure 2: Dispersion curve of the allowed and the silent modes. The dispersion curves meet near E = 62 meV [5].

Near E = 62 meV, the dispersion of the phason modes emanating from the two magnetic satellite peaks merges. For $E > 62$ meV, only scattering from the spin waves is observed.

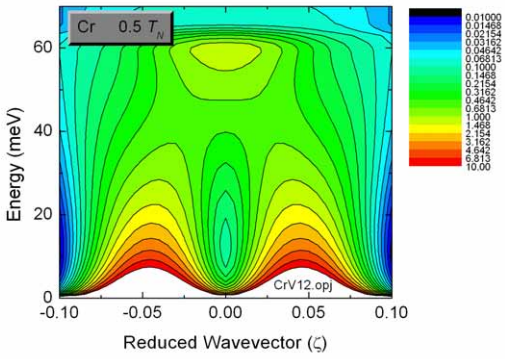

Figure 3: Calculated intensity contours of the dispersion of the magnetic excitations along the [100]*-direction using the 3-band model [3].*

Our data resolves the long standing problem of interpreting the tilted dispersion cones in Cr and identifies unambiguously the dispersion of the phason mode. The magnetic scattering in Cr does resemble closely the lower part of the 'hour glass' dispersion in the cuprates. One may speculate that the relevant excitations in the cuprates are also the phason modes.

References

[1] J. Tranquada et al. *Nature*, 429:534, 2004.
[2] C. R. Fincher et al. *Phys. Rev. B*, 24:1312, 1981.
[3] R. S. Fishman and S. H. Liu. *Phys. Rev. Lett.*, 76:2398, 1996.
[4] T. Fukuda et al. *J. Phys. Soc. Jpn.*, 65:1418, 1996.
[5] Y. Endoh and P. Böni. *J. Phys. Soc. Jpn.*, 75:111002, 2006.

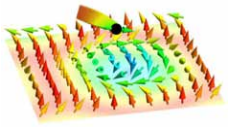

Skyrmion Lattices in Metallic and Semiconducting B20 Transition Metal Compounds

Tim Adams[1], Andreas Bauer[1], Sebastian Mühlbauer[1], Andreas Neubauer[1], Wolfgang Münzer[1], Florian Jonietz[1], Christian Franz[1], Michael Schmidt[2], Robert Georgii[2], Christian Pfleiderer[1], Peter Böni[1], Björn Pedersen[2], and Achim Rosch[3]

[1] *Physik Department E21, Technische Universität München, D-85748 Garching, Germany*
[2] *Forschungsneutronenquelle Heinz Maier-Leibnitz (FRM II), Technische Universität München, D-85748 Garching, Germany*
[3] *Institut für Theoretische Physik, Universität zu Köln, D-50937 Köln, Germany*

A comprehensive series of small angle neutron scattering measurements have been carried out on the cold diffractometer MIRA at FRM II that show that skyrmion lattices occur quite generally in metallic and semi-conducting B20 transition metal compounds. These studies establish magnetic order composed of topologically stable knots in the spin structure as a general phenomenon.

Recently we identified a completely new type of magnetic order, a skyrmion lattice, in the cubic B20 system MnSi [1, 2]. In the skyrmion lattice the spins form a hexagonally closest packed arrangement of topologically stable knots, a type of vortices, parallel to an applied magnetic field. The topological properties of this lattice give rise to a new form of Hall effect: the topological Hall effect [2]. The observation of the skyrmion lattice in MnSi raises the question for further magnetic materials with skyrmion lattices and if skyrmion lattices are a more general phenomenon. We have approached this question in two different ways, performing studies comprising single-crystal growth by optical float-zoning, measurements of the bulk properties and small angle neutron scattering on the cold diffractometer MIRA at FRM II.

On the one hand we performed comprehensive substitutional doping studies in the isostructural B20 series $Mn_{1-x}Fe_xSi$ and $Mn_{1-x}Co_xSi$. Here Fe- and Co-doping of MnSi suppresses the helimagnetic transition temperature and introduces moderate site disorder. Nevertheless we find that the skyrmion lattice forms in a small field for temperatures just below T_c as before and remains a stable feature of the magnetic phase diagram [3]. In addition our studies even suggest the formation of more complex forms of topological order when approaching the quantum phase transition.

On the other hand we have performed a detailed study of the helimagnetic order that stabilizes under substitutional Co doping of the paramagnetic insulator FeSi. Here we find the formation of a skyrmion lattice in a doped semiconductor with strong site disorder [4]. Our study in $Fe_{1-x}Co_xSi$ (x = 0.2) revealed two additional features. First the scattering pattern in the zero-field cooled state of $Fe_{1-x}Co_xSi$ (x = 0.2) is remarkably similar to partial order in MnSi under high pressure [4]. Second, the formation of skyrmion lattice domains when the magnetic field is applied parallel to a ⟨100⟩ direction of the cubic crystal structure [5].

The existence of skyrmion lattices in anisotropic chiral magnets was first suggested theoretically by Bogdanov and Yablonskii in 1989 using a mean-field description [6]. The theoretical description of the skyrmion lattice in MnSi [1, 2], showed that Gaussian fluctuations may stabilize skyrmion lattices in applied magnetic fields even in cubic materials. Since the theoretical framework is very general, our experimental studies of metallic and semiconducting B20 transition metal compounds establish the formation of skyrmion lattices as the first representatives of a very general phenomenon. In fact, they point at the existence of a much wider range of spin textures with non-trivial topology.

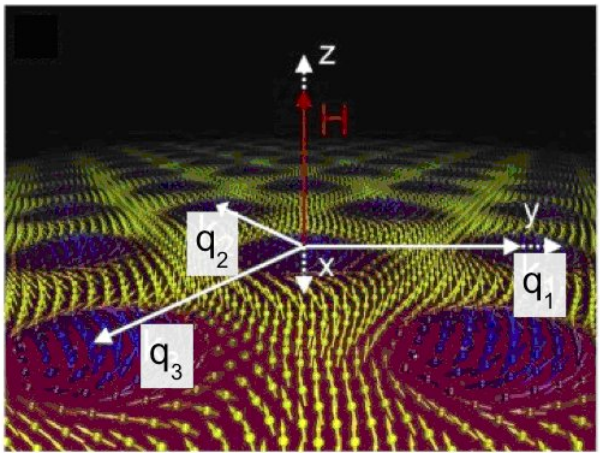

Figure 1: Top view of the skyrmion lattice in metallic and semiconducting B20 transition metal compounds. The skyrmion lattice represents a hexagonally closest packed arrangement of a type of vortex lines. The full spin structure is akin to a triple-Q structure with additional higher harmonic contributions (not indicated). It stays always strictly perpendicular to the applied magnetic field.

References

[1] S. Mühlbauer, B. Binz, F. Jonietz, C. Pfleiderer, A. Rosch, A. Neubauer, R. Georgii, and P. Böni. *Science*, 323:915, 2009.

[2] A. Neubauer, C. Pfleiderer, B. Binz, A. Rosch, R. Ritz, P. G. Niklowitz, and P. Böni. *Phys. Rev. Lett.*, 102:186602, 2009. Selected for "Viewpoint in Physics".

[3] C. Pfleiderer, T. Adams, A. Bauer, W. Biberacher, B. Binz, F. Birkelbach, P. Böni, C. Franz, R. Georgii, M. Janoschek, F. Jonietz, R. Ritz, S. Mühlbauer, W. Münzer, A. Neubauer, B. Pedersen, and A. Rosch. *J. Phys.: Cond. Matter*, in press 2010. Invited contribution at International Conference of Magnetism, Karlsruhe 2009.

[4] W. Münzer, A. Neubauer, T. Adams, S. Mühlbauer, C. Franz, F. Jonietz, R. Georgii, P. Böni, B. Pedersen, M. Schmidt, A. Rosch, and C. Pfleiderer. *Phys. Rev. B (Rapid Communications)*, 81:041203, 2010. "Editor's choice".

[5] T. Adams, S. Mühlbauer, A. Neubauer, W. Münzer, F. Jonietz, R. Georgii, B. Pedersen, P. Böni, A. Rosch, and C. Pfleiderer. *J. Phys.: Conf. Series*, in press 2010. Contribution at the International Conference of Magnetism, Karlsruhe 2009.

[6] A. N. Bogdanov and D. A. Yablonskii. *JETP Lett.*, 68:101, 1989.

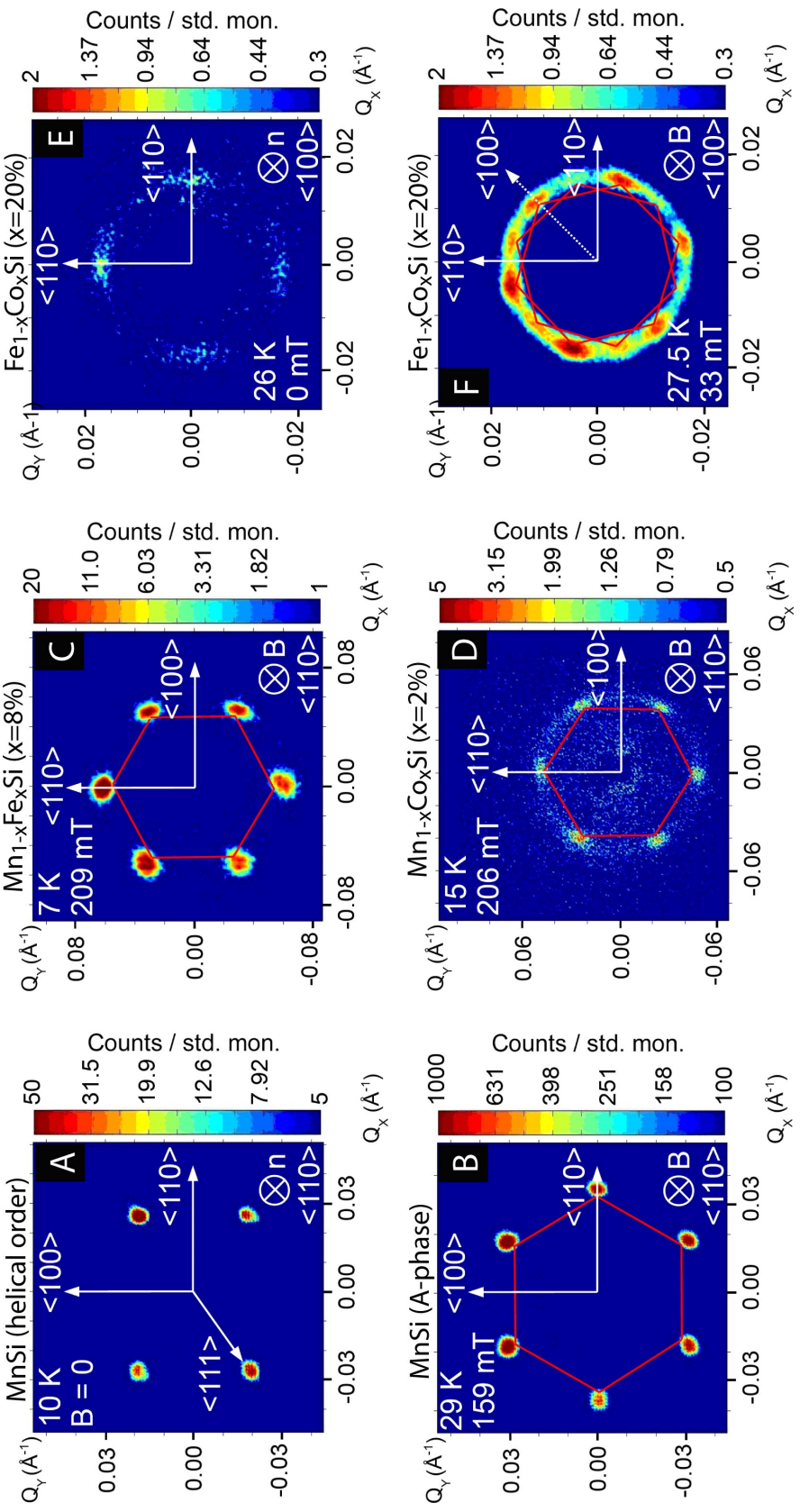

Figure 2: Typical scattering patterns as observed in our small angle neutron scattering studies of B20 transition metal compounds on the cold diffractometer MIRA. (A) Normal helical order in MnSi, where the helical propagation vector is parallel to the ⟨111⟩ cubic space diagonal. (B) Hexagonal scattering pattern for neutrons parallel to the skyrmion lattice in MnSi [1, 2]. (C) Hexagonal scattering pattern parallel to the skyrmion lattice in $Mn_{1-x}Fe_xSi$ (x = 0.08) [3]. (D) Hexagonal scattering pattern parallel to the skyrmion lattice in $Mn_{1-x}Co_xSi$ (x = 0.02) [3]. (E) Zero-field cooled state in $Fe_{1-x}Co_xSi$ (x = 0.2) showing partial magnetic order (broad intensity maxima for ⟨110⟩) [4]. (F) Two six-fold scattering patterns of the domain populations of the skyrmion lattice in $Fe_{1-x}Co_xSi$ (x = 0.2) for magnetic field parallel ⟨100⟩ [4, 5].

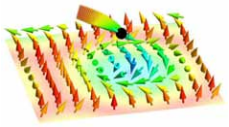

Search for ferromagnetic quantum criticality with polarized neutron imaging

A. Neubauer[1], M. Schulz[1,2], C. Franz[1], P. Böni[1], and C. Pfleiderer[1]

[1] *Physik Department E21, Technische Universität München, D-85748 Garching, Germany*
[2] *Forschungsneutronenquelle Heinz Maier-Leibnitz (FRM II), Technische Universität München, D-85748 Garching, Germany*

Quantum phase transitions are phase transitions that are driven by quantum fluctuations. In practice this implies that quantum phase transitions occur at zero temperature as a function of non-thermal control parameters such as pressure, magnetic field, uniaxial stress or chemical composition [1]. Since the many-body wave-function of systems at a quantum phase transition are exact, a cornucopia of unexpected novel electronic states may occur. Amongst the most prominent examples are superconductivity at the border of antiferromagnetism or deep inside ferromagnetic states [2], as well as various forms of heterogeneities [1]. The latter are viewed as partial forms of magnetic or electronic order that share certain similarities with nematic or smectic order in liquid crystals. In turn experimental methods, that allow to track the evolution of heterogeneities across large sample volumes as a function of temperature and non-thermal control parameters are of great interest.

We have explored the use of neutron depolarization imaging in a comprehensive search for ferromagnetic quantum criticality. Neutron depolarization imaging has recently attracted interest as a method that allows to map out magnetic fields in complex solenoids or type 2 superconductors [3]. It is hence also suited as a method to address scientific challenges in ferromagnetic materials. As our non-thermal control parameters we used hydrostatic pressure and compositional tuning. Ferromagnetic quantum phase transitions have thereby long attracted great interest as a particularly simple example for a quantum phase transition.

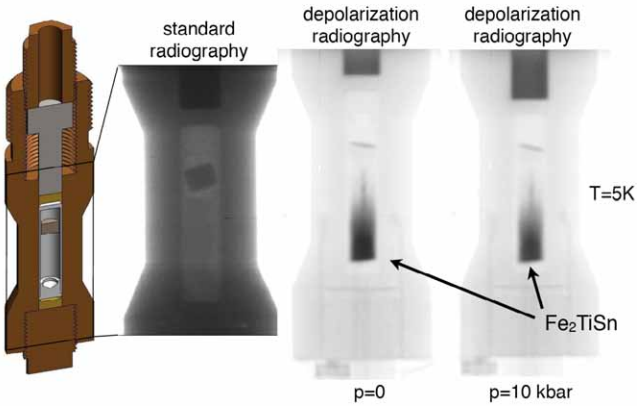

Figure 1: (Left) Schematic cut-away view of the clamp type pressure cell used in our studies of Fe_2TiSn. (2nd from Left) Standard radiography of the central part of the pressure cell. (Right) Depolarization radiography at ambient pressure and high pressure (10 kbar). The ferromagnetic properties are suppressed with increasing pressure. Note the lower position of the WC piston under pressure.

In order to establish the best experimental set up we have at first performed a series of studies in which we compared various types of polarizer and analyzer, notably ^{3}He, solid state benders and a periscope. For a detailed account of the advantages of the various methods we refer to Ref. [4, 5, 6]. Subsequently we demonstrated the possibility of a tomographic reconstruction [7]. Further, in a study of the weak itinerant ferromagnet Ni_3Al we have demonstrated that neutron depolarization tomography is ideally suited to track the pressure dependence of ferromagnetic materials [8].

Recently we have applied neutron depolarization radiography to a wide range of ferromagnetic materials. An important example is the Heusler compound Fe_2TiSn, which is believed to display weak ferromagnetism due to site disorder [8]. However, in single crystals of Fe_2TiSn grown with optical float-zoning, we find a wide range of magnetic properties ranging from ferromagnetism all the way to paramagnetism. Since the application of hydrostatic pressure tends to stabilize magnetic order in Heusler compounds [9] we have also studied the pressure dependence of the ferromagnetism by means of neutron depolarization.

In our study we find that the ferromagnetic properties are suppressed, consistent with the metallurgical complexity as the origin of the ferromagnetism. Closer inspection of the ferromagnetic regime using EDX finally revealed the presence of metallurgical segregation as the possible origin of the ferromagnetism. Combining our tomography results with the growth conditions used in optical float-zoning promises important insights how to improve the preparation of high purity single crystals.

Financial support through DFG Forschergruppe FOR 960 (Quantum Phase Transitions) and DFG Transregio TRR80 (From Electronic Correlations to Functionality) is gratefully acknowledged.

References

[1] H. v. Löhneysen, A. Rosch, M. Vojta, and P. Wölfle. *Rev. Mod. Phys.*, 79:1015, 2008.
[2] C. Pfleiderer. *Rev. Mod. Phys.*, 81:1551, 2009.
[3] N. Kardjilov, I. Manke, M. Strobl, A. Hilger, W. Treimer, M. Meissner, T. Krist, and J. Banhart. *Nature Physics*, 4:399, 2008.
[4] M. Schulz, P. Böni, E. Calzada, M. Mühlbauer, A. Neubauer, and B. Schillinger. *Nucl. Inst. Meth. A*, 605:43, 2009.
[5] M. Schulz, A. Neubauer, M. Mühlbauer, E. Calzada, B. Schillinger, C. Pfleiderer, and P. Böni. *J. Phys.: Conf. Series*, 200:112009, 2010.
[6] M. Schulz, P. Böni, C. Franz, A. Neubauer, E. Calzada, M. Mühlbauer, B. Schillinger, C. Pfleiderer, A. Hilger, and N. Kardjilov. *J. Phys.: Conf. Series*, 251:012068, 2010.
[7] M. Schulz, A. Neubauer, S. Masalovich, M. Mühlbauer, E. Calzada, B. Schillinger, C. Pfleiderer, and P. Böni. *J. Phys.: Conf. Series*, 211:01225, 2010.
[8] A. Ślebarski, M. B. Maple, E. J. Freeman, C. Sirvent, D. Tworuszka, M. Orzechowska, A. Wrona, A. Jezierski, S. Chiuzbaian, and M. Neumann. *Phys. Rev. B*, 62:3296, 2000.
[9] E. Şaşioğlu, L. M. Sandratskii, and P. Bruno. *Phys. Rev. B*, 71:214412, 2005.

Quantum phase transitions in single-crystal $Mn_{1-x}Fe_xSi$ and $Mn_{1-x}Co_xSi$: crystal growth, magnetization, AC susceptibility, and specific heat

A. Bauer[1], A. Neubauer[1], C. Franz[1], W. Münzer[1], M. Garst[2,3], and C. Pfleiderer[1]

[1] *Physik Department E21, Technische Universität München, D-85748 Garching, Germany*
[2] *Physik Department, Technische Universität München, D-85748 Garching, Germany*
[3] *Institut für Theoretische Physik, Universität zu Köln, D-50937 Köln, Germany*

The magnetic ordering temperature in MnSi may be suppressed by hydrostatic pressure [1] or substitutional doping of Fe or Co on the Mn-sites. To explore differences of the pressure and composition tuned quantum phase transition we have grown high quality single crystals of $Mn_{1-x}Fe_xSi$ (x = 0.04, 0.08, 0.12, 0.16, 0.19, and 0.22) and $Mn_{1-x}Co_xSi$ (x = 0.02 and 0.04) by means of optical float-zoning. A comprehensive study of the magnetization, susceptibility and specific heat was carried out [2] to address two related issues: (i) Does $Mn_{1-x}(Fe,Co)_xSi$ also display evidence for a non-Fermi liquid phase and partial magnetic order such as pure MnSi under pressure? (ii) What is the fate of the magnetic phase diagram and the skyrmion lattice phase [3] in the A-phase?

In our studies we find that the transition temperature T_c as derived from Arrott and Curie plots vanishes at critical concentrations of $x_{c,Fe} \approx 0.19$ and $x_{c,Co} \approx 0.09$, respectively. The spontaneous magnetic moment $m_{s,0}$ tracks T_c suggesting a second order phase transition (see Fig. 2). Moreover the initial inverse susceptibility vanishes at the critical concentration and the electronic part of the heat capacity shows a logarithmic divergence. Hence, in contrast to MnSi under pressure there is strong evidence that substitutional doping leads to a quantum critical point.

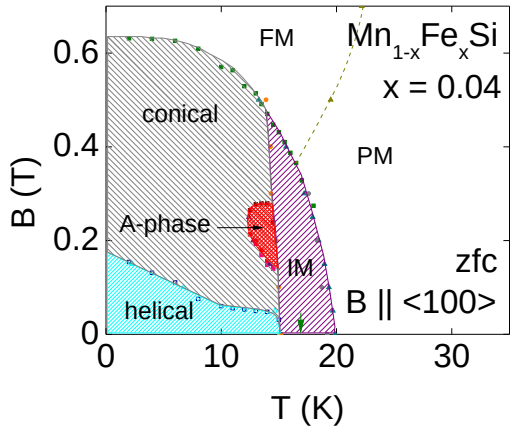

Figure 1: Magnetic phase diagram of $Mn_{0.96}Fe_{0.04}Si$ for $B \parallel \langle 100 \rangle$ after zero field cooling.

The magnetic phase diagrams of the doped systems (see Fig. 1 for an example) may be derived from the AC susceptibility. They are reminiscent of MnSi. While the T_c is suppressed, the second critical field B_{c2} only changes slightly. Moreover the helical phase shows some dependence the orientation of the magnetic field and differences between zero field and field cooling. The A-phase in the highly doped systems exists over a larger field interval and down to lowest temperatures available. In both MnSi and the doped systems an intermediate regime (IM), which may be related to more complex spin textures, exists between the paramagnetic phase and the helimagnetic ones. This regime extends with increased doping concentration and dominates the behaviour in the vicinity of x_c (see Fig. 3).

Taken together, the effect of Fe- and Co-doping may be plotted on a normalized concentration scale. The bulk properties thereby reveal a rich phase diagram which is dominated by a combination of a putative ferromagnetic quantum critical point and complex helical spin textures.

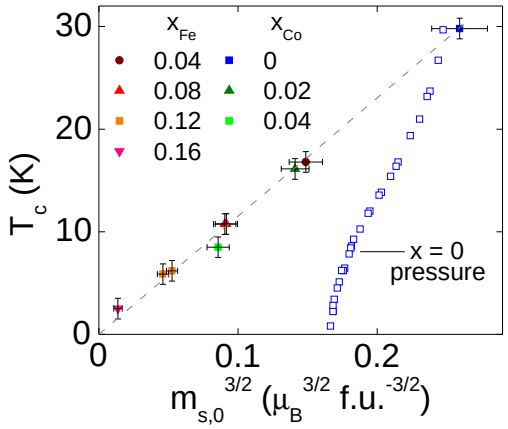

Figure 2: The critical temperature T_c over the spontaneous magnetic moment $m_{s,0}$ suggesting a putative ferromagnetic quantum critical point.

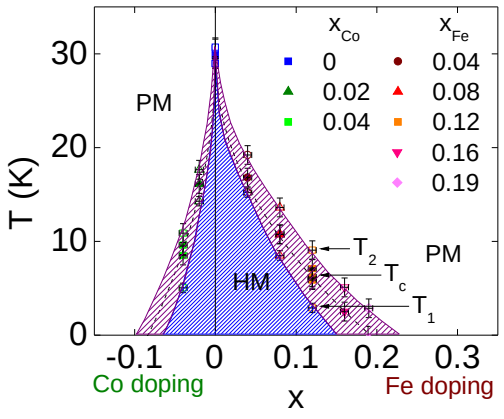

Figure 3: Phase diagram at B = 0 showing paramagnetic (PM) and helimagnetic (HM) behavior. The purple area represents an intermediate regime of unidentified nature.

References

[1] C. Pfleiderer et al. *Science*, 316:1871–1874, 2007.
[2] A. Bauer et al. *Phys. Rev. B*, 82:064404, 2010.
[3] S. Mühlbauer et al. *Science*, 323:915–919, 2009.

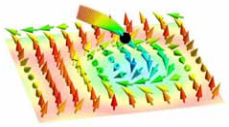

Magnetization of $Pd_{1-x}Ni_x$ near Quantum Criticality

Christian Franz[1], Christian Pfleiderer[1], Andreas Neubauer[1], Michael Schulz[1,2], Björn Pedersen[2], and Peter Böni[1]

[1] *Physik Department E21, Technische Universität München, D-85748 Garching, Germany*
[2] *Forschungsneutronenquelle Heinz Maier-Leibnitz (FRM II), Technische Universität München, D-85748 Garching, Germany*

In recent years so-called quantum phase transitions (QPT), representing a new class of phase transitions, have been attracting great interest. In contrast to conventional entropy-driven thermal phase transitions QPT are driven by quantum fluctuations and result from a competition of dominant contributions in the internal energy. An important question concerns whether a given QPT is first or second order and whether the underlying dynamical properties are those of a pure or a disordered compound. A prototypical example for a QPT and the perhaps best studied class concerns the border of itinerant ferromagnetism in three-dimensional systems. For clean systems mean field behavior is expected. $Pd_{1-x}Ni_x$ is a rare example of a system in which a QPT can be reached without the application of pressure. As a function of Ni concentration ferromagnetic order emerges in $Pd_{1-x}Ni_x$ for $x > 2.5\%$. The temperature dependence of the specific heat, resistivity and susceptibility suggest the properties of a clean ferromagnetic quantum critical point. We have revisited this issue using complimentary measurements of the magnetization as a function of magnetic field, thereby directly investigating the order parameter.

We have measured the magnetization of a sample containing $\approx 2.5\%$ Ni as a function of magnetic field up to 9 T at temperatures in the range 4 K to 60 K (Fig. 1). In the simplest scenario the non-linear magnetization may be accounted for by a magnetic equation of state derived from a fourth order Ginzburg Landau free energy. The magnetic field B which stabilizes the magnetization M is then expected to vary as $B = aM + bM^3$ where a and b are material specific phenomenological parameters. a represents the inverse linear susceptibility, which limits for $T \to 0$ to the so-called inverse initial susceptibility $a_0 = a(T \to 0)$. The parameter b represents the lowest approximation of the effects of mode-mode coupling.

To better explore the nature of the non-linear field dependence we show in Fig. 1(B) the inverse DC susceptibility B/M as a function of M^2. At high temperatures a straight line is observed for all fields (and thus values of M). This is characteristic of a conventional mean field relationship between the susceptibility and the magnetization. As the temperature decreases the mean field behavior survives for sufficiently large values of M, notably to the right hand side of the arrows at high fields. The arrows hence mark the location of a cross-over, where we find for low values of M and T a behavior that is more complex.

The anomalous behavior we observe in the Arrott plots for $Pd_{1-x}Ni_x$ near the quantum critical Ni concentration is summarized in Fig. 2. Shown in panel (A) is the inverse susceptibility as a function of temperature. The behavior at low fields and low temperatures is shown by black data points. A pronounced Curie-Weiss dependence is observed with a large fluctuating moment of $\approx 1\mu_B$. The susceptibility provides clear evidence of a ferromagnetic transition at $T_c \sim 11$ K. The properties suggested by the inverse susceptibility shown in Fig. 2 (A) are strongly supported by the ordered magnetic moment M_s inferred from the Arrott plots as the value of M for $B \to 0$ (Fig. 2 (B)). The ordered moment vanishes at a Curie temperature $T_c \sim 11$ K. As a final point to illustrate the increased curvature shown in Fig. 1 (B) we plot in Fig. 2 (C) an estimate of the initial slope of the Arrott plots for small fields. The mode-mode coupling parameter appears to be anomalously large when approaching low temperatures.

Our measurements of the magnetic field dependence of the magnetization clearly reveal a regime at low fields and low temperatures, where strong deviations emerge from the conventional mean field predictions of a ferromagnetic quantum critical point in the clean limit. We expect that microscopic heterogeneities and clustering of the Ni atoms represent aspects that have to be taken into account for a full description.

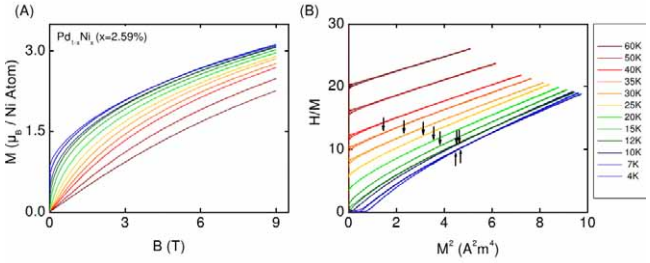

Figure 1: (A) Magnetization of $Pd_{1-x}Ni_x$ as a function of magnetic field. (B) Arrott plots of the data shown in panel (A).

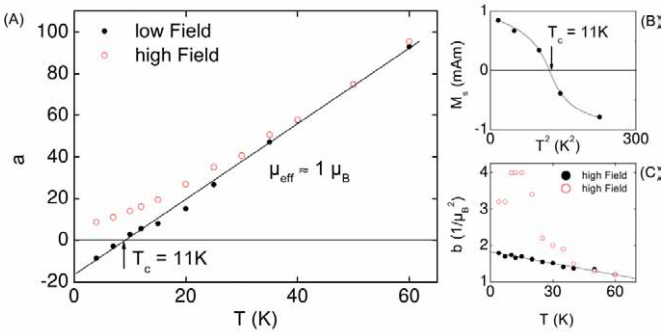

Figure 2: Information inferred from the data shown in Fig. 1. (A) Inverse susceptibility inferred from the Arrott plots. (B) Ordered moment inferred from the intercept of the Arrott plots. (C) Temperature dependence of the mode-mode coupling parameter B.

Magnetism in geometrically frustrated systems under extreme conditions

Michael Wagner[1], Vladimir Tsurkan[2], Sarah Dunsiger[1], and Christian Pfleiderer[1]

[1] *Physik Department E21, Technische Universität München, D-85748 Garching, Germany*
[2] *Zentrum für Elektronische Korrelationen und Magnetismus, Institut für Physik, Universität Augsburg, D-86159 Augsburg, Germany*

Geometrically frustrated spin systems on a pyrochlore lattice are prone to competing antiferromagnetic and ferromagnetic interactions. In turn highly degenerated ground states may form, that are sensitive to small perturbations and additional interactions. Under hydrostatic pressure the relative strength of the various magnetic interactions may be changed driving phase transitions of the ground state. For instance, changes of the lattice constant may generate magnetic as well as a metal-insulator transition. An open issue is thereby the interplay of metal-insulator transitions with the spin order in geometrically frustrated systems.

To address the question of the interplay of geometric frustration in the metallic state we decided to study the chromium spinel $HgCr_2Se_4$, a ferromagnetic semiconductor. First high pressure studies suggested the existence of a insulator to metal transition at room temperature under pressures exceeding 17 kbar [1]. We have measured the magnetization under pressure to search for evidence of the metal insulator transition. Our measurements were carried out on single crystals prepared by chemical transport reaction. Fig. 1 shows schematically the pressure cell used for our measurements of the magnetization. The signal of the empty pressure cell was measured separately and subtracted.

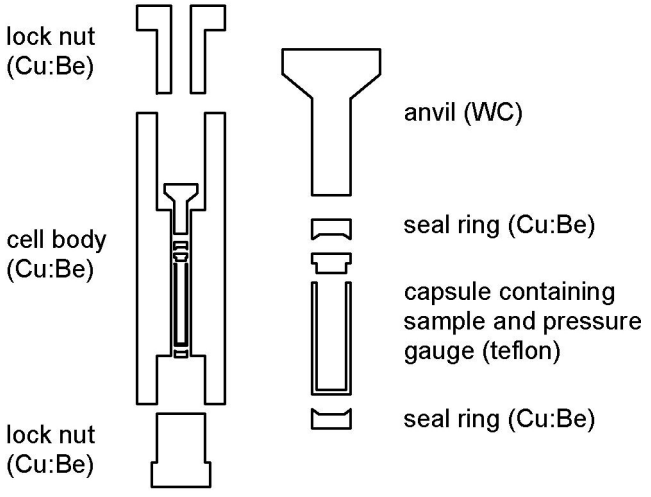

Figure 1: Schematic view of the miniature clamp cell used for measurements of the magnetization. The inner part is shown enlarged on the right hand side.

At ambient pressure and 4 K the saturation magnetization is 6 μ_B/f.u. dominated by the contribution of the two Cr^{3+} atoms (see Fig. 2). With increasing pressure the saturation magnetization at 4 K slightly increases, where tiny systematic errors cannot be ruled out. Essentially no hysteresis is observed. As a function of temperature the magnetization vanishes at the curie temperature T_c, which decreases as a function of pressure consistent with literature [2] (see Fig. 3). Thus the ordered moment and Curie temperature do not seem to track each other in a simple manner. To confirm that the ferromagnetic properties are essentially unchanged under pressure, we will measure the resistivity and Hall effect in the near future.

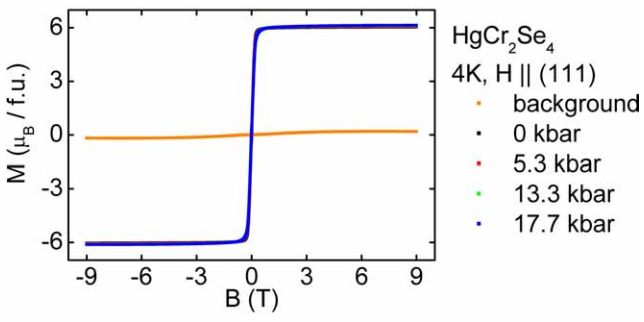

Figure 2: Magnetic field dependence of the magnetization of $HgCr_2Se_4$ under pressure. The signal of the empty pressure cell is shown in orange.

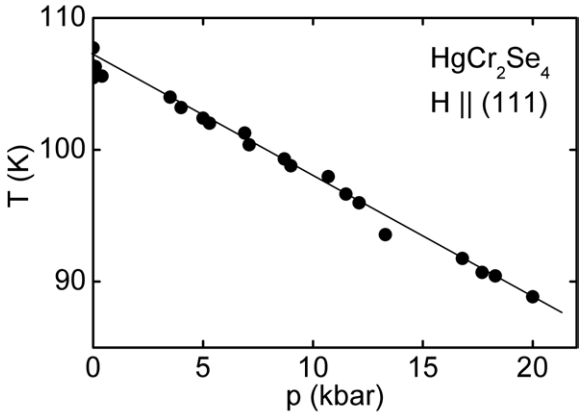

Figure 3: Curie temperature T_c as a function of pressure in $HgCr_2Se_4$. The line is a guide to the eye.

References

[1] P. Kistaiah, K. Satyanarayana Murthy, and K. V. Krishan Rao. *Journal of the Less-Common Metals*, 98:L13, 1984.
[2] T. Kanomata, K. Shirakawa, and T. Kaneko. *J. Magn. Magn. Mater.*, 54-57:1499, 1986.

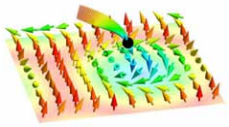

Vibrating Coil Magnetometry in $LiHoF_4$

Stefan Legl[1], Christian Pfleiderer[1], and Karl Krämer[2]

[1] *Physik Department E21, Technische Universität München, D-85748 Garching, Germany*
[2] *Department of Chemistry, University of Bern, CH-3012 Bern, Switzerland*

$LiHoF_4$ attracts great interest, because the ferromagnetic transition at T_c = 1.54 K is still not understood [1, 2]. Moreover, for fields transverse to the Ising axis a quantum phase transition is observed [3, 4].

To test the performance of our newly developed vibrating coil magnetometer (VCM, see page 48 in this issue) we have measured the magnetization of the dipolar Ising ferromagnet $LiHoF_4$ [5], for which no magnetization data below 1.5 K have been reported in the literature. In contrast to other methods, such as Faraday magnetometry, our vibrating coil magnetometer is insensitive to magnetization components transverse to the field direction. This permits in particular to measure proper hysteresis loops as a function of applied magnetic field.

Shown in Fig. 1 (a) is the susceptibility and in Fig. 1 (b) the inverse susceptibility for the easy-axis in a small applied field of 10 mT. Data below T_c = 1.54 K are dominated by demagnetizing fields, where χ = const for $T < T_c$ = 1.54 K corresponds roughly to the demagnetising factor of the sample.

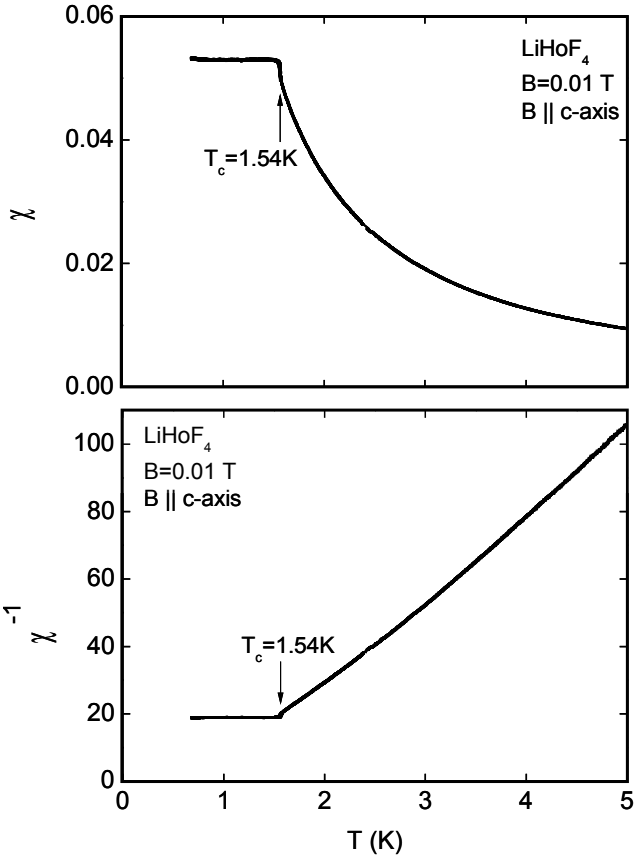

Figure 1: Susceptibility, $\chi = M/B$, (a) and inverse susceptibility, $\chi^{-1} = B/M$, (b) as a function of temperature with the magnetic field along the Ising-axis. χ = const for $T < T_c$ = 1.54 K corresponds roughly to the demagnetising factor of the sample (see text).

Fig. 2 shows the easy-axis magnetisation as a function of magnetic field for temperatures as low as 60 mK. Black and red curves denote VCM measurements, where the red curve was taken at T_c = 1.54 K. Data shown in blue were recorded with a conventional VSM. Data shown in Fig. 1 and 2 are in excellent agreement with the literature, where data has been reported (e.g. Ref. [3, 6]).

For the large signal of $LiHoF_4$ a sensitivity of 10^{-3} emu was achieved equivalent to a resolution better than 10^{-5}. In addition, the VCM signal may be amplified by toroidal low temperature transformers, where we readily achieved a sensitivity of 10^{-4} emu and further improvements seem possible.

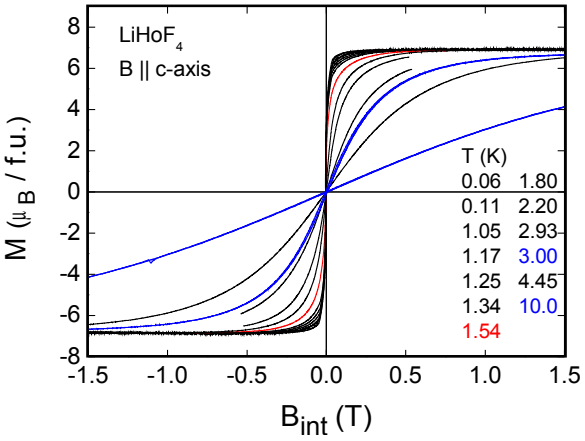

Figure 2: Easy-axis magnetisation as a function of magnetic field for temperatures as low as 60 mK. Black and red curves denote VCM measurements, where the red curve was taken at T_c = 1.54 K. Data shown in blue were recorded with a conventional VSM.

References

[1] P. B. Chakraborty, P. Henelius, H. Kjonsberg, A. W. Sandvik, and S. M. Girvin. Theory of the magnetic phase diagram of $LiHoF_4$. *Phys. Rev. B*, 70:144411, 2004.

[2] A. Biltmo and P. Henelius. The ferromagnetic transition and domain structure in $LiHoF_4$. *Eur. Phys. Lett.*, 87:27007, 2009.

[3] D. Bitko, T. F. Rosenbaum, and G. Aeppli. Quantum Critical Behavior for a Model Magnet. *Phys. Rev. Lett.*, 77:940, 1996.

[4] H. M. Ronnow, R. Parthasarathy, J. Jensen, G. Aeppli, T. F. Rosenbaum, and D. F. McMorrow. Quantum Phase Transition of a Magnet in a Spin Bath. *Science*, 308:389, 2005.

[5] S. Legl, C. Pfleiderer, and K. Krämer. Vibrating coil magnetometer for milli-Kelvin temperatures. *Rev. Sci. Instr.*, 81:043911, 2010.

[6] A. H. Cooke, D. A. Jones, J. F. A. Silva, and M. R. Wells. Ferromagnetism in lithium holmium fluoride-$LiHoF_4$. I. Magnetic measurements. *J. Phys. C: Solid State Phys.*, 8:4083, 1975.

Distribution of Lattice Constants in $CePt_3Si$ observed by Larmor Diffraction and SANS

R. Ritz[1], S. Mühlbauer[1], C. Pfleiderer[1], T. Keller[2], J. White[3], M. Laver[3], E. M. Forgan[3], R. Cubitt[4], C. Dewhurst[4], P. G. Niklowitz[5], A. Prokofiev[6], and E. Bauer[6]

[1] *Physik Department E21, Technische Universität München, D-85748 Garching, Germany*
[2] *MPI für Festkörperforschung, Heisenbergstr. 1, D-70569 Stuttgart, Germany*
[3] *School of Physics and Astronomy, University of Birmingham, Birmingham B15 2TT, UK*
[4] *Institut Laue-Langevin, BP 156, F-38042 Grenoble, France*
[5] *Dep. of Physics, Royal Holloway, University of London, Egham TW20 0EX, UK*
[6] *Fakultät für Physik, Institut für Festkörperphysik, TU Wien, A-1040 Wien, Austria*

In recent years a large number of f-electron heavy fermion superconductors have been discovered that are prime candidates for non-electron-phonon pairing mechanisms and unconventional pairing symmetries [1]. A prominent example is the non-centrosymmetric f-electron compound $CePt_3Si$ [2]. At ambient pressure $CePt_3Si$ orders antiferromagnetically below $T_N = 2.2\,\mathrm{K}$, followed by a superconducting transition, where $T_s = 0.45\,\mathrm{K}$ for high quality samples and $T_s = 0.75\,\mathrm{K}$ for lower quality samples. Under hydrostatic pressure the antiferromagnetism in $CePt_3Si$ is suppressed above a critical pressure of $p_N = 8\,\mathrm{kbar}$, while the superconductivity vanishes above $p_s \approx 16\,\mathrm{kbar}$ [3]. Unconventional superconductivity is well known to respond very sensitively to both magnetic and non-magnetic defects. This raises the question, why samples of seemingly better quality have a *reduced* superconducting transition temperature. We have used neutron Larmor diffraction to measure the temperature dependence and distribution of the lattice constants in a single crystal of $CePt_3Si$ with $T_s = 0.75\,\mathrm{K}$ [4, 5].

Fig. 1 (A,B) shows the relative change of lattice constant $\Delta d/d$ as a function of temperature for the a- and the c-axis. Evidently the thermal expansion of $CePt_3Si$ is highly anisotropic. Fig. 1(C) shows the polarization of the signal for the a- and the c-axis as a function of total Larmor phase. Our data are best explained by invoking the presence of two Gaussian distributions of lattice constants which yields $\Delta a/a \approx \Delta c/c \approx 10^{-3}$. The wide distribution of lattice constants seen in LD may be interpreted as a wide range of microscopic pressures Δp across the sample volume. With $\Delta p = K\Delta V/V$ and the modulus of compressibility of copper $K_{\mathrm{Cu}} = 125 \cdot 10^9\,\mathrm{N/m^2}$ as an first estimate we find $\Delta p \approx 4\,\mathrm{kbar}$ which translates into $\Delta T_s \approx 0.15\,\mathrm{K}$ according to the published T-p-phase diagram of $CePt_3Si$ [3]. This implies that the increased value of T_s in low quality samples is due to an effective negative pressure.

Small angle neutron scattering suggests an abundance of defects along the lattice planes. We find strong scattering intensity along the crystallographic a-axis (Fig. 2(A)). Closer inspection of the intensity variation as a function of wave vector and scattering angle 2θ seen in rocking scans suggests that considerable intensity shifts from large scattering angles to small scattering angles with decreasing rocking angle ω (see Fig. 2(B)). This behavior is atypical of simple small angle diffraction. Rather it is the signature of an abundance of reflections confined to the crystallographic ac-plane.

As a possible explanation for the sample dependence of T_s the SANS data suggest, e.g., the presence of fissures parallel to the lattice planes causing reflections. The associated q-values suggest that these fissures may be quite large, exceeding the superconducting coherence length. In turn this suggests, that the material is comparatively free of defects on microscopic scales while the fissures may generate local strains.

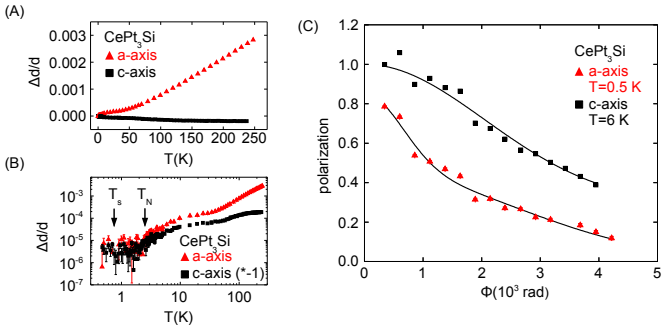

Figure 1: (A) $\Delta d/d$ of $CePt_3Si$ as a function of temperature for the a- and the c-axis. (B) The same data shown as a double logarithmic plot. The c-axis data was multiplied by -1 for logarithmic display. The arrows indicate $T_N = 2.2\,\mathrm{K}$ and $T_s = 0.75$, K. (C) Polarization as a function of total Larmor phase. The strong decrease of polarization is due to a large distribution of lattice constants $\Delta G/G \approx 10^{-3}$ in both directions.

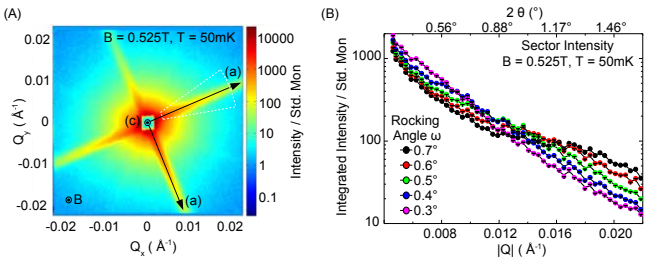

Figure 2: (A) SANS intensity pattern for the intermediate quality single crystal of $CePt_3Si$ investigated in our study. An abundance of scattering is observed along the ac-lattice planes, where the a- and c-axis are labelled as (a) and (c), respectively. (B) Scattering intensity in the sector shown in panel (A) as a function of wave vector or scattering angle 2θ for various rocking angles. The variation of the intensity as a function rocking angle ω is characteristic of reflections rather than small angle diffraction.

References

[1] C. Pfleiderer. *Rev. Mod. Phys.*, 81:1551, 2010.
[2] E. Bauer et al. *Phys. Rev. Lett.*, 92:027003, 2004.
[3] M. Nicklas et al. *Physica B*, 359:386, 2005.
[4] M. T. Rekveldt et al. *Eur. Phys. Lett.*, 54:342–346, 2001.
[5] R. Ritz et al. *J. Phys.: Conf. Series*, 200:012165, 2010.

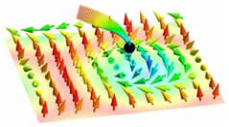

Larmor diffraction in the ferromagnetic superconductor UGe_2

R. Ritz[1], D. Sokolov[2], T. Keller[3], A. D. Huxley[2], and C. Pfleiderer[1]

[1] *Physik Department E21, Technische Universität München, D-85748 Garching, Germany*
[2] *School of Physics and Astronomy, and Centre for Science at Extreme Conditions, The University Edinburgh, Edinburgh EH9 3JZ, UK*
[3] *MPI für Festkörperforschung, D-70569 Stuttgart, Germany*

It was long thought that ferromagnetism and superconductivity may not coexist microscopically. Only in the year 2000 superconductivity was reported to occur in UGe_2 under pressures between 9 kbar and 16 kbar deep inside the ferromagnetic phase, where $T_{sc} \ll T_C$ [1]. The superconducting transition temperature T_{sc} has a maximum at a pressure $p_X \approx 12$ kbar where a transition T_X between two ferromagnetic phases with different magnetic moments, FM1 and FM2, is suppressed [2]. Hence the T_X transition seems to play a vital role for the coexistence of superconductivity and ferromagnetism in UGe_2.

The most prominent scenario proposed to explain the superconductivity in UGe_2 assumes that an abundance of ferromagnetic spin fluctuations near p_X drives the superconductive pairing [3]. This is scenario is perfectly compatible with the first order suppression of the FM2 state at p_X inferred from the magnetization. However, more recent proposals recognize, that the Uranium 5f electrons are subject to strong spin-orbit-coupling. Theoretical calculations thereby suggest the existence of two ground states that differ in the Uranium orbital moment, where the T_X transition separates these two orbital states. It has therefore been argued that orbital fluctuations near T_X may act as the pair building mechanism [4].

To resolve this issue we have tracked the signatures of the ferromagnetic phase transition as a function pressure simultaneously in the thermal expansion using Larmor diffraction as well the ferromagnetic moment using normal neutron diffraction for all three crystallographic axes under pressures up to 12.2 kbar.

All of our measurements were carried out at the spectrometer TRISP at the FRM II using Larmor diffraction. Larmor diffraction permits high-intensity measurements of lattice constants with an unprecedented high resolution of $\Delta d/d \approx 10^{-6}$. This is achieved by encoding the lattice spacing in the Larmor phase of a polarized neutron beam rather than in the scattering angle as in conventional scattering experiments. A detailed description of Larmor diffraction is given in references [5, 6].

For measurements of changes of the lattice constant ($\Delta d/d$) under pressure Larmor diffraction is especially suited since no apparatus needs to be installed inside the pressure cell containing the sample and the sample is floating completely free in the pressure medium. Also, it is possible to measure $\Delta d/d$ and the intensity of ferromagnetic Bragg peaks – which is proportional to the magnetization $M(T)$ squared – in the same setup. Hence transition temperatures as seen in $\Delta d/d$ and $M(T)$ may be compared directly. This makes Larmor diffraction unique in comparison with other techniques for measuring $\Delta d/d$ such as capacitive dilatometers or strain gauges.

Since Larmor diffraction requires polarized neutrons it was long believed that samples that depolarize the neutron beam, such as ferromagnets or superconductors, cannot be studied. However, after demagnetizing our samples in a small AC-magnetic field while cooling through the Curie temperature T_C even the strong ferromagnetism in UGe_2 ($\mu_{S,FM1} = 1.2\mu_B$/U; $\mu_{S,FM2} = 1.5\mu_B$/U [7]) did not completely demagnetize the neutron beam and measurements were possible. This behavior may be attributed to the Ising anisotropy of UGe_2.

For our experiment we used five single crystals of UGe_2 ($\approx$ 0.4 g – 1.3 g) grown in Edinburgh by the Czochralski technique under a purified Ar atmosphere. For measurements under pressure the single crystals were mounted in piston-cylinder pressure cells with a fluorinert mixture as pressure medium. Pressures up to 12.2 kbar were applied.

We found that the transition T_X between the two ferromagnetic phases which is believed to drive superconductivity and which can be seen in the magnetization as $T_{X,M}$ can also be clearly observed in the thermal expansion (TE) as $T_{X,TE}$ along the b- and c-axes. However, we also find $T_{X,TE}$ to be systematically a few Kelvin higher than $T_{X,M}$ and $T_{X,TE}$ along the a-axis as sketched in Fig. 1. In turn this suggests the existence of an additional energy scale. Notably, the suppression of $T_{X,TE}$ may be controlled by orbital fluctuations as proposed in Ref. [4].

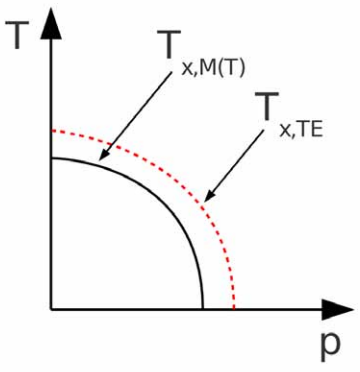

Figure 1: Sketch of T_X transition in $M(T)$ and thermal expansion (TE).

References

[1] S. S. Saxena et al. *Nature*, 406:587, 2000.
[2] A. Huxley et al. *Phys. Rev. B*, 63:144519, 2001.
[3] K. G. Sandeman et al. *Phys. Rev. Lett.*, 90:167005, 2003.
[4] A. B. Shick et al. *Phys. Rev. B*, 70:134506, 2004.
[5] T. Keller et al. *Appl. Phys. A*, 74:127, 2002.
[6] T. Rekveldt et al. *Eur. Phys. Lett.*, 54:342, 2001.
[7] C. Pfleiderer et al. *Phys. Rev. Lett.*, 89:147005, 2002.

Helimagnon Bands in MnSi

Marc Janoschek[1,2], Florian Bernlochner[1], Sarah Dunsiger[1], Christian Pfleiderer[1], Peter Böni[1], Bertrand Roessli[2], Peter Link[3], and Achim Rosch[4]

[1] *Physik Department E21, Technische Universität München, D-85748 Garching, Germany*
[2] *Laboratory for Neutron Scattering, Paul Scherrer Institut & ETH Zürich, CH-5232, Villigen, Switzerland*
[3] *Forschungsneutronenquelle Heinz Maier-Leibnitz (FRM II), Technische Universität München, D-85748 Garching, Germany*
[4] *Institut für Theoretische Physik, Universität zu Köln, D-50937 Köln, Germany*

The dispersion of low-energy spin excitations in ferro- or antiferromagnetic compounds can be deduced from simple symmetry arguments: the spontaneous breaking of a continuous symmetry in the magnetically ordered state implies the existence of Goldstone modes. The resulting spin wave theory does not depend on microscopic details, yielding a distinct universal shape of the dispersion. In ferromagnets, where the order parameter is a conserved quantity, spin waves show a quadratic dispersion while in antiferromagnets the superposition of the normal modes of the sublattices leads to the well-known linear dispersion at low energies [1, 2]. This makes the measurement of spin waves in ferromagnets or antiferromagnets an unique tool to probe the magnetic energy scales and is therefore of general importance. In addition, this raises the question about the nature of spin excitations in more general magnetic materials.

We have addressed this question in a detailed combined experimental and theoretical investigation of the spin wave spectrum in a helimagnetic system. From a more general viewpoint, all forms of complex order can be interpreted as a superposition of helimagnetic order [3]. Our experiments have been carried out using the B20 compound MnSi that is ideally suited to study the collective spin excitations of helimagnets experimentally. Below T_c = 29.5 K and in zero magnetic field a long-wavelength spin spiral ($\lambda_h \approx 180$ Å) that propagates along the cubic space diagonal stabilizes due to competing ferromagnetic exchange and Dzyaloshinskii-Moriya (DM) interactions [4]. MnSi has recently attracted great interest as a candidate for a genuine non-Fermi liquid metallic state in a three-dimensional metal at high pressure [5]. Moreover, a skyrmion lattice, was recently identified unambiguously at ambient pressure in a small phase pocket just below T_c [6]. The determination of the low lying excitations in MnSi is hence of great interest in its own right.

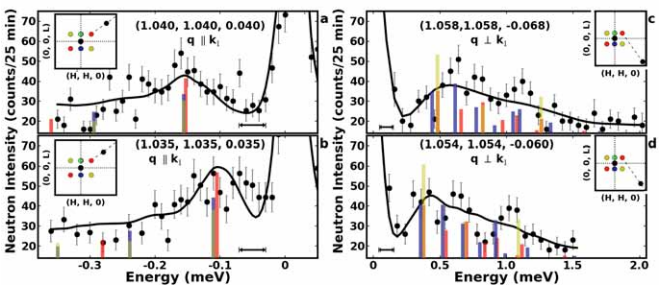

Figure 1: Measured low-energy spin excitations spectrum measured in the helical phase of MnSi at 20 K.

Our experiments were carried out on the cold triple axis spectrometers TASP (PSI) and PANDA (FRM II). All spectra were recorded in energy scans at fixed momentum Q. Examples of typical scans are provided in Figs. 1 (a) and (b). The observed excitations are characterized by fairly broad dispersive maxima. A naive interpretation of the data suggests an extreme form of broadening caused by damped modes. However, using a parameter free model we quantitatively establish that these excitations represent broad spin wave bands that are purely caused by the tiny magnetic propagation vector of the helix. The small magnetic Brillouin zone leads to multiple Umklapp interactions and thus many helimagnon modes as demonstrated in Fig. 2. Here the different colors denote the contributions from the four different configuration domains. The theory developed to describe our data [7] is only based on three parameters, namely the spin-wave stiffness of the modes, the length of propagation vector and a *single* scale factor for the intensities of *all* measured data. The first two are known from previous experiments and only the scale factor was free in the fits to our data (cf. black lines in Fig. 1).

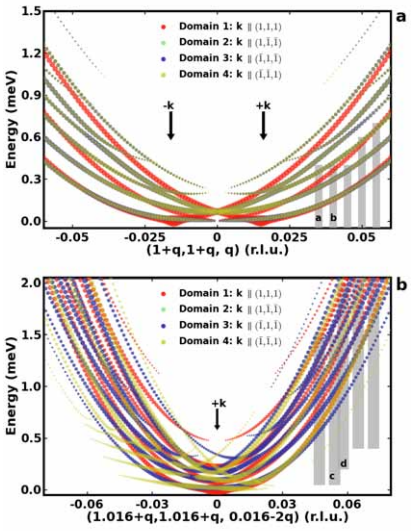

Figure 2: Dispersion of the helimagnon bands as derived from our fits.

Our study [7] provides first insights in collective spin excitations of complex forms of magnetic order. In addition, the developed theory demonstrates how spin waves may be radically modified even in simple systems by seemingly harmless small magnetic propagation vectors.

References

[1] C. Kittel. *Introduction to Solid State Physics*. John Wiley & Sons, Inc., New York, 1996.
[2] F. Keffer et al. *Am. J. Phys.*, 21:250, 1953.
[3] L. M. Sandratskii. *Adv. Phys.*, 47:91, 1998.
[4] M. Ishida et al. *J. Phys. Soc. Jpn.*, 54:2975–2982, 1985.
[5] C. Pfleiderer et al. *Science*, 2871:8330–8338, 2007.
[6] S. Mühlbauer et al. *Science*, 323:915, 2009.
[7] M. Janoschek et al. *Phys. Rev. B*, 81:214436, 2010.

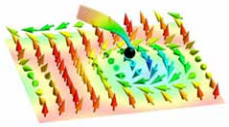

Parasitic small moment antiferromagnetism in the hidden order of URu_2Si_2

P. G. Niklowitz[1,2], C. Pfleiderer[1], T. Keller[3], M. Vojta[4], Y.-K. Huang[5], and J. A. Mydosh[6]

[1] *Physik Department E21, Technische Universität München, D-85748 Garching, Germany*
[2] *Department of Physics, Royal Holloway, University of London, Egham, United Kingdom*
[3] *Max-Planck-Institut für Festkörperforschung, Stuttgart, Germany*
[4] *Institut für Theoretische Physik, Universität zu Köln, D-50937 Köln, Germany*
[5] *Van der Waals-Zeeman Institute, University of Amsterdam, Amsterdam, The Netherlands*
[6] *Kamerlingh Onnes Laboratory, Leiden University, Leiden, The Netherlands*

We have used Larmor diffraction to establish that the small moment antiferromagnetism in the hidden order phase of the heavy-fermion superconductor URu_2Si_2 is parasitic. We also showed that the hidden order and the large moment antiferromagnetism, which emerges under pressure, must have a different symmetry. This makes an exotic origin of the hidden order, such as orbital currents, helicity order or multipolar order, most likely.

For over twenty years one of the most prominent unexplained properties of f-electron materials has been a phase transition of URu_2Si_2 at $T_0 \approx 17.5$ K into a state known as 'hidden order' (HO) [1]. The discovery of the HO was soon followed by the observation of a small, antiferromagnetic moment (SMAF), $m_s \approx 0.03\mu_B$ per U atom [2], long believed to be an intrinsic property of the HO. The discovery of large-moment antiferromagnetism (LMAF) with $m_s \approx 0.4\mu_B$ per U atom [3] under pressure, consequently prompted intense theoretical efforts to connect the LMAF with the SMAF and the HO. In particular, models have been proposed that are based on competing order parameters of the same symmetry and hence linearly coupled in a Landau theory; such models assume that the SMAF is intrinsic to the HO. This is contrasted by proposals for the HO parameter such as incommensurate orbital currents, multipolar order, or helicity order, where HO and LMAF break different symmetries.

Prior to our study, some neutron scattering studies of the temperature-pressure phase diagram suggested that the HO-LMAF phase boundary ended in a critical end point [4], while other studies concluded that it meets the boundaries of HO and LMAF in a bicritical point [5, 6, 7]. The lack of consistency is accompanied by considerable variations in the size and pressure dependence of the moment reported for the SMAF, whereas NMR and μ-SR studies suggested the SMAF to be parasitic [8]. It was therefore long suspected that the conflicting results are due to a distribution of lattice distortions arising from defects. Notably, uniaxial stress studies showed that LMAF is stabilized if the c/a ratio η of the tetragonal crystal is increased by the small amount $\Delta\eta/\eta \approx 5\times10^{-4}$ [9]. Hence, the SMAF may, in principle, result from a distribution of η across the sample, its magnitude being dependent on sample quality and experimental conditions.

For the first time, simultaneous measurements have been carried out of the lattice constants, the distribution of the lattice constants and the antiferromagnetic moment of URu_2Si_2 as a function of temperature, for pressures up to 18 kbar, employing Larmor and conventional diffraction [10]. Our measurements were carried out at the spectrometer TRISP at FRM II.

Larmor diffraction (LD) permits high-intensity measurements of lattice constants with an unprecedented high resolution of $\Delta a/a \approx 10^{-6}$, by encoding the lattice spacing in the Larmor phase of a polarized neutron beam. For more details see Ref. [11, 12].

The distribution of lattice constants may be inferred from the change of polarization as a function of the Larmor frequency. A quantitative analysis establishes that the distribution we observed experimentally accounts for the size of the SMAF in the same sample, which must be purely parasitic. In addition, we find a rather abrupt transition from HO to LMAF, which extends from $T = 0$ up to a bicritical point (Fig. 1). Our study demonstrates that the transition from HO to LMAF is intrinsically first order, i.e., the HO and LMAF must have different symmetry [10]. This supports exotic scenarios of the HO, such as incommensurate orbital currents, helicity order or multipolar order.

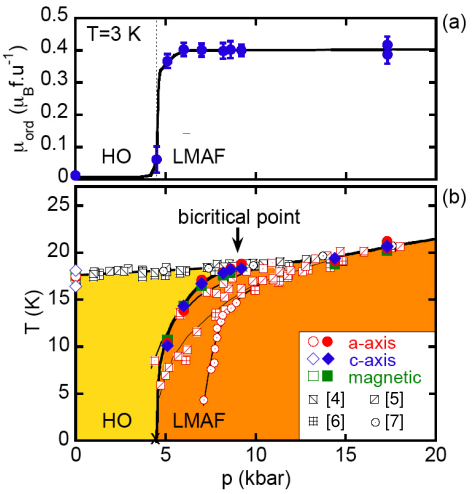

Figure 1: Key features and pressure versus temperature phase diagram of URu_2Si_2. (a) Pressure dependence of the low temperature magnetic moment m_s. (b) Phase diagram based on Larmor diffraction and conventional magnetic diffraction data. The onset of LMAF and HO in our data is marked by full and empty symbols, respectively (x marks a transition near base temperature). For better comparison data of T_N and T_0 from Refs. [4, 5, 6, 7] are shown, where red symbols refer to T_N and black symbols to T_0.

References

[1] T. T. M. Palstra et al. *Phys. Rev. Lett.*, 55:2727, 1985.
[2] V. P. Mineev et al. *Phys. Rev. B*, 72:014432, 2005.
[3] H. Amitsuka et al. *Phys. Rev. Lett.*, 83:5114, 1999.
[4] J. R. Jeffries et al. *J. Phys.: Cond. Matter*, 20:095225, 2008.
[5] S. Uemura et al. *J. Phys. Soc. Jpn.*, 74:2667, 2005.
[6] E. Hassinger et al. *Phys. Rev. B*, 77:115117, 2008.
[7] G. Motoyama et al. *J. Phys. Soc. Jpn.*, 77:123710, 2008.
[8] K. Matsuda et al. *J. Phys.: Cond. Matter*, 15:2363, 2003.
[9] M. Yokoyama et al. *Phys. Rev. B*, 72:214419, 2005.
[10] P. G. Niklowitz et al. *Phys. Rev. Lett.*, 104:106406, 2010.
[11] T. Rekveldt et al. *Eur. Phys. Lett.*, 54:342, 2001.
[12] T. Keller et al. *Appl. Phys. A*, 74:127, 2002.

Low energy μSR study of homogeneous ferromagnetism in (Ga,Mn)As

S. R. Dunsiger[1,2], J. P. Carlo[1], T. Goko[1,3], G. Nieuwenhuys[4], T. Prokscha[4], A. Suter[4], E. Morenzoni[4], D. Chiba[5,6], Y. Nishitani[6], T. Tanikawa[5,6], F. Matsukura[5,6], H. Ohno[5,6], J. Ohe[7,8], S. Maekawa[7,8], and Y. J. Uemura[1]

[1] *Department of Physics, Columbia University, New York, New York 10027, USA*
[2] *Physik Department E21, Technische Universität München, D-85748 Garching, Germany*
[3] *TRIUMF, 4004 Wesbrook Mall, Vancouver, British Columbia, V6T 2A3, Canada*
[4] *Paul Scherrer Institut, Laboratory for Muon Spin Spectroscopy, CH-5232 Villigen PSI, Switzerland*
[5] *ERATO Semiconductor Spintronics Project, Japan Science and Technology Agency, Sanban-cho 5, Chiyoda-ku, Tokyo 102-0075, Japan*
[6] *Laboratory for Nanoelectronics and Spintronics, Research Institute of Electrical Communication, Tohoku University, 2-1-1 Katahira, Sendai 980-8577, Japan*
[7] *Institute for Materials Research, Tohoku University, Sendai 332-0012, Japan*
[8] *CREST, Japan Science and Technology Agency (JST), Sanbancho, Tokyo 102-0075, Japan*

Ferromagnet-Semiconductor heterostructures show immense promise for device applications [1], in particular for the injection of polarised spins into a semiconducting substrate. More fundamentally, prototypical systems like the III-V semiconducting materials $Ga_{1-x}Mn_xAs$/GaAs exhibit unusual long range indirect exchange interactions mediated by charge carriers in the semiconductor host. This unusual interplay between magnetism and transport properties opens up the interesting and potentially technologically useful possibility of modulating magnetic behaviour by controlling the charge carrier properties and vice versa. Artificial heterostructures based on these ferromagnetic semiconductors may be produced in thin film form using non-equilibrium techniques such as molecular beam epitaxy [2]. Investigations using local probes which are sensitive to magnetic structure on a nanometre length scale are therefore invaluable.

We undertook measurements on the low-energy μSR beamline at the Paul Scherrer Institute (PSI). Using an incident momentum of 5 keV, muons were controllably implanted with an average depth of 30 nm and a spread (half-width at half-maximum) of 10 nm. μSR time spectra in a number of $Ga_{1-x}Mn_xAs$ films were obtained in a weak transverse field (WTF) of 100 G. A marked damping of the signals seen at $T = 5$ K is due to inhomogeneous quasistatic internal fields from ordered Mn moments. We also notice a long-lived component with slower relaxation persisting with a significantly reduced amplitude. It represents muons in a non- or paramagnetic environment. The amplitude of this signal is shown in Fig. 1. The background signal level is calibrated by means of WTF measurements on a thin ferromagnetic Ni plate having the same areal dimension as the (Ga,Mn)As films, which yields the estimate shown by the dashed line. The full signal from the non-/paramagnetic environment was calibrated by a dry run on a silver plate. Fig. 1 demonstrates that all of the films show transitions from a full paramagnetic volume to a nearly full volume of static magnetism, with a rather sharp onset.

The ferromagnetic exchange interaction between Mn moments was initially explained by a model with itinerant hole carriers in the valence band provided by Mn impurities, that is, the pd Zener model [3]. More recently, a picture with carriers in the Mn impurity band has been proposed on the basis of optical and other studies [4, 5]. For ferromagnetism in insulating films, recent theoretical proposals [6, 7] involve the hybridization of locally polarized valence band states and Mn impurity states where the Fermi level lies between the impurity bound states and the valence band. The present results demonstrate that homogeneous ferromagnetism develops smoothly across the metal-insulator transition point. The resistivity values of semiconducting $x = 0.03$ (ag) and metallic 0.034 (ag) films differ by more than a factor of 200 at $T = 2$ K, whereas their T_C values differ by only a factor of 1.5, and essentially identical responses are observed by μSR and magnetization. This feature implies that a sizable exchange interaction between Mn moments may be mediated by holes before they become fully itinerant, and that the existence of the metallic state is not a precondition for formation of a homogeneous ferromagnetic state.

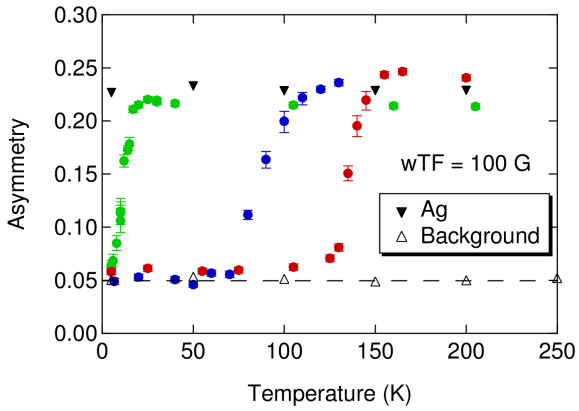

Figure 1: Muon precession asymmetry, representing muons in para- or non-magnetic environments, observed in a WTF of 100 G. Green symbols correspond to a $Ga_{1-x}Mn_xAs$ film with $x = 0.012$ (ag) ($T_C = 16$ K); blue symbols to a (Ga,Mn)As film with $x = 0.07$ (ag) ($T_C = 90$ K). The red symbols represent the behaviour of the $x = 0.07$ sample after annealing in air for 60 minutes at 240° C.

References

[1] I. Žutić, J. Fabian, and S. Das Sarma. *Rev. Mod. Phys.*, 76:323–410, 2004.
[2] H. Ohno. *Science*, 281:951–956, 1998.
[3] T. Dietl, H. Ohno nad F. Masukura, J. Cibert, and D. Ferrand. *Science*, 287:1019–1022, 2000.
[4] K. S. Burch, D. D. Awschalom, and D. N. Basov. *J. Magn. Magn. Mater.*, 320:3207–3228, 2008.
[5] K. S. Burch et al. *Phys. Rev. Lett.*, 97:087208, 2006.
[6] J. Ohe et al. *J. Phys. Soc. Jpn.*, 78:083703, 2009.
[7] N. Bulut, K. Tanikawa, S. Takahashi, and S. Maekawa. *Phys. Rev. B*, 76:045220, 2007.

Electrical transport properties of single-crystal $Nb_{1-y}Fe_{2+y}$

Max Hirschberger[1,2], William Duncan[3], Andreas Neubauer[2], Manuel Brando[4], Christian Pfleiderer[2], and Malte Grosche[1]

[1] *Cavendish Laboratory, University of Cambridge, Cambridge, UK*
[2] *Physik Department E21, Technische Universität München, D-85748 Garching, Germany*
[3] *Department of Physics, Royal Holloway, University of London, Egham, UK*
[4] *Max-Planck-Institute for Chemical Physics of Solids, Dresden, Germany*

The Laves phase system $Nb_{1-y}Fe_{2+y}$ displays a marginal Fermi liquid breakdown close to the critical composition $y = -0.015$ [1]. For $y > -0.015$, various bulk properties suggest the formation of hitherto unidentified electronic order at low temperatures akin a spin-density wave (SDW) state [2, 3]. Poly-crystalline feed rods of $Nb_{1-y}Fe_{2+y}$ were grown at Royal Holloway and consecutively used to obtain large single crystals by means of a bespoke image furnace [4] in Munich. The magnetic order in this system is highly sensitive to small changes in doping [5]. In the present study, we investigated a slightly niobium-rich sample at $y = -0.007$, a stoichiometric sample at $y = 0$ and three slightly iron-rich samples from the same crystal at $y = 0.006$.

Resistivity data down to 2 K was taken using a Quantum Design PPMS cryostat. A simple measurement setup has been mounted on a proprietary PPMS sample holder ("PUK"), shown in Fig. 1. The relative angle ϕ_{cH} between the magnetically easy c axis and the magnetic field H can be changed mechanically by turning a screw on the modified PUK. The angle ϕ_{cH} was obtained by evaluation of digital photographs. We estimate a systematic observational error of $\Delta\phi_{cH} \approx 3°$. Resistivity data has been taken using a four-point technique. A wide range of field orient

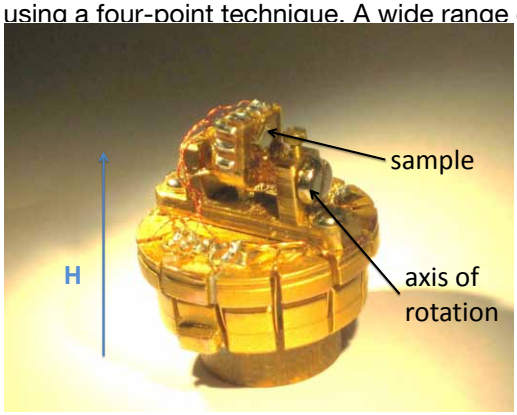

Figure 1: Measurement setup on Quantum Design PPMS PUK. The sample is fixed on a platform that can be rotated with respect to the applied magnetic field H. The sample resistivity $\rho(H)$ is measured using a four-point technique.

In all five samples, we observed a strong anisotropy of the magnetoresistance between fields along the magnetically easy c-axis and the magnetically hard ab-plane. In the slightly iron-rich samples ($y = 0.006$), a pronounced peak in $\rho(H)$ emerges for magnetic fields H perpendicular to the c-axis. The effect is constrained to a temperature range of 10 to 30 K. As an example, we show data for $T = 18$ K and various angles ϕ_{cH} in Fig. 2. The peak disappears quickly as H is turned out of the ab-plane. Moreover, hysteresis can be clearly observed at the low-field side of $\rho(H)$ when H is parallel to the a-axis. Temperature scans of the iron-rich sample (data not shown) reveal a rapid drop in resistivity around the critical temperature $T_c \approx 28$ K for $H \parallel a$. This behaviour could hint towards a first order transition at T_c.

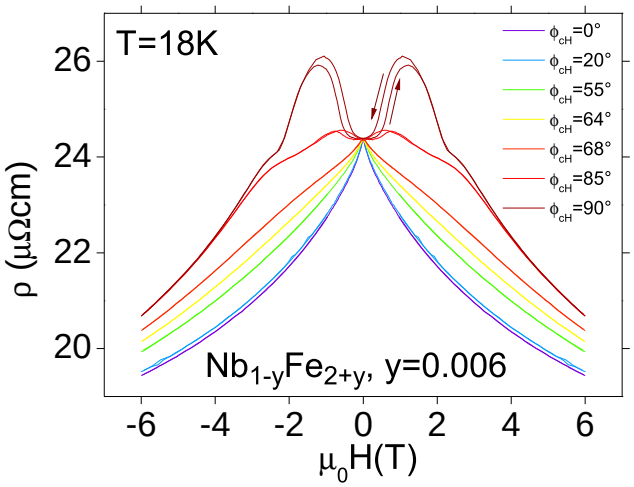

Figure 2: Iron-rich $Nb_{1-y}Fe_{2+y}$ ($y = 0.006$). We show resistivity in magnetic field $\rho(H)$ for fixed temperature $T = 18$ K at different angles ϕ_{cH} between H and the magnetically easy c-axis. The current density j was applied along the a-axis. The in-plane component of H was parallel to j for all these measurements. Data for $H > 0$ have been mirrored onto the negative half-plane.

As an alternative to a SDW scenario, we propose the strong anisotropy between the easy c-axis and hard ab-plane to be the signature of a putative, uniaxial Ising ferromagnet. A field H applied in the ab plane acts as a tuning parameter, suppressing the critical temperature of magnetic ordering. We believe that a peak in $\rho(H)$ at a fixed temperature can emerge if scattering from spin fluctuations is the dominant process contributing to ρ in this material. In this scenario, spin fluctuations would be particularly strong just before entering the ordered phase, leading to a distinct rise in ρ at that point. At high fields, spin fluctuations are suppressed, resulting in a negative magnetoresistance. If the field H is aligned parallel to the easy c-axis, the up-down Ising symmetry is broken, there cannot be a ferromagnetic phase at finite fields and in conclusion we do not observe a peak in $\rho(H)$.

As a next step, measurements of torque magnetisation on the samples mentioned above have been scheduled. This will allow us to map the magnetic anisotropies in this material and to test our hypothesis of a uniaxial Ising system.

References

[1] M. Brando et al. *Phys. Rev. Lett.*, 101:026401, 2008.
[2] Y. Yamada and A. Sakata. *J. Phys. Soc. Jpn.*, 57:46, 1988.
[3] M. R. Crook and R. Cywinski. *J. Magn. Magn. Mater.*, 140:71, 1995.
[4] A. Neubauer et al. *Rev. Sci. Instrum.*, 82:013902, 2011.
[5] D. Moroni-Klementowicz et al. *Phys. Rev. B*, 79:224410, 2009.

Neutron Depolarization Imaging of the Kondo system $CePd_xRh_{1-x}$

Philipp Schmakat[1], Michael Schulz[2], Peter Böni[1], Christian Pfleiderer[1], Manuel Brando[3], Christoph Geibel[3], Micha Deppe[3], Elbio Calzada[2], and Sergey Masalovich[2]

[1] *Physik Department E21, Technische Universität München, D-85748 Garching, Germany*
[2] *Forschungsneutronenquelle Heinz Maier-Leibnitz (FRM II), Technische Universität München, D-85748 Garching, Germany*
[3] *Max-Planck-Institut für Chemische Physik fester Stoffe, D-01187 Dresden, Germany*

Introduction

The heavy fermion compound $CePd_xRh_{1-x}$ undergoes a quantum phase transition as a function of Rh content x, where ferromagnetism is continuously suppressed for large x [1]. In the concentration-dependent magnetic phase diagram the curvature of the phase boundary at $T_C(x)$ changes sign at $x \approx 0.65$. For Rh concentrations $x > 0.70$ spin-glass behaviour has been reported, which may be the manifestation of a so-called Kondo-Cluster-Glass [2]. Metallurgical inhomogeneities and a random distribution of Kondo temperatures due to the statistical distribution of the Pd and Rh atoms result in cluster formation. For this range of concentrations the low temperature properties are dominated by a freezing transition of these clusters [3].

We have used Neutron Depolarisation Imaging (NDI) to explore the nature of the spin freezing in $CePd_xRh_{1-x}$. NDI was recently set up at the beam line ANTARES at FRM II [4]. The depolarization of a polarized neutron beam, transmitting the sample, is thereby analyzed. The beam is well collimated, as the instrument is built for radiography. A CCD camera in combination with a LiF/ZnS converter and scintillator film is used as the detector. This permits to spatially resolve the polarization across the entire sample.

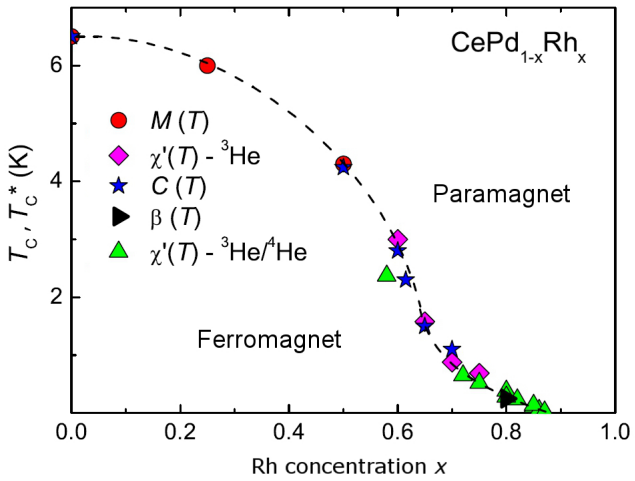

Figure 1: Temperature versus concentration phase diagram of the Kondo lattice system $CePd_xRh_{1-x}$ as a function of Rh content x. When ferromagnetism is suppressed continuously a Kondo screened state emerges. The curvature of the phase boundary changes sign at $x \approx 0.65$. After Ref. [3].

For studies of samples with elevated Rh concentration and thus a transition temperature in the milli-Kelvin range we combined the NDI technique with the standard pulse tube cryostats of the sample environment group at FRM II. This allowed measurements at temperatures down to 370 mK and 75 mK using a ^{3}He insert and a ^{3}He/^{4}He dilution insert, respectively.

A bespoke pair of Helmholtz coils surrounding the cryostat at the sample position allowed us to apply small fields up to 22.5 mT.

Experimental Results

Typical NDI data are shown in Fig. 2 of samples with a Rh concentration $x = 0.40$ and $x = 0.60$, respectively. The T_C maps were derived from temperature scans in a small magnetic field of $B = 7.5$ mT. The maps show the distribution of the magnetic ordering temperature over the sample. The color coding in the histogram below each map represents the corresponding transition temperature. As can be seen from the histograms, the distribution of transition temperatures of the sample with $x = 0.60$ is wider than the distribution measured in the sample with $x = 0.40$. This may be a signature of the increasing disorder introduced by the chemical substitution.

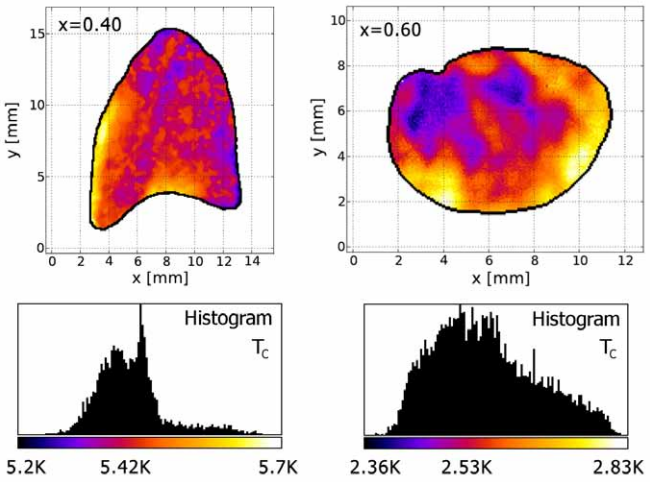

Figure 2: The T_C maps of $CePd_xRh_{1-x}$ for $x = 0.40$ and $x = 0.60$. The color coding in the corresponding histogram below each map represents the T_C distribution over the sample.

NDI measurements on zero-field-cooled (zfc) as well as field-cooled (fc) samples under field-heating (fh) underscore the role of applied magnetic fields. Fig. 3 shows typical depolarisation data from zfc-fh and fc-fh measurements on three $CePd_xRh_{1-x}$ samples with Rh concentrations $x = 0.40$, $x = 0.60$ and $x = 0.65$, respectively.

The sample with $x = 0.40$ shows the typical behaviour expected of a ferromagnet. The depolarisation sets in at the transition temperature and remains strong for $T \rightarrow 0$. Measurements on the sample with $x = 0.60$ suggest a freezing transition of the magnetic moments under zero-field-cooling. When a small magnetic field of 7.5 mT is applied after zero-field-cooling the depolarization remains nearly constant. Increasing the temperature

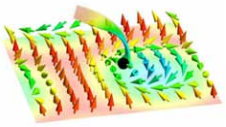

restores the long-range ferromagnetic order in the sample and leads to a stronger depolarisation. Evidence for an intermediate state may be seen for concentrations $x \geq 0.65$ where the depolarisation vanishes after zero-field-cooling and does not change if a small external field is applied. With increasing temperature the ferromagnetic behaviour is reentrant in a finite temperature interval. At the slightly higher transition temperature the paramagnetic phase is reached.

Fig. 4 shows typical depolarisation curves measured for the same three samples, but with different magnetic field histories. The samples were heated and thereby measured in the same magnetic field as they were cooled down. Data were recorded for three different field strengths of B = 7.5 mT, B = 15.0 mT and B = 22.5 mT. For comparison zero-field data are shown for each sample.

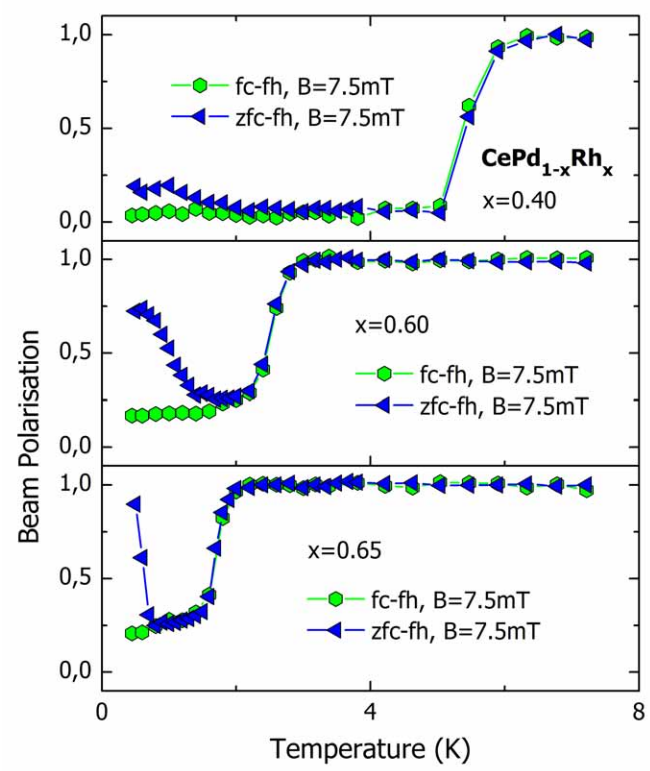

Figure 3: Typical depolarisation curves extracted from both zfc-fh and fc-fh data recorded in $CePd_xRh_{1-x}$ with Rh concentrations x = 0.40, x = 0.60 and x = 0.65, respectively. The signature of the cluster-glass formation is associated with the onset of the splitting of the curves.

As expected from the zfc-fh measurements, the external magnetic field leads only to a small enhancement of the depolarisation of the sample with x = 0.40. The onset of the competition of the long-range and short-range order can be seen in the sample with x = 0.60. The small field of 7.5 mT can enhance the depolarisation remarkably. The sample with x = 0.65 shows a vanishing depolarisation after zero-field-cooling. This means that the long-range order is nearly suppressed, but can be induced by the external magnetic field.

Discussion

For a Rh concentration x = 0.40 we find a clear ferromagnetic transition in the depolarisation curves. The formation of short-range order at intermediate Rh concentrations may be associated with the onset of the splitting of the depolarisation curves which is reminiscent of spin-glass behaviour in the magnetisation. Disorder in this concentration range leads to a distribution of Kondo temperatures which results in cluster formation. These clusters emerge in a surrounding of Kondo screened moments, thereby interacting through RKKY interactions. This results in frustration and random freezing of the clusters at low temperatures.

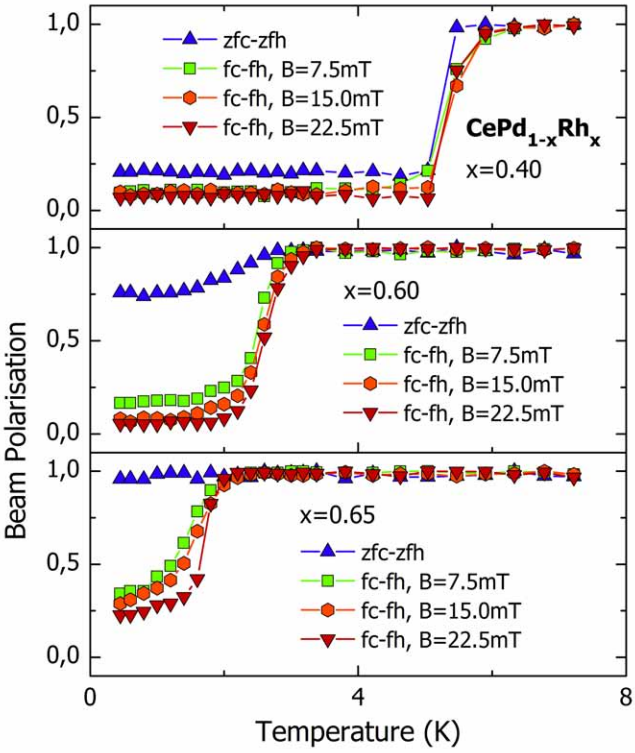

Figure 4: Comparison of zfc-fh and fc-fh data of the $CePd_xRh_{1-x}$ with Rh concentrations x = 0.40, x = 0.60 and x = 0.65 under applied magnetic fields of B = 7.5mT, B = 15.0mT and B = 22.5mT, respectively.

A small external magnetic field enhances the long-range magnetic correlations in this concentration regime. For Rh concentrations $x > 0.65$ short-range order should dominate, since the depolarisation after zero-field-cooling vanishes completely. Further measurements on samples with higher Rh concentrations will need to confirm these considerations.

Support from the German Science Foundation under FOR960 (Quantum Phase Transitions) and from the collaborative research network TRR80 (From Electronic Correlations to Functionality) is gratefully acknowledged.

References

[1] J. G. Sereni, T. Westerkamp, R. Küchler, N. Caroca-Canales, P. Gegenwart, and C. Geibel. Ferromagnetic quantum criticality in the alloy $CePd_{1-x}$ Rh_x. *Phys. Rev. B*, 75:024432, 2007.

[2] T. Westerkamp, M. Deppe, R. Küchler, M. Brando, C. Geibel, P. Gegenwart, A. P. Pikul, and F. Steglich. Kondo-Cluster-Glass State near a Ferromagnetic Quantum Phase Transition. *Phys. Rev. Lett.*, 102:206404, 2009.

[3] T. Westerkamp. *Quantenphasenübergänge in den Schwere-Fermionen-Systemen $Yb(Rh_{1-x}M_x)_2Si_2$ und $CePd_{1-x}Rh_x$*. PhD thesis, Technische Universität Dresden, 2009.

[4] M. Schulz. *Radiography with polarized neutrons*. PhD thesis, Technische Universität München, 2010.

Optical float-zoning growth of Cu_2MnAl single crystals

Andreas Neubauer[1], Florian Jonietz[1], Martin Meven[2], Robert Georgii[2], Georg Brandl[1,2], Günter Behr[3], Peter Böni[1], and Christian Pfleiderer[1]

[1] *Physik Department E21, Technische Universität München, D-85748 Garching, Germany*
[2] *Forschungsneutronenquelle Heinz Maier-Leibnitz (FRM II), Technische Universität München, D-85748 Garching, Germany*
[3] *IFW Dresden, PF 270116, D-01171, Dresden, Germany*

Polarized neutrons are indispensable for numerous techniques to study the magnetic properties of solids [1]. Examples are the examination of the handedness of chiral magnetic order [2] or, as a new method, neutron depolarization radiography, which may be used to investigate non-destructively the magnetic distributions in materials [3]. The growing importance of polarized neutron scattering underlines the need for methods that produce and analyze polarized neutrons with a high accuracy and efficiency.

The Heusler compound Cu_2MnAl is a prominent example of a material used for monochromators, where the (111) Bragg reflection is typically used to generate a beam of polarized neutrons [4]. The main challenge in the preparation of monochromators for polarized neutron scattering from Cu_2MnAl Heusler crystals lies in the growth of large and homogeneous crystals with a well defined mosaic spread. Previous studies established that crystals prepared by the Bridgman technique are characterized by very large anisotropies of the mosaic distribution depending on the growth direction [5].

We carried out single crystal growth of Cu_2MnAl with the optical floating zone method. Altogether eight single crystals were grown, two in a vertical double ellipsoid image furnace (URN-2-ZM, MPEI, Moscow) at the IFW in Dresden and six in a refurbished high-purity four-mirror image furnace [6] in Munich. The high-purity conditions at TUM were found to promote stable growth conditions, resulting in a mono-crystalline structure throughout the entire cross-section of the rods.

For these crystals growth rates of 10-12 mm/h were used, except for OFZ10, where the rate was increased from 5 mm/h to 10 mm/h during the growth. The feed and seed rods were counter-rotating at 10 rpm and 30 rpm, respectively. Prior to each growth the image furnace was carefully baked out (10^{-8} mbar) and filled with 6N argon gas, that was additionally purified with a getter furnace. Each growth took place in a static argon atmosphere of $p \sim 1.5$ bar.

The investigation of the mosaic spread of four large single crystalline samples cut from OFZ3, OFZ5, OFZ6 and OFZ10 was carried out at the single crystal diffractometer HEIDI at FRM II. For each crystal rocking scans with respect to the {400} and {111} lattice planes were carried out. For OFZ10 the {333} lattice planes were studied. An overview of the Bragg scattering intensities as a function of the rocking angle ϕ is shown in Fig. 1. The width of the rocking curves, presented in terms of the full-width-half-maximum (FWHM) in Table 1, provides information on the isotropy of the mosaic spread. The FWHM values were obtained directly by means of the measurement software at HEIDI through extrapolation of the measured intensities.

OFZ3 (a, b), OFZ5 (c, d), and OFZ6 (e, f) show highly homogeneous rocking curves for all {400} and {111} reflections, characteristic of an isotropic mosaic spread. In contrast, different behavior is found for OFZ10 (g, h) where two intensity maxima are observed. This signature is most likely due to the change of growth velocity. This sensitivity of the mosaic distribution to variations of the growth rate might be advantageous, if varied in a more moderate way, for the preparation of optimized monochromator crystals with a mosaic spread between 0.5° and 1°.

In summary we showed that optical float zoning growth leads to an isotropic distribution of the mosaic spread of Cu_2MnAl single crystals, hence avoiding the main drawback of the Bridgman technique. The high purity conditions of the image furnace at TUM were found to be indispensable to promote stable growth conditions. Investigations of the polarizing properties indicate a high polarization efficiency of float-zoned Cu_2MnAl crystals [7]. For technical applications as monochromator crystals, however, the size of the float-zoned crystals has to be increased.

FWHM \ Crystal	OFZ3	OFZ5	OFZ6	OFZ10
(400)	0.31°	0.25°	0.49°	0.52°
(040)	0.34°	0.26°	0.42°	0.33°
(004)	0.27°	0.28°	0.27°	1.28°
(111) (333) for	0.41°	0.41°	0.43°	0.74°
$(\bar{1}11)$ OFZ10	0.39°	0.41°	0.53°	0.72°
$(1\bar{1}1)$	0.42°	0.41°	0.46°	0.65°
$(11\bar{1})$	0.42°	0.43°	0.73°	0.26°

Table 1: Summary of the Bragg diffraction FWHM values of the Cu_2MnAl crystals measured at HEIDI.

References

[1] W. G. Williams. *Polarized Neutrons*. Clarendon Press, Oxford, New York, 1988.
[2] Y. Ishikawa, Y. Noda, Y. J. Uemura, C. F. Majkrzak, and G. Shirane. Paramagnetic spin fluctuations in the weak itinerant-electron ferromagnet MnSi. *Phys. Rev. B*, 31:5884, 1985.
[3] M. Schulz, P. Böni, E. Calzada, M. Mühlbauer, A. Neubauer, and B. Schillinger. A polarizing neutron periscope for neutron imaging. *Nucl. Instrum. and Methods in Physics A*, 605:43, 2009.
[4] A. Delapalme, J. Schweizer, G. Couderchon, and R. Perrier de la Bathie. Étude de l'alliage de Heusler (Cu_2MnAl) comme monochromateur de neutrons polarisés. *Nucl. Instrum. and Methods*, 95:589, 1971.
[5] P. Courtois. Characterization of Heusler crystals for polarized neutrons monochromators. *Physica B: Cond. Matter*, 267-268:363, 1999.
[6] A. Neubauer, J. Bœuf, A. Bauer, B. Russ, H. v. Löhneysen, and C. Pfleiderer. Ultra-high vacuum compatible image furnace. *Rev. of Sci. Instr.*, 82:013902, 2011.
[7] A. Neubauer. PhD thesis, Technische Universtität München, 2011.

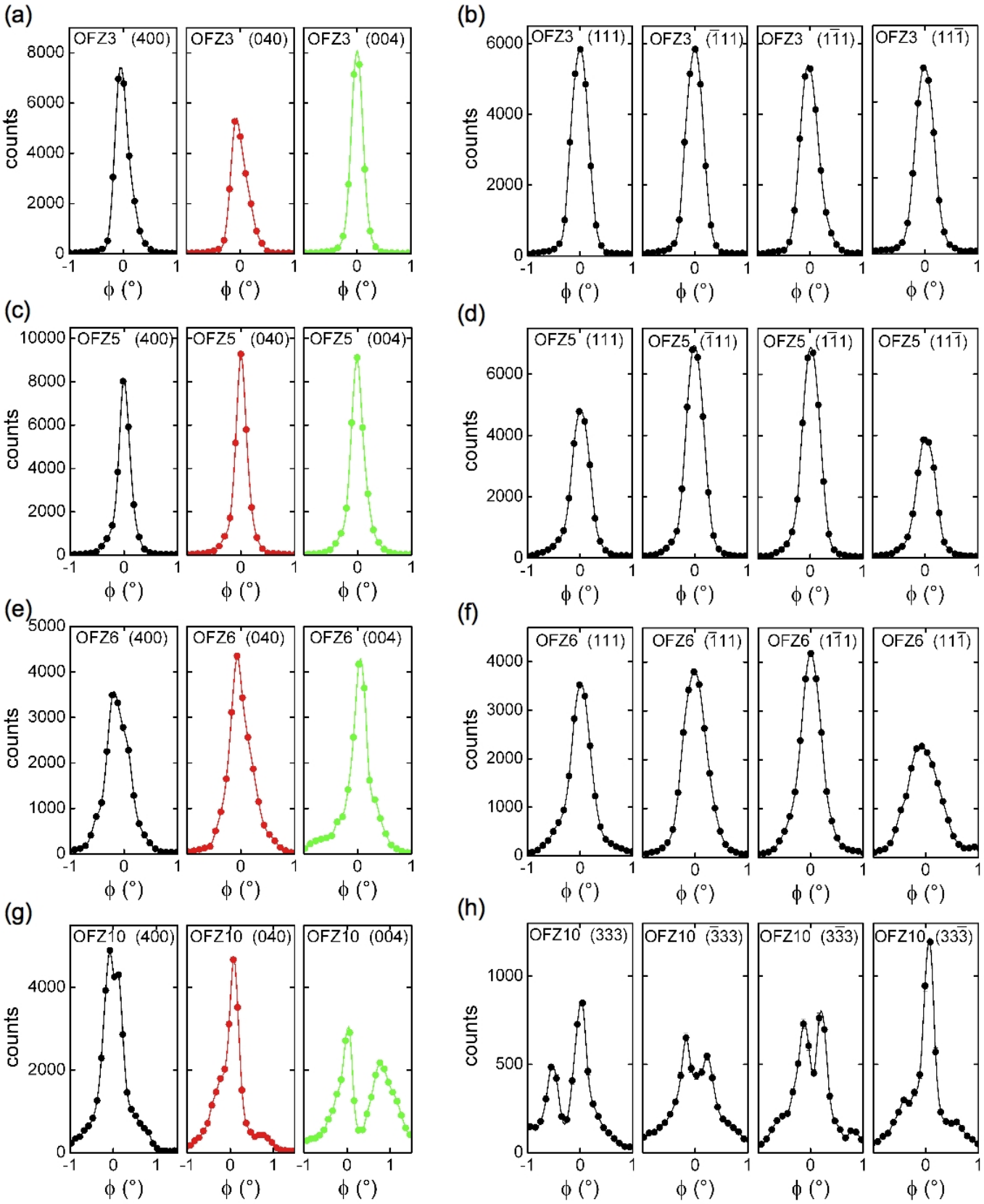

Figure 1: Overview of the {400} and {111} Bragg reflection intensities as a function of the rocking angle ϕ. Cu_2MnAl crystals OFZ3 (a, b) and OFZ5 (c, d) show highly homogeneous rocking curves for all {400} and {111} planes. For OFZ6 (e, f) the curves are slightly broadened. The inhomogeneous peak structure of crystal OFZ10 (g, h) is most likely due to a change of the growth rate during crystal growth. The instrumental resolution of the FWHM is $\pm 0.1°$.

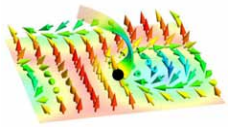

Chapter 2

Nuclear and Fundamental Physics

Transmission measurements of guides for ultra cold neutrons using UCN capture activation analysis of vanadium

A. Frei[1], K. Schreckenbach[1], B. Franke[1], J. Hartmann[1], T. Huber[1], R. Picker[1], S. Paul[1], and P. Geltenbort[2]

[1] Physik Department E18/E21, Technische Universität München, D-85748 Garching, Germany
[2] Institut Laue-Langevin, F-38042 Grenoble, France

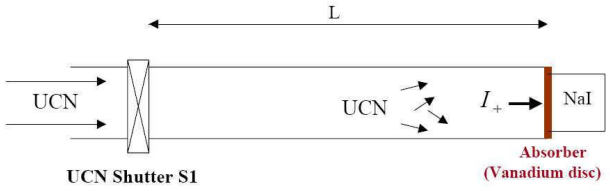

Figure 1: Scheme of the UCN current measurement for the determination of the transmission of UCN guides of length L. The UCN beam spectrum was shaped before entering the beam line.

The transport of ultra cold neutrons (UCN) in guides from the source to the experimental site is a major issue for the planned UCN beam port at the FRM II with a distance of 40 m from the source. We have developed a novel method for UCN transmission measurement [1]. At the PN2 TES beam at the ILL [2] the UCN were absorbed at the end of the guide in a vanadium plate. At a vanadium surface UCN reflection is small due to the Fermi potential of -7 neV. The UCN absorption produces a beta unstable nucleus ^{52}V with a half live of 3.74 min and a 1434 keV gamma ray following the beta decay. It was measured by a NaI detector system. UCN guides (66 mm diameter) of the repliqua type from PNPI and from S-DH Heidelberg were investigated and the UCN loss per meter was measured by varying the guide length (up to 2 m). By an absolute calibration of the gamma detection system we deduced also the absolute value of the UCN current absorbed in the vanadium plate.

Fig. 2 shows schematically the built up of the activity in the vanadium disc. For the background measurement the valve S1 was kept closed. The result for the transmission was $95.6 \pm 0.6\%$ per m for the PNPI guide and $96.4 \pm 0.6\%$ per m for the Heidelberg guide, but the guides were not gap free. The NaI detector set-up yields 4.7(2)% efficiency as calibrated later at the FRM II in a comparative measurement with an HPGe detector of the health physics group.

In conclusion we have developed a technique for measuring reliably the UCN current at the end of an UCN guide and have determined the transmission of repliqua type UCN guides. For a guide of a diameter as planned for the FRM II UCN line (120–160 mm diameter) and avoiding UCN leakages from gaps, a transmission for a 40 m guide of the order of 50% may be achieved. The presented activation method is well suited for a limited application of UCN detection cases, where an accumulated detection of the UCN ensemble is adequate and may be used also off-line.

Acknowledgements

Supported by the DFG cluster of excellence 'Origin and structure of the universe'. The authors acknowledge the technical support by the ILL. We are thankful to S. Wolff from the FRM II for the comparative HPGe measurements in the absolute calibration of the NaI detector.

References

[1] A. Frei, K. Schreckenbach, B. Franke, J. Hartman, T. Huber, R. Picker, S. Paul, and P. Geltenbort. *Nucl. Inst. Meth. A*, 612:349, 2010.
[2] A. Steyerl et al. *Phys. Lett. A*, 116:347, 1986.

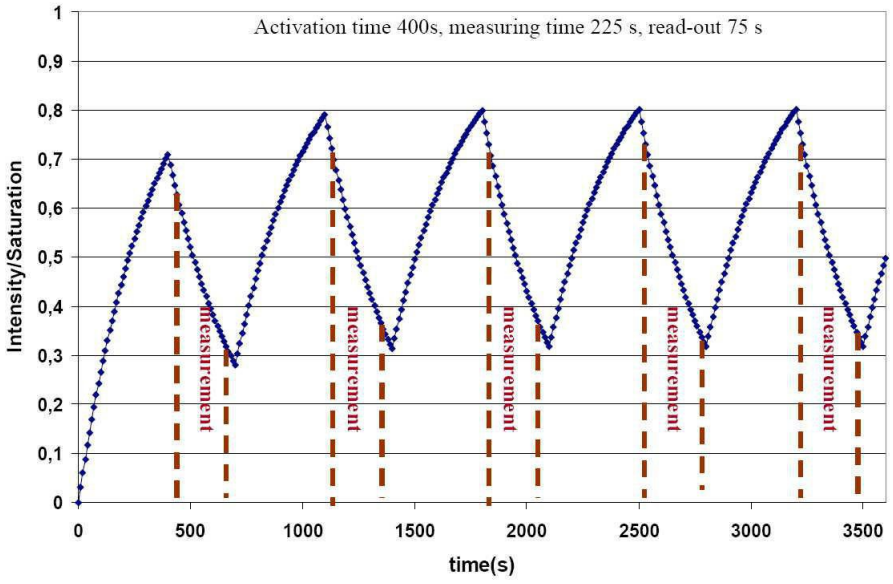

Figure 2: Alternate activation and decay measurement with the vanadium UCN beam absorber. The number of ^{52}V is given in units of saturation. The time slabs for the measurement of the 1434 keV gamma line are indicated.

Neutron lifetime measurement with the UCN trap-in-trap MAMBO II

A. Pichlmaier[1], V. Varlamov[3], K. Schreckenbach[1], and P. Geltenbort[2]

[1] *Physik Department E21, Technische Universität München, D-85748 Garching, Germany*
[2] *Institut Laue-Langevin, F-38042 Grenoble, France*
[3] *Petersburg Nuclear Physics Institute, Gatchina, Russia*

We have measured the free neutron lifetime τ_n by storage of ultra-cold neutrons (UCN) in a Fomblin coated UCN trap of in-situ variable size. The method was initially developed by W. Mampe et al. with MAMBO I and improved by the addition of a prestorage volume yielding a well defined UCN spectrum for storage in the main trap. By extrapolation to infinite trap size using the time scaling method we obtain for the free neutron lifetime = (880.7 $\pm$ 1.3 $\pm$ 1.2) s. Data from different UCN spectra, trap temperatures and storage times were used for the evaluation. The present result is compared with other experimental neutron lifetime data [1].

The beta decay of the free neutron is of importance as fundamental semileptonic weak interaction decay. The constants g_A and g_V and the CKM matrix element V_{ud} can be deduced from the neutron decay alone and used as sensitive tests of the Standard Model. τ_n is of relevance in astrophysics and cosmology. It enters as a parameter in the primordial element formation. The cross section for the pp-cycle in stars is proportional to g_A^2 of the neutron apart from strong interaction corrections and the cross section of antineutrinos with protons is inversely proportional to τ_n.

In recent years τ_n measurements converged to 885.7(0.8) s adapted by the PDG in 2008 [2]. But the recent experiment by Serebrov et al. with (878.5 $\pm$ 0.7 $\pm$ 0.3) s [3] is far off the world average and was even not yet considered for the average by PDG 2008, which claimed for that reason the present world average value as 'suspect'; see also the recent review on τ_n measurements by S. Paul [4]. The experimental approach MAMBO II (MAMpe BOttle) is the successor of MAMBO I, which was a break-through in precision for UCN storage experiments. Based on their experience Mampe et al. started the concept and design of MAMBO II. The early death of W. Mampe prevented him from carrying out the experiment, but his ideas were the essential prerequisite for the present work.

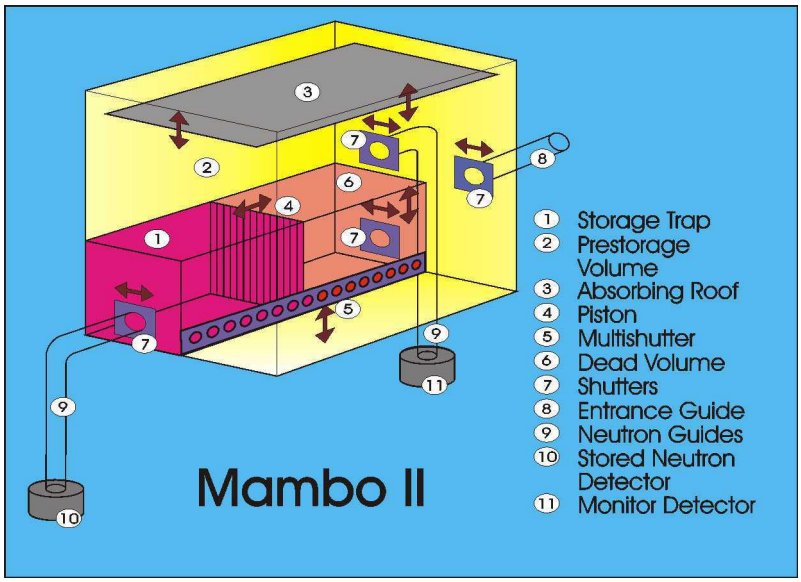

Figure 1: Schematic view of MAMBO II. The storage walls are covered with UCN reflecting fomblin oil. The prestorage volume shapes the UCN spectrum by gravity and absorbing roof. The storage trap length can be change in-situ moving the piston. The free neutron lifetime is derived from a proper extrapolation of the storage time to infinite size of the storage trap.

In comparison to other τ_n measurements the present MAMBO II value lies below the PDG 2008 average by 2.5σ and above the result [3] by 1.1σ. The full set of τ_n data scatters significantly more than by their uncertainty allowed and lead to an average of 881.8 (1.4) s, where the error is scaled up by a factor of 2.7 according to the PDG rules.

Acknowledgements

Supported by DFG 375 and by the DFG Cluster of Excellence 'Origin and Structure of the Universe'. We appreciate very much the contribution of M. Pendlebury to the concept of MAMBO II and the idea of the scaling method, of F. Schorr to the realization of the set-up and of V. Nesvizhevsky on error assessments. We thank S. Neumaier, I. Krasnoshekova and A. P. Serebrov for fruitful discussions and for excellent technical support at the TU Munich and ILL Grenoble, especially by Th. Brenner, H. Just, H. Nagel and F.-X. Schreiber.

References

[1] A. Pichlmaier, V. Varlamov, K. Schreckenbach, and P. Geltenbort. *Phys. Lett. B*, 693:221, 2010.
[2] C. Amsler et al., Particle Data group. *Phys. Lett. B*, 667:1, 2008.
[3] A. P. Serebrov et al. *Phys. Rev. C*, 78:035505, 2008.
[4] S. Paul. *Nucl. Inst. Meth. A*, 611:157, 2009.

Bremsstrahlung information for the non-destructive characterization of radioactive waste packages

Benjamin Rohrmoser[1]

[1] *Zentrale Techn.-Wiss. Betriebseinheit Radiochemie München RCM, Technische Universität München, D-85748 Garching, Germany*

Non-destructive techniques are the preferred methods for the characterization of radioactive waste packages. Compared to destructive methods it minimizes the radiation dose for the personal, the secondary radioactive waste production, and is less time consuming. In routine gamma-spectroscopy, applied successfully over decades, identification and quantification of gamma-emitting nuclides is practiced. This method does not consider any information on beta-emitting nuclides embedded in the waste matrix. But there is the phenomenon of charged particle radiation called Bremsstrahlung, which may be detected in gamma scans, too. This possibility of an identification of beta-emitters is not considered in data evaluation at present. A feasibility study shall investigate, if the identification of beta-emitters in the gamma-spectra via their Bremsstrahlung is possible. First experiments have been started at laboratory dimensions. The first experiment consisted of three measurements with a HPGe detector. As sample ^{60}Co, ^{133}Ba, ^{137}Cs, and ^{241}Am calibration standards were used as gamma-emitters and a ^{170}Tm sample, produced at FRM II, as a Bremsstrahlung emitting nuclide. The selection of the latter was based on [1]. First, the spectrum of ^{170}Tm only was recorded. Then only the gamma emitters ^{60}Co, ^{133}Ba, ^{137}Cs, and ^{241}Am were recorded. For the third measurement all samples were measured together. Fig. 1 shows the results as well as the difference of the third to the second measurement resulting in the same distribution as the measurement of only ^{170}Tm.

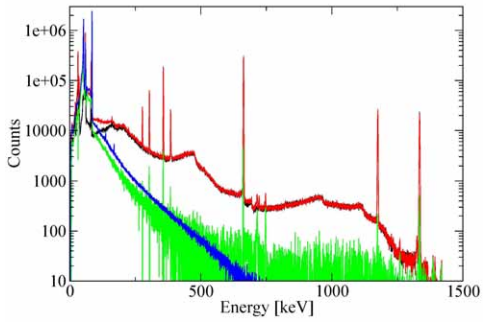

Figure 1: Black: Spectrum of ^{60}Co, ^{133}Ba, ^{137}Cs, ^{241}Am; Red: Spectrum of ^{60}Co, ^{133}Ba, ^{137}Cs, ^{241}Am and ^{170}Tm; Blue: Spectrum of ^{170}Tm (identical to the difference of the red and black spectra (Green)).

As a first result, it was demonstrated that in this simple set-up the extraction of the Bremsstrahlung-part from different gamma-emitters is possible, simply by subtracting the spectra. In a second experiment with ^{170}Tm-samples of different activities the limits of the method were investigated, i.e. the minimum activity of the beta-emitter required for definite identification in dependence of the activities of the gamma-emitters being present. This value is defined as beta-to-gamma ratio. Fig. 2 shows the spectra of ^{60}Co ($3.0 \cdot 10^4$ Bq) and ^{60}Co together with ^{170}Tm ($5.7 \cdot 10^7$ Bq).

In the spectrum of ^{60}Co and ^{170}Tm shoulders on the right hand side of the characteristic gamma-peaks of ^{60}Co at 1173.3 and 1332.5 keV are noticeable, not being present in the spectrum of only ^{60}Co. The only explanation is a contribution by ^{170}Tm having an endpoint energy of about 970 keV. This becomes clear in Fig. 2, which also shows the difference of the two measured spectra. Up to about 700 keV the characteristics of the pure ^{170}Tm is visible. Between 1100 keV and 1500 keV also summation effects take place, as well known in pure gamma-spectroscopy [2]. The peaks at 1257 keV and 1418 keV, respectively, are the results of the summations of the two cobalt peaks with the only thulium peak at 84.3 keV. In Fig. 2, the pure ^{170}Tm spectrum is added to the right side of the 1173.3 keV ^{60}Co peak for better illustration. It indicates the trend of the ^{170}Tm spectrum between 60–200 keV, thus reflecting the summation effect. These shoulders might be used for the determination of Bremsstrahlung-emitters in the future. In this case the beta-to-gamma-ratio has an extremely high value of about 2000.

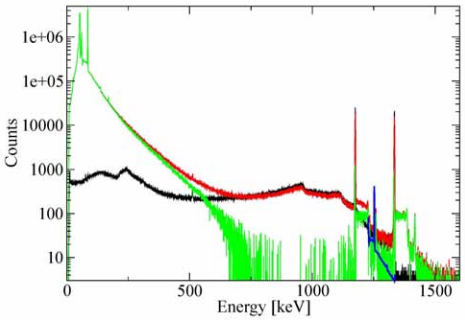

Figure 2: Black: ^{60}Co spectrum, Red: spectrum of ^{60}Co with ^{170}Tm. Green: Difference-spectrum of ^{60}Co and ^{170}T measured together minus the ^{60}Co only spectrum. Blue: The energy range from 60–200 keV of the ^{170}Tm spectrum is added to the right side of the 1173.3 keV ^{60}Co peak for better illustration.

The experiment was repeated with ^{170}Tm ($2.8 \cdot 10^6$ Bq) and ^{137}Cs ($2.3 \cdot 10^5$ Bq). Here the beta-to-gamma- ratio is only about 12. Converted with the use of the their decay constants, the number of cesium-atoms was seven times bigger than the number of thulium-atoms. The problem here is, that the 661.7 keV Cs-peak occurs within the region of the Tm-spectrum. However the same effect as discussed above for ^{60}Co is still distinguishable, although less distinctive. The appearance of these summation effects may simplify the search for beta-emitters in radioactive waste matrices. Additional experiments as well as computer simulations will be performed to demonstrate the applicability of this method in practice. Special focus will be given on the influence of absorbing matrices surrounding the gamma- and beta-emitters.

References

[1] A. S. Dhaliwal and S. Amarjit. *Nucl. Inst. Meth. B*, 198:32–36, 2002.

[2] G. Gilmore and J. Hemingway. *Practical Gamma-ray Spectroscopy*. John Wiley and Sons, 1995.

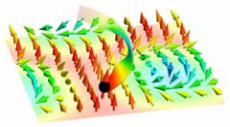

Chapter 3

Positron Physics

Determination of core annihilation probabilities with PAES

Jakob Mayer[1,2], **Christoph Hugenschmidt**[2], **and Klaus Schreckenbach**[1,2]

[1] *Physik Department E21, Technische Universität München, D-85748 Garching, Germany*
[2] *Forschungsneutronenquelle Heinz Maier-Leibnitz (FRM II), Technische Universität München, D-85748 Garching, Germany*

Introduction

Positron annihilation induced **A**uger **E**lectron **S**pectroscopy (PAES) is a very surface sensitive, non destructive analysis method. Up to now data acquisition times of several days were typical, but the high intense positron source NEPOMUC at the FRM II allows now measurements within less than one hour. Hence, it is for the first time possible to observe dynamic processes at the surface with PAES. Routinely the measurement of PAES-spectra of pure metals is now possible. This offers a new approach to measure the core annihilation probability of different elements.

Principle of PAES

Electron induced Auger Electron Spectroscopy (EAES) is a widely used method in solid state physics to characterize the chemical composition of surfaces. Though EAES is accepted as a surface sensitive method it probes not only the topmost atomic layer, but -depending on the kinetic energy of the Auger electron- up to five atomic layers. Furthermore, since the energy of the incoming electrons must be chosen very high (at least 1keV), the incident beam might damage slightly bound molecules at the surface. Positron annihilation induced Auger Electron Spectroscopy (PAES), in contrast, uses low energy positrons (20 eV) since the primary hole, necessary for the Auger process, is produced via electron-positron annihilation instead of impact ionization. Thus, the secondary electron background ends at 20eV, and no secondary electron background is detected in the range of the Auger peaks. Due to the short thermalization times of a few ps and the long lifetime of positrons in bulk materials of several hundred ps the positron can diffuse back to the surface, where it is trapped in the attractive surface potential. Hence, the majority of the detected Auger electrons stem from the topmost atomic layer [1]. With the high intense positron beam NEPOMUC at the FRM II PAES reached for the first time acquisition times which are comparable with conventional EAES.

Measurements and results

In the following, the results of the measurement of clean metals (Fe, Ni, Cu, Zn, Pd, and Au) are presented. The determination of the intensities of different Auger transitions give a possibility to determine the core annihilation probabilities. Only a few, reasonable assumptions are made. First, the primary positron flux at the sample position is considered to be constant. Hence, the time normalized spectra can be compared directly. Secondly, the different positron reflexion, which increases with higher nuclear charge, is not taken into account.

With this assumptions it is possible to plot the intensities of each Auger transition versus the binding energy of the respective electron level. This is a measure for the so called core annihilation probability p.

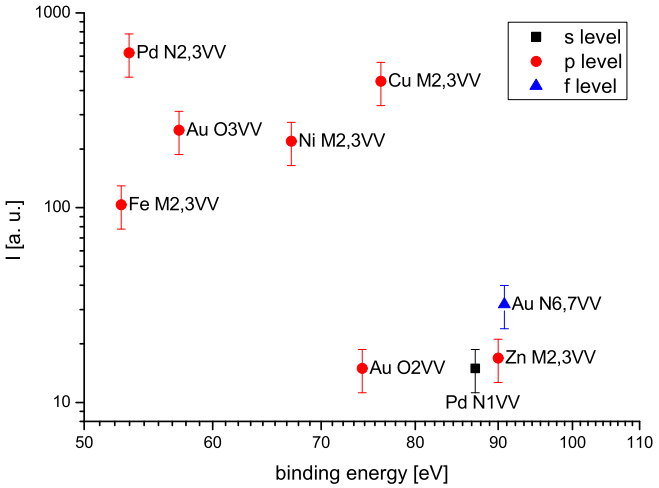

Figure 1: Relative Auger intensities as a function of the binding energy of the annihilated electron [2].

The data in Fig. 1 clearly shows a negative slope with higher Auger intensities for lower binding energies. A comparison of the experimental data with the theoretical formula for p, $p = 600 \cdot N(E_B) \cdot E_B^{-1.6}$ [1] shows considerable qualitative correlation. In the formula p is the core annihilation probability in %, E_B is the binding energy in eV and $N(E_B)$ is the number of electrons with E_B. Though such a plot is not a direct measurement of the core annihilation probability, it is at least possible to test the theory for the determination of the core annihilation probability.

Outlook

In the next measurement periods it is planned to install a sample manipulator with controllable temperature (100–1000 K) in order to influence the processes at the surface, e.g. diffusion of thin metallic films into the bulk and adsorption/desorption of gases.

References

[1] P. Coleman, editor. *Positron Beams and their applications*. World Scientific Publishing Co. Pte. Ltd., 2000.

[2] C. Hugenschmidt, J. Mayer, and K. Schreckenbach. High-resolution Auger-electron spectroscopy induced by positron annihilation on Fe, Ni, Cu, Zn, Pd, and Au. *J. Phys.: Conf. Series*, 225:012015, 2010.

Measurement of the Ps^- Decay Rate

Hubert Ceeh[1], Klaus Schreckenbach[1], Stefan Gärtner[3], and Christoph Hugenschmidt[1,2]

[1] *Physik Department E21, Technische Universität München, D-85748 Garching, Germany*
[2] *Forschungsneutronenquelle Heinz Maier-Leibnitz (FRM II), Technische Universität München, D-85748 Garching, Germany*
[3] *Fakultät für Physik, Ludwig-Maximilians-Universität, D-85748 Garching, Germany*

Ps^- is a bound system consisting of two electrons and a positron. Its three constituents are point-like and stable leptonic particles with the same mass, which are only subject to the electro-weak and the gravitational force. Hence Ps^- represents an ideal object to study the quantum-mechanics of three-body systems. Using a time-of-flight method we performed several high-yield lifetime measurements at the NEPOMUC facility, in order to critically test recent relativistic calculations of the decay rate.

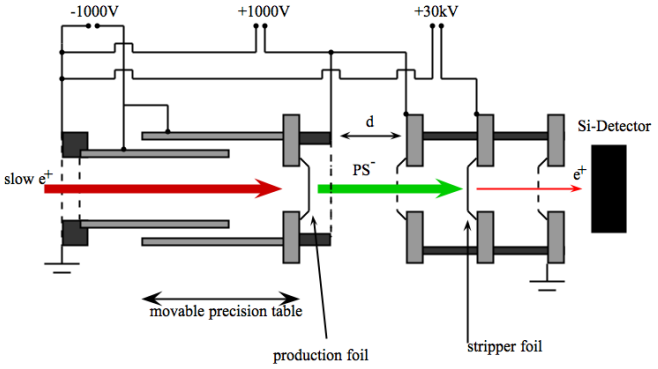

Figure 1: Schematic of the setup used for production and detection of Ps^-.

Experimental Setup

We applied a beam-foil-technique to produce Ps^-. Therefore a positron beam with an energy of 800–1200 eV is directed onto a DLC-foil (Diamond-like Carbon). The positron subsequently picks up two electrons to create Ps^-. After the first electron is captured the emerging positronium can acquire an additional electron by inelastic scattering with a carbon atom. This is possible if the impact energy is insufficient to ionize the carbon atom but suffices to lift one of the outer shell electrons into the bound state of Ps^-. The produced Ps^- ions are accelerated by an electric field between the production foil and a fine meshed grid to energies of 1000–4000 eV. Passing the acceleration grid the Ps^- ions enter the field-free decay volume which is terminated by an second fine meshed grid. The distance between this two grids and therefore the time-of-flight can be adjusted by a high precision linear positioning stage. The surviving Ps^- ions are accelerated towards a second DLC-foil, to which a voltage of +30 kV is applied. When the Ps^- ions impinge the foil, the two electrons are stripped off and the remaining positron is again accelerated towards a grounded grid. At the exit of this tandem-accelerator-like setup the positrons have an energy of 40 keV and are guided towards a silicon particle detector. In order to increase the signal-to-noise-ratio a chicane is mounted in front of the detector, which can only be passed by positrons with the right energy of 40 keV. Secondary electrons an ions are deflected and cannot reach the detector. The Ps^- vacuum decay rate can hence be calculated from the measured decay constant.

Results

The results of a previous measurement of the Ps^- decay rate Γ performed by Frank Fleischer in Heidelberg were confirmed within the error bounds. In two days of beam time at the NEPOMUC facility we were able to measure the decay rate with an accuracy of 1.1% [1] to:

$$\Gamma = 2.083(23)\,\mathrm{ns}^{-1}$$

This value is in good agreement with the theoretical value [2] of $\Gamma_{Th} = 2.087963(12)\,\mathrm{ns}^{-1}$ as well with the value obtained in Heidelberg [3] $\Gamma_{Exp} = 2.089(15)\,\mathrm{ns}^{-1}$. However, the measurement in Heidelberg took over three month to reach this precision, since a laboratory positron source was used. This can now be achieved within two days using the current production setup and the high intensity positron beam provided by NEPOMUC.

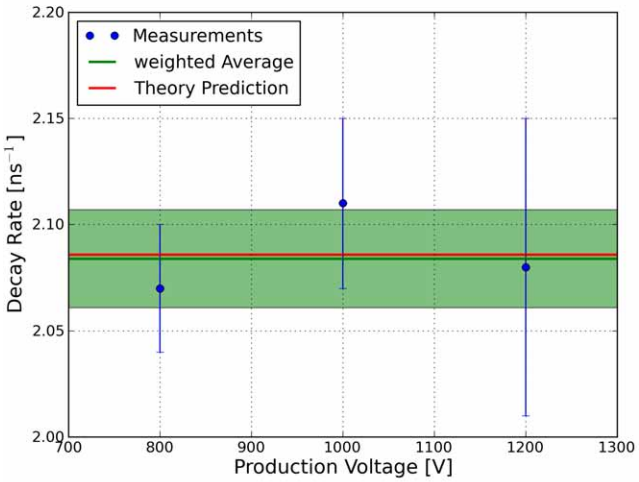

Figure 2: Decay rate Γ obtained for three different production voltages. The theoretical prediction is also shown for comparison.

Outlook

The limit for the accuracy of the decay rate, that can be achieved with this setup in a reasonable beam time of $\approx$ 2 weeks is of the order of 0.2%. This will allow first tests of the lowest order QED contributions to the decay rate, which are of the order of 0.3%.

References

[1] H. Ceeh. Produktion und Lebensdauermessung des negativ geladenen Positroniumions. Diploma thesis, Technische Universität München, 2009.
[2] M. Puchalski and A. Czarnecki. *Phys. Rev. Lett.*, 99:203401, 2007.
[3] F. Fleischer et al. *Phys. Rev. Lett.*, 96:063401, 2006.

Positron Experiments at NEPOMUC

Christoph Hugenschmidt[1,2], Günther Dollinger[3], Hubert Ceeh[1,2], Werner Egger[3], Gottfried Kögel[3], Elisabeth Lachner[1], Benjamin Löwe[2,3], Jakob Mayer[1,2], Philip Pikart[1,2], Christian Piochacz[1,2], Markus Reiner[1], Florin Repper[2], Peter Sperr[3], Alexander Wolf[2], and Klaus Schreckenbach[1,2]

[1] *Physik Department E21, Technische Universität München, D-85748 Garching, Germany*
[2] *Forschungsneutronenquelle Heinz Maier-Leibnitz (FRM II), Technische Universität München, D-85748 Garching, Germany*
[3] *Inst. für Angewandte Physik und Messtechnik (LRT2), Universität der Bundeswehr München, D-85577 Neubiberg, Germany*

The positron beam facility NEPOMUC at FRM II provides the world highest intensity of a mono-energetic positron beam of $(9.0 \pm 0.8) \cdot 10^8$ moderated positrons per second. The energy of the positrons, which are extracted from the in-pile positron source, amounts to 1 keV. Outside the biological shield, the beam brilliance is improved by a positron remoderation unit, which is operated with an W(100) single crystal in back reflexion geometry. The intensity was determined to $(5.0 \pm 1.0) \cdot 10^7$ remoderated positrons per second, and the beam diameter amounts to < 2 mm (FWHM) in a longitudinal magnetic guide field of 5 mT.

The energy of the remoderated positron beam was set to 20 eV for all experiments. The beam properties are adapted to the respective experimental requirements such as magnetic or/and electrostatic beam guidance, pulsing mode, and additional acceleration to the desired kinetic energy.

The main beam characteristics are summarized in table 1.

Instrument	e+ Energy [keV]	Beam Transport	Beam Mode
PLEPS	1 .. 18	magnetic	pulsed, 50MHz, 100-150ps
SPM	0.2 .. 25 (planned)	magnetic/electr.	pulsed, 50MHz, 100-150ps
CDBS	0.2 .. 30	electrostatic	dc
PAES	0.02	electrostatic	dc
Open Port	0.02	magnetic	dc
Positronium-Ion	0.1 .. 5	magnetic	dc

Table 1: Main beam characteristics of positron instruments

An overview of the present status of the NEPOMUC beam facility with the five different instruments is shown in Fig. 1. In the following, the instruments are briefly presented, and recent experimental results are exemplarily given.

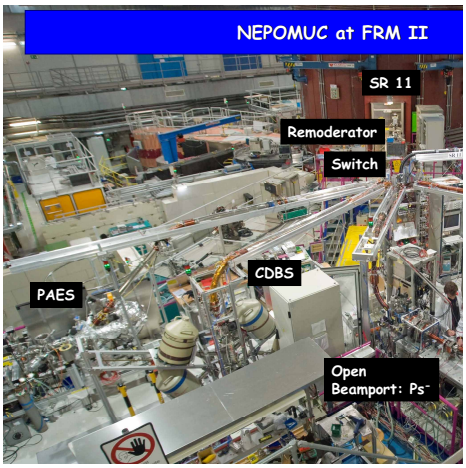

Figure 1: The positron beam facility NEPOMUC at FRM II.

PLEPS - Pulsed Low-Energy Positron System

The positron lifetime in matter is correlated to the size and concentration of lattice defects such as mono-vacancies or vacancy clusters or to the free volume in polymers. For this reason, PLEPS is a unique instrument for positron lifetime measurements near the surface or for layered samples by using the mono-energetic positron beam at NEPOMUC. In 2009, features of the lifetime spectrometer such as the lateral stability of the beam in the whole energy range (0.2–18 keV) were further improved. PLEPS, which was developed at the UniBW, delivers now a pulsed beam with a time resolution of 260 ps, a repetition rate of 50 MHz, and a high peak-to-background ratio of typically $2 \cdot 10^4$. In addition, a first AMOC (Age-MOmentum-Correlation) measurement was performed where the lifetime and the electron momentum was detected in coincidence.

SPM - Scanning Positron Microscope

It is planned to transfer the SPM from the UniBW to NEPOMUC. For this reason, an SPM-interface was installed with an additional remoderation unit for brightness enhancement. Furthermore, a new pulsing set-up with a chopper and two bunching units was developed and taken in operation for the first time. [1]

CDBS - Coincident Doppler Broadening Spectrometer

The CDBS can be operated in two modes: Conventional DBS (Doppler Broadening Spectroscopy) by using Ge-detectors independently and CDBS, where pairs of Ge-detectors are used in coincidence in order to suppress the background effectively. DBS is applied for depth dependent (up to a few µm) and spatially resolved (300 µm) defect spectroscopy. It is applied for the investigation of interfaces of layered samples, defects after mechanical or thermal load, and irradiation induced

defects in specimens. As an example Fig. 2 shows a 2D-scan of am asymmetrically and plastically deformed Al sample. [2] Due to the extremely low background, annihilation events with high Doppler-shifts, and hence high electron momenta, can be detected with CDBS. Since CDBS allows to study the chemical surrounding of the positron annihilation site nano-scopic precipitates, metal-vacancy complexes and embedded metallic layers are examined.

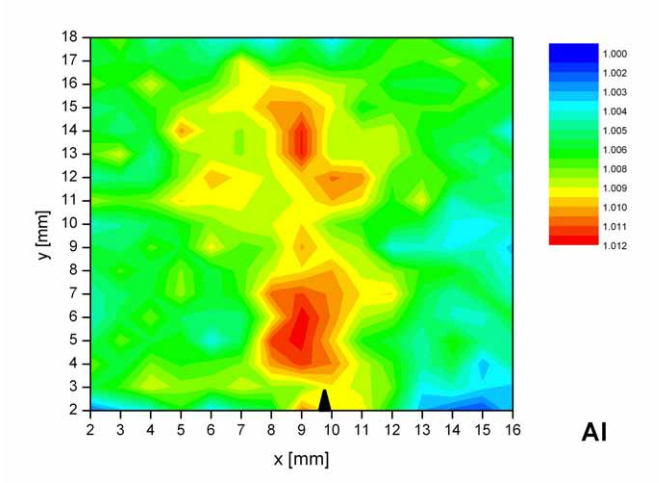

Figure 2: Asymmetrical deformed Al-sample with a notch after tensile test: The 2D S-parameter scan with a step width of 1 mm clearly indicates regions of large density of dislocations and vacancy-lie defects in front of the micro-crack. [2]

PAES - Positron annihilation induced Auger Electron Spectrometer

In contrast to conventional electron induced AES, PEAS has several advantages such as extreme surface sensitivity and superior signal-to-noise ratio. Hence PAES is particularly suited as a non-destructive and element selective surface technique.

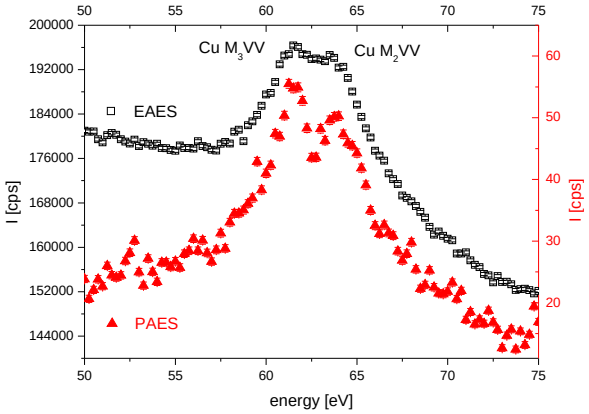

Figure 3: High-resolution PAES on Cu: The double-peak structure of the $Cu_{2,3}MVV$ Auger transition is clearly observable. EAES for comparison (open symbols).

Within the last reactor cycle, we succeeded to obtain PAES spectra in the systems Cu/Pd and Cu/Fe within exceptional short measurement times ($<$ 1 h). Due to the high positron intensity available at NEPOMUC, PAES with 20 eV positrons enables the observation of segregation and alloying at surfaces, and the measurement of Auger transition with high energy resolution ($\approx 0.5\,eV$) [3]. As an example, a high-resolution spectrum of the $Cu_{2,3}MVV$ Auger transition is shown in Fig. 3.

Open Beam Port: Production of Ps^-

The open multi-purpose beamport is dedicated to various experimental set-ups, which can be connected to the positron beamline. During 2009 this experimental position was mainly used for the production of the negatively charged positronium ion Ps^-. This experiment was performed in collaboration of the positron group at TUM with the Max-Planck institute for nuclear physics at Heidelberg and the physics department of the LMU. At NEPOMUC, we succeeded to reproduce the value for the Ps^- decay rate with an statistical error of 1.1 % within 2 days: $\Gamma = 2.083(33)\,ns^{-1}$. [4] During the next beam time, the statistics will be further improved by a factor of 4 within about 5 days of measurement time compared to the Heidelberg experiment with a duration of 3 months.

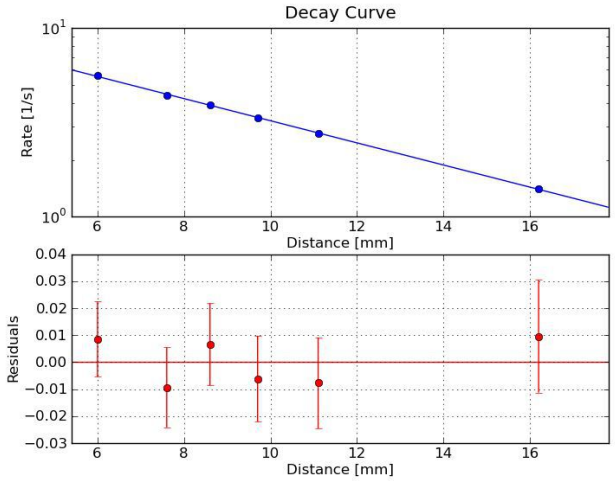

Figure 4: In-flight decay of Ps^-: Surviving Ps^- as function of the flight distance. [4]

References

[1] C. Piochacz. *Generation of a high-brightness pulsed positron beam for the Munich scanning positron microscope*. PhD thesis, Technische Universität München, 2009.

[2] C. Hugenschmidt, N. Qi, M. Stadlbauer, and K. Schreckenbach. Correlation of the mechanical stress and the Doppler-broadening of the positron annihilation line in Al and Al alloys. *Phys. Rev. B*, 80:224203, 2009.

[3] C. Hugenschmidt, J. Mayer, and K. Schreckenbach. High-resolution Auger-Electron Spectroscopy Induced by Positron Annihilation on Fe, Ni, Cu, Zn, Pd, and Au. *J. Phys.: Conf. Series*, 225:012105, 2010.

[4] H. Ceeh. Produktion und Lebensdauermessung des negativ geladenen Positroniumions. Diploma thesis, Technische Universität München, 2009.

Direct Observation of the Surface Segregation of Cu in Pd by Time-Resolved Positron-Annihilation-Induced Auger Electron Spectroscopy

Christoph Hugenschmidt[1,2], **Jakob Mayer**[1,2], **and Klaus Schreckenbach**[1,2]

[1] *Physik Department E21, Technische Universität München, D-85748 Garching, Germany*
[2] *Forschungsneutronenquelle Heinz Maier-Leibnitz (FRM II), Technische Universität München, D-85748 Garching, Germany*

Pure Pd and Pd-based alloys are important materials, e.g., for hydrogen storage, hydrogen purification, and heterogeneous catalysis. In particular, in Cu-Pd alloys the amount of Cu atoms and their exact position strongly affect the mechanical stability and the catalytic properties of Pd membranes. Density functional theory calculations for Cu-Pd alloys predict the segregation of Cu in the second atomic layer of Pd [1], but the available experimental data for this system are still poor and the experiments done so far do not unambiguously confirm the theory. In the presented experiment we investigate the stability and dynamics of thin Cu layers on the Pd surface. In our approach, we use the extremely surface sensitive and elemental selective analysis method of positron-annihilation-induced Auger electron spectroscopy (PAES) for the direct measurement of the surface segregation. In contrast to electron-induced Auger electron spectroscopy (EAES), which was applied as well, PAES intrinsically analyzes the topmost atomic layer of a sample almost exclusively. In addition to the high surface sensitivity that arises from the efficient trapping of the positrons in a delocalized surface state, one benefits from the positron affinity which makes PAES a highly elemental selective technique.

Up to now, the time for a single PAES measurement amounted to several days, and hence it was not possible to investigate dynamic surface processes. We cope with this challenge by using the PAES spectrometer [2] at the high intensity neutron-induced positron source Munich (NEPOMUC) which delivers $9 \cdot 10^8$ monoenergetic positrons per second. Additionally, the experimental setup was improved in order to enable time dependent PAES and hence to monitor the dynamic behavior of Cu atoms on a Pd surface for the first time. Two samples were prepared with different Cu covers on Pd: 2.88 monolayers (ML) Cu on Pd and 5.77 ML Cu on Pd. The measured fractions of the Auger intensities from Cu and Pd, respectively, as a function of time are shown in Fig. 1.

The exponential intensity profile for both Cu-covered Pd samples is attributed to the migration of Cu atoms from the surface into the second atomic layer of Pd. Alternative interpretations such as surface contamination are dismissed since an increase of the Auger fraction of Pd at the expense of the Cu intensity is observed. Bulk diffusion is also excluded since it would lead to a vanishing Cu intensity, which is in contrast to the measured saturation values for both samples. Also, surface diffusion is ruled out because it would require time scales of several minutes, which is well below the observed value of 1.38 h. A more detailed presentation can be found in [3]. Hence, the observed increase of the Pd Auger intensities at the expense of the Cu intensities until reaching a saturation value is attributed to the segregation of Cu in Pd. The reason for this segregation is that the most stable configuration for Cu is in the second atomic layer of Pd in thermodynamical equilibrium. This is supported by the calculated segregation energy of 6 kJ/mol according to 63 meV per Cu atom [1].

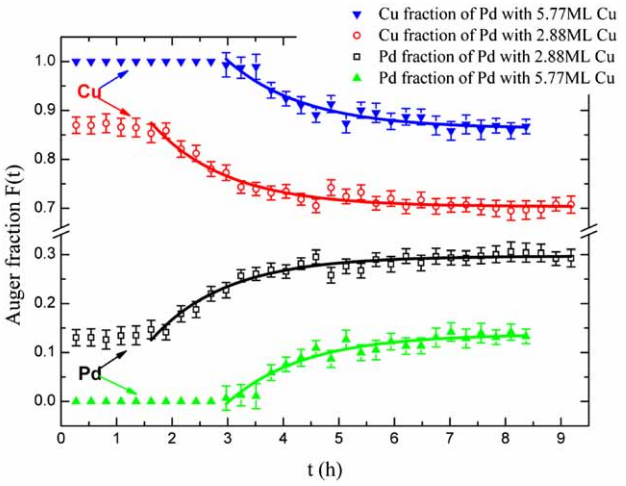

Figure 1: Fraction of the Auger intensities from Cu and Pd, respectively, as a function of time for two different Cu initial covers on Pd: 2.88 ML Cu on Pd and 5.77 ML Cu on Pd. In both cases a similar time dependency is observed due to the segregation of Cu in the second atomic layer of Pd. The exponential fit (solid lines) reveals the time constant of segregation of τ = 1.38(0.21) h [3].

We succeeded to record PAES spectra of Cu and Pd with the unprecedented short measurement time of only seven minutes. Thus, it was possible to observe directly the segregation of Cu in the second atomic layer of Pd by time-dependent PAES. The theoretically predicted result of the stable final configuration was confirmed experimentally. Moreover, the migration process itself was observed with a characteristic time constant of τ = 1.38(0.21) h. Time-dependent PAES enables the investigation of elemental selective dynamic processes such as heterogeneous catalysis, surface alloying, or corrosion processes of numerous systems with unprecedented measurement times and extremely high surface sensitivity.

References

[1] O. M. Lovvik. Surface segregation in palladium based alloys from density-functional calculations. *Surface Science*, 583:100–106, 2005.

[2] J. Mayer. *High energy resolution and first time-dependent positron annihilation induced Auger electron spectroscopy*. PhD thesis, Technische Universität München, 2010.

[3] J. Mayer, C. Hugenschmidt, and K. Schreckenbach. Direct observation of the surface segregation of Cu in Pd by time-resolved positron-annihilation-induced Auger electron spectroscopy. *Phys. Rev. Lett.*, 105(20):207401, 2010.

First Measurements at the SPM Interface

Christian Piochacz[1,2] and Gottfried Kögel[3]

[1] *Physik Department E21, Technische Universität München, D-85748 Garching, Germany*
[2] *Forschungsneutronenquelle Heinz Maier-Leibnitz (FRM II), Technische Universität München, D-85748 Garching, Germany*
[3] *Inst. für Angewandte Physik und Messtechnik (LRT2), Universität der Bundeswehr München, D-85577 Neubiberg, Germany*

For decades the positron has been used as a very sensitive micro probe for defect spectroscopy. One of the most meaningful observable is the positron lifetime, which is measured by the Munich Scanning Positron Microscope (SPM). Today, the SPM is operated by a ^{22}Na source from which a beam with a diameter of about 2 mm is created. To be able to measure also short positron lifetimes of about 100 ps the positron beam is pulsed by several bunching units. The re-moderation technique is used to reduce the phase volume occupied by the initial beam and hence enabling positron microscopy. Thus and by varying the implantation energy between 0.5 and 20 keV the measurement of 3D defect maps with a lateral resolution of about 1 µm is possible. Because of the low intensity of the ^{22}Na source the measurement of a lifetime map lasts several weeks and therefore comprehensive examinations are impeded.

At the FRM II the positron beam facility NEPOMUC provides the world most intense slow positron beam with up to $9 \times 10^8 \frac{e^+}{s}$ and hence more than three orders of magnitude higher intensity than available at the SPM laboratory beam. On the other hand, the phase space volume occupied by the NEPOMUC beam is about four orders of magnitude larger than in the laboratory. Hence, the NEPOMUC beam has to be prepared for the usage with the SPM by a special interface (see Fig. 1) [1].

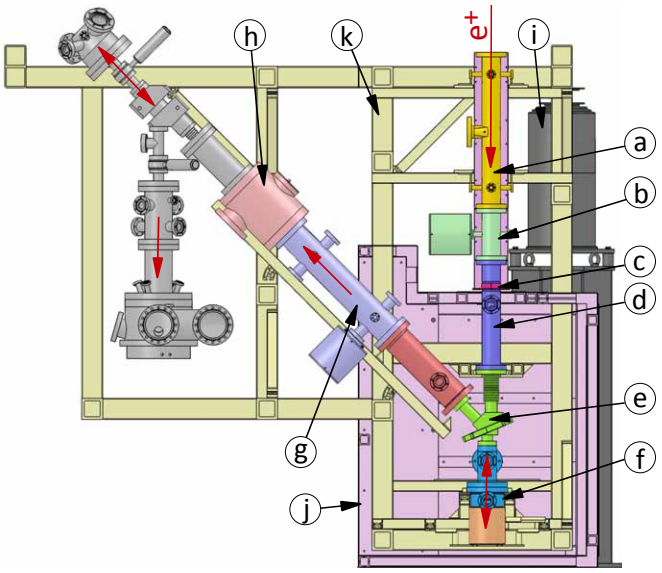

Figure 1: Overview of the SPM and the SPM interface: a) pre-buncher b) 1. sine buncher c) magnetic field termination d) static accelerator e) beam switch f) re-moderator g) 2. sine buncher / chopper h) ac accelerator i) vibration damping j) magnetic shielding k) rack construction. Parts of the last optical column of the SPM are shown in gray (without magnetic shielding).

This interface consists of newly developed pulsing components, which convert the continuous NEPOMUC beam highly efficient into a pulsed beam with a repetition rate of 50 MHz. An additional positron re-moderator enhances the phase space density of the beam in order to be compatible with the SPM. This re-moderator is also incorporated into the pulsing concept and allows an aberration free pulsing and hence pulses below 50 ps.

For the first time all pulsing components and the re-moderation stage of the SPM interface were operated successfully together. Due to the combination of a sawtooth buncher (a) and a sine wave buncher (b) the intensity in the time peak is 14 times higher than in the same time frame of the dc beam (see Fig. 2). All bunching units (a,b,d) operated together with the chopper (e), which is used to reduce the background between the time peaks, compress more than 56 % of the continuous beam into the final peaks. The peak to background ratio reached more than 260:1 already in the first measurements without an optimized setup.

Due to the installation of the pulsing components and the re-moderator the beam is now prepared for the subsequent ac acceleration and the SPM. The successful measurements demonstrated the high efficiency not only of the bunchers, but also of the beam transport and the re-moderator. They showed that by implementing the SPM at the NEPOMUC source high resolved lifetime maps can be measured within only one day.

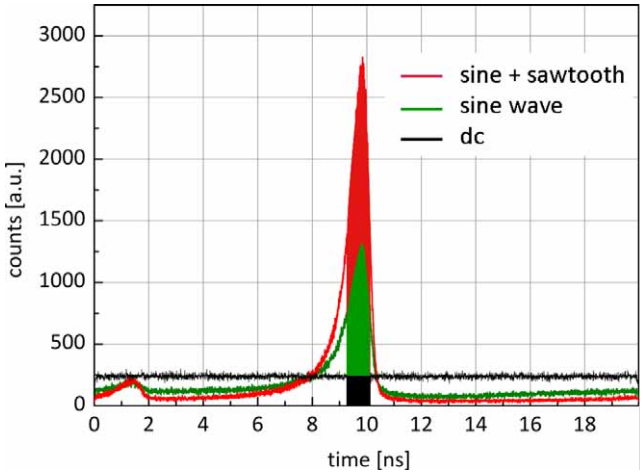

Figure 2: Intensity enhancement due to the combination of a high efficient sawtooth pre-buncher and high amplitude sine wave buncher.

References

[1] C. Piochacz, W. Egger, C. Hugenschmidt, G. Kögel, K. Schreckenbach, P. Sperr, and G. Dollinger. Implementation of the Munich scanning positron microscope at the positron source NEPOMUC. *physica status solidi (c)*, 4(10):4028–4031, 2007.

High sensitive analysis of metallic layers using a positron beam

Philip Pikart[1,2], **Christoph Hugenschmidt**[1,2], **and Klaus Schreckenbach**[1,2]

[1] *Physik Department E21, Technische Universität München, D-85748 Garching, Germany*
[2] *Forschungsneutronenquelle Heinz Maier-Leibnitz (FRM II), Technische Universität München, D-85748 Garching, Germany*

Positron annihilation spectroscopy is widely used as a non-destructive technique in material science due to its high sensitivity for lattice defects in the volume of the sample. Furthermore embedded layers and clusters of very low concentration can be detected with positrons too. For this type of measurement, the element-dependent positron affinity is essential to be known because it greatly affects the technique's sensitivity for different substances. When a positron is implanted into the sample, it diffuses before annihilation. During the diffusion process it can be trapped at attractive locations, and the annihilation radiation carries a signature of the chemical composition of the trapping site. To analyze annihilation events with highly shifted gamma signature, a coincident setup of two high-purity Germanium detectors is required.

Sample Setup

In the sample volume, regions of higher positron affinity form a potential well and can trap the diffusing positron. Hence, the trapping efficiency for clusters of a high affinity is greatly enhanced [1]. For a systematic study on this effect layers of different elements of various thickness were grown on an aluminum substrate and covered by an aluminum layer of constant thickness.

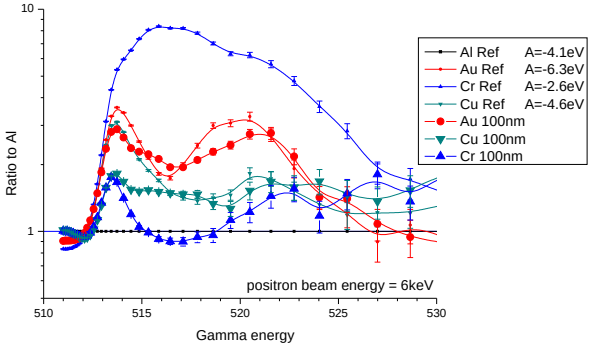

Figure 1: Coincident Doppler spectra of reference materials (thick lines) and layered samples with 100 nm intermediate films (thin lines). All curves are normalized to the aluminum reference.

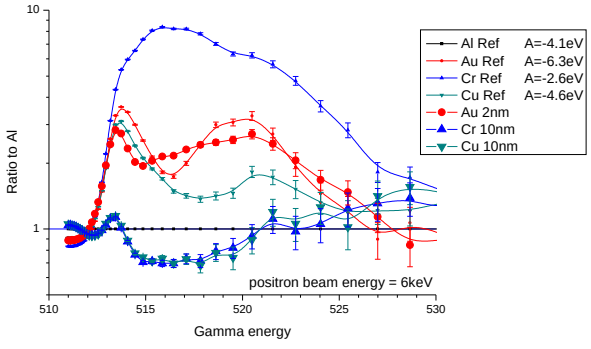

Figure 2: The same as Fig. 1 with thin intermediate layers.

CDB measurements

In the layered samples, it is of interest if the positron is trapped and annihilates in the intermediate layer or in the aluminum substrate. Therefore, reference data of the used elements have been recorded with annealed samples of high purity ($>$ 99.99%). The obtained data are normalized to the spectrum of the aluminum reference which is shown as a baseline in the resulting spectrum (Fig. 1 and 2). Due to this normalization the element specific shapes of the references get visible and are shown as thick lines in the graphs.

Fig. 1 shows a set of samples with a thick intermediate layer of 100 nm of gold, copper and chromium, respectively. As expected, the signature of gold and copper gets clearly visible, because the largest fraction of the positrons is implanted in the layer and the positron affinity ratio does not allow diffusion of positrons out of the layer. A different picture is seen at the chromium layer, which has a higher positron affinity than the substrate by 1.5 eV. This results in a diffusion process of the positrons out of the layer, so that practically no chromium signature can be detected. Fig. 2 shows samples with a very thin intermediate layer. Now the signature of chromium vanishes totally, only the influence of defects caused by the lattice mismatch between chromium and aluminum is visible. The same is visible for copper which has nearly the equal affinity as aluminum. But for gold, with its high affinity, a layer of only 2 nm is clearly visible although implantation calculations show that only 2.7% of the positrons are implanted directly in the layer. This is explained by the diffusion of the positrons after the implantation which leads to an effective trapping in the potential well formed by the thin layer or clusters of gold.

Conclusion and Outlook

This measurement on thin metallic layers is fundamental for application of the CDB-technique in material sciences. Many experiments with positrons on binary metallic alloys have been already performed. However, it is still challenging to get quantitative results because there are few experimental data about the trapping at metallic clusters. The presented measurements show the high suitability of CDBS to studay layered systems; in addition the influence of theoretically calculated positron affinities to the sensitivity of the measurement was confirmed. For further measurements, a heatable sample holder will allow to measure growth of precipitates which are observed in the non-deformed, undisturbed volume of the metallic sample. Due to these developments, CDBS with a monoenergetic positron beam becomes a unique method for elementally selective and high sensitive measurements on embedded structures of appropriate positron affinity.

References

[1] C. Hugenschmidt et al. *Phys. Rev. B*, 77:092105, 2008.

Temperature dependent Doppler broadening spectroscopy

Markus Reiner[1,2], Philip Pikart[1,2], and Christoph Hugenschmidt[1,2]

[1] *Physik Department E21, Technische Universität München, D-85748 Garching, Germany*
[2] *Forschungsneutronenquelle Heinz Maier-Leibnitz (FRM II), Technische Universität München, D-85748 Garching, Germany*

At our DB(Doppler broadening)-spectrometer positrons provided by the high intense positron beam NEPOMUC of the FRM II are used for defect spectroscopy in material science. The positron beam can be implanted into the sample with an energy up to 30 keV in order to adjust the mean penetration depth which is given by the Makhovian implantation profile. Before annihilation with electrons the positrons diffuse in the sample and are likely to get trapped in vacancies or at grain boundaries. For lower implantation energies back diffusion to the surface and trapping in surface states becomes more and more dominant.

Dependent on the electronic surrounding of the annihilation site a Doppler broadening of the 511 keV annihilation line can be seen. The broadening of the line is described by a lineshape parameter, the so called S-parameter. As there is a lower probability for annihilation with high energetic core electrons when positrons are trapped in defects, the broadening of the 511 keV-line decreases and hence results in a higher S-parameter. In our experimental setup for the spectroscopy of the annihilation radiation 8 HPGe detectors can be used. By performing a depth resolved scan of the S-parameter (S(E)-scan) the positron diffusion length can be extracted which reveals information about the concentration of open volume defects such as grain boundaries or vacancies.

In order to study and characterize annealing processes a new heating device has been installed at the DB-spectrometer. An aluminium reflector is used to concentrate light of a high intense filament lamp onto the backside of the sample. For measurement of the temperature two methods have been applied. Instead of using a thermocouple a pyrometer is used during measurements at high voltage at the sample. With the recently installed reflector with a diameter of 5 cm temperatures up to 1000 K have been achieved. Presently, we are working on further improvement of the heating system to enable measurements at even higher temperatures.

Annealing in thin metallic layers

In order to establish the determination of positron diffusion length to measure defect concentration in thin films, measurements on model systems with thin metallic films have been performed. Thin films of Copper and Gold with a thickness between 20 nm and 500 nm have been deposited on glass and silicon substrates. These systems were produced by use of the electron beam evaporation system of the sample preparation chamber of the NEPOMUC PAES-facility. For controlling the thickness of the deposited layers a quartz thickness monitor was used.

Here we present two S(E)-scans of an Au-Si system with a thickness of the Au-layer of 90 nm. The first measurement was made at room temperature, then the sample was heated up to a temperature of 648 K for the second scan. In the shown figure the points represent the measurement data, the lines are results of fits to the data that were performed to extract the diffusion length.

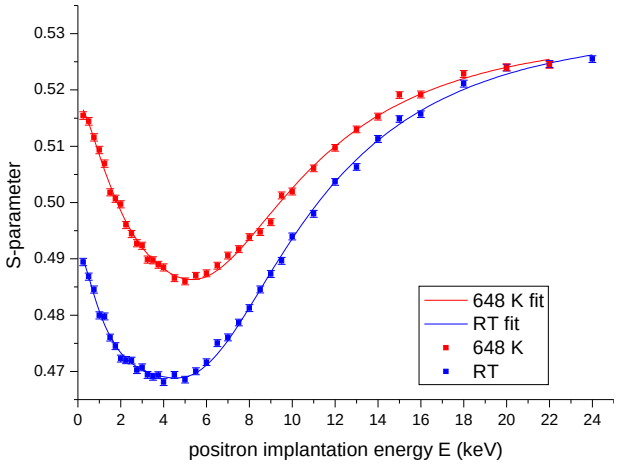

Figure 1: S(E)-scans on a 90 nm Au-layer on a Si-substrate.

For both temperatures three characteristic S-parameters can be seen. For low energies (0 keV) the surface S-parameter represents positrons annihilating in surface states. In the energy region close to 5 keV the S-parameter of positrons annihilating in the Au-layer is measured. An energy of 5.65 keV corresponds to a mean positron implantation depth of 45 nm. For high energies above 20 keV the S-parameter corresponds to positrons annihilating in the Si-substrate. The shape of the transition between the three S-parameter values is determined by the implantation profile and the positron diffusion length.

While the S-parameter in the Si-substrate does not change when the sample is heated, the S-parameters at the surface and in the Au-layer increase. The increase of the S-parameter at the surface can be explained by thermal desorption of positrons from the surface states under formation of Positronium with electrons from the surface region. The change of the S-parameter in the Au-layer indicates that at higher temperatures the positrons are trapped in different kind of defects.

The results of the fits, which take into account the positron implantation profile and the positron diffusion, reveal that the positron diffusion length increased from 5 nm at room temperature to 43 nm at 648 K. These results clearly show that the concentration of trapping centers, such as vacancy-like defects, has been decreased during heating due to annealing at elevated temperature. In addition, CDB measurements which were performed to investigate processes at the Au-Si interface did not show any change in the chemical surrounding of defects.

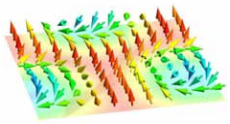

Chapter 4

Radiography and Tomography

Tomographic Reconstruction of Neutron Depolarization Data

Michael Schulz[1,2], Christian Franz[1], Philipp Schmakat[1,2], Andreas Neubauer[1], Elbio Calzada[1,2], Burkhard Schillinger[1,2], Peter Böni[1], and Christian Pfleiderer[1]

[1] *Physik Department E21, Technische Universität München, D-85748 Garching, Germany*
[2] *Forschungsneutronenquelle Heinz Maier-Leibnitz (FRM II), Technische Universität München, D-85748 Garching, Germany*

The combination of neutron imaging with polarization analysis is a new and powerful method which has proven to be useful in the investigation of magnetic phenomena [1, 2]. In particular, the depolarization of the neutron beam may be used to map out variations of ferromagnetic properties as a function of external parameters such as stress, pressure, applied magnetic and electric field or temperature as well as internal characteristics such as chemical composition, defects and strain. In this article we will present a 3D reconstruction of neutron depolarization data, which yields a volume model of the sample and its magnetic properties on a macroscopic scale using a standard filtered backprojection algorithm. Depolarization tomography is based on the spatially resolved measurement of the polarisation of a neutron beam after transmission of a sample under different projection angles.

The longitudinal polarisation analysis setup used for our experiment was installed at the radiography beam line ANTARES at FRM II and consists of a ^{3}He polarizer and analyzer, a precession coil spin flipper, a closed-cycle cryostat with a base temperature of 3.5 K, which holds the sample and a position sensitive CCD detector that records the image on a LiF/ZnS scintillator. We investigated a polycrystalline $Pd_{1-x}Ni_x$ sample, which was grown with the Czrochalski technique and has a nominal Ni concentration of $x = 2.67\%$. The sample has a cylindrical shape with a diameter of 11 mm and a length of 26 mm. $Pd_{1-x}Ni_x$ is a weak itinerant ferromagnet with a strong dependence of the Curie-temperature T_C on the Ni concentration x [3]. A tomography with a total measurement time of approx. 30 h, during which the sample was rotated over 180° with angular steps of 1° was recorded at a temperature of 8 K.

We were able to show that the neutron depolarisation data can be reconstructed using a standard filtered back projection algorithm [4]. Both the polarisation and the absorption data were reconstructed separately and then visualised as shown in Fig. 1. Here, the paramagnetic regions of the sample are displayed in grey, whereas the ferromagnetic regions are shown in blue. Image a) shows an outside view of the absorption data of the crystal as an overview. At the bottom of the sample the glue which was used to fix the sample on the sample holder is visible. Furthermore at the top of the sample one can clearly see an edge which was cut off the crystal for bulk measurements. For images b) through f) the paramagnetic regions of the sample were rendered more transparently to visualize the ferromagnetic parts inside the sample. Furthermore images c) through f) show horizontal cuts through the absorption data for better visibility of the depolarisation data. For all images the orientation of the 3D object was the same. One can readily see that the sample is extremely inhomogeneous and has vast paramagnetic regions. Furthermore the ferromagnetic parts of the sample tend to arrange in horizontal layers, which are however, also not perfectly homogeneous. This might be due to the crystal growth process, which was perpendicular to these planes. A change in the growth parameters (i.e. the growth velocity) could be responsible for variations in the Ni concentration and consequently in the magnetic properties of the sample.

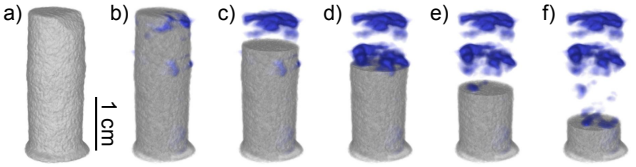

Figure 1: 3D Reconstruction of the ND data. a) View of the crystal; b) through f) Paramagnetic regions of the sample are shown in light grey. Ferromagnetic regions are displayed in blue. Several cuts through the sample are shown from c) to f).

Our experiment shows that 3D information on the distribution of magnetic properties of a sample can be obtained by using a tomographic method. This could help to improve the understanding of substances showing a strong dependence of the Curie temperature on the composition or phase separation. Furthermore this method allows to locate regions of desired magnetic properties from a 3D model and later cut these out of the sample for further investigation with bulk or neutron scattering measurement methods. Several other substances such as Ni_3Al and Heusler alloys have already been studied with this method and it turns out that many samples, which were thought to be of very high quality show drastic variations of their magnetic properties on a macroscopic scale [5]. This observation becomes especially important if neutron scattering studies are performed on such samples, since these use a large beam which performs an implicit average over the sample volume. We are currently as well studying the influence of different crystal growth conditions on the resulting crystal quality and will try to identify the ideal parameters for high quality crystals using radiography and tomography with polarized neutrons.

Acknowledgements

We wish to thank A. Hilger and N. Kardjilov from CONRAD at HZB, Berlin for giving us the opportunity to do first tomography measurements at their beam line. Financial support through DFG Forschergruppe FOR 960 on Quantum Phase Transitions and Transregio TRR 80 is gratefully acknowledged.

References

[1] N. Kardjilov et al. *Nature Physics*, 4:399, 2008.
[2] M. Schulz et al. *J. Phys.: Conf. Series*, 251:012068, 2010.
[3] M. Nicklas et al. *Phys. Rev. Lett.*, 82:4268, 1999.
[4] M. Schulz et al. *J. Phys.: Conf. Series*, 211:12025, 2010.
[5] M. Schulz. PhD thesis, Technische Universität München, 2010.

Quantitative determination of hydrogen effusion in ferrous alloys using neutron imaging

Axel Griesche[1], Katrin Beyer[1], Thomas Kannengießer[1], and Burkhard Schillinger[2,3]

[1] *BAM Bundesanstalt für Materialforschung und -prüfung, 12205 Berlin, Germany*
[2] *Forschungsneutronenquelle Heinz Maier-Leibnitz (FRM II), Technische Universität München, D-85748 Garching, Germany*
[3] *Physik Department E21, Technische Universität München, D-85748 Garching, Germany*

We studied the hydrogen diffusion in-situ in differently treated steels at different temperatures using a mirror furnace on ANTARES. Neutron radiography allows to measure the hydrogen distribution for small concentrations as a function of space and time due to the high contrast between H and Fe.

The samples were charged with hydrogen in the home lab and stored and transported in liquid nitrogen in order to prevent hydrogen losses. Transmission images of charged samples and non-charged reference samples were recorded simultaneously. Furthermore, three different mixtures of TiH_2 and SiC (containing 0, 10, and 200 ppm_H) serve as calibration standards for hydrogen concentration. The change of the hydrogen concentration in the charged samples is recorded for a sufficient long time in each experiment run.

The suspended samples and references and the concentration standards were located in the isothermal zone of the mirror furnace. Openings in the furnace housing with Al windows left a clear view from source to detector at the positions of sample, reference and standards (Fig. 1).

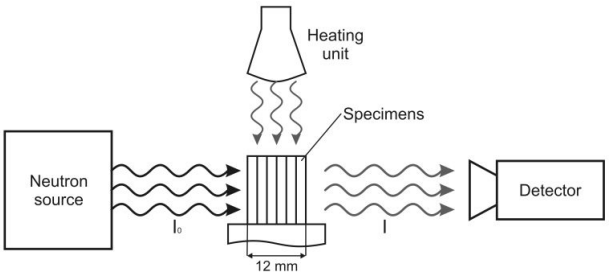

Figure 1: Neutron radiography experimental setup at FRM II with analysed specimen stack.

The temperature was measured with one thermocouple inside of the furnace close to the sample. The furnace was operated automatically. Temperature stability was within one Kelvin. The samples were quickly heated to the annealing temperature. The individual samples and references with the measures $40 \times 5 \times 2\,mm^3$ H × W × T used for the experiments were assembled as stacks, each consisting of 6 such plates resulting in 12 mm absorption length.

The L/D = 400 setup was used for the experiments. The scintillator screen was placed approximately 10 cm away from the centres of sample, reference and standards. The L/D = 800 setup offered slightly better resolution at a lower flux. This positively benefited our experiment. The exposure time was set to 20 s making optimum use of the dynamic range of the detector.

20 different samples were measured. Sample materials were technical iron, austenitic stainless steel and duplex stainless steel. The annealing temperature was varied as well as the initial hydrogen concentration, the method of charging the samples with hydrogen, and the dislocation density of the materials.

The first neutron radiographic experiment to study hydrogen diffusion at the ANTARES instrument in 2009 gave the proof that hydrogen concentrations can be measured down to 20 ppm_H. The newly developed mirror furnace based on the previous design allowed to study samples at much better isothermal conditions. The use of concentration standards will hopefully allow to detect contrast differences between sample and reference quantitatively with much better statistics at even lower concentrations.

In Fig. 2 a preliminary evaluation of a corrected and normalized image series is shown.

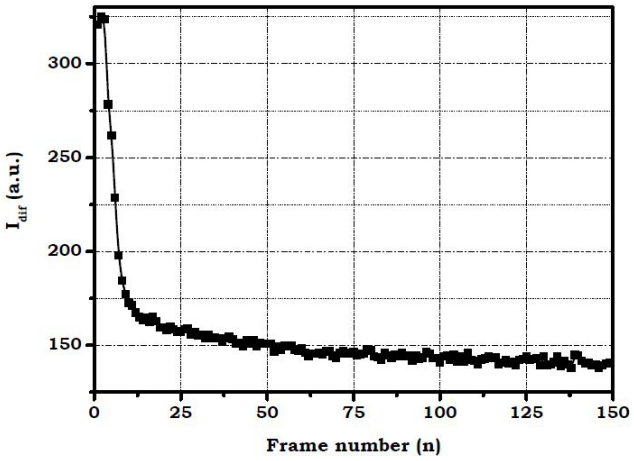

Figure 2: Intensity difference $I_{diff} = I_{sample} - I_{reference}$ of a charged duplex stainless steel sample and a non-charged duplex stainless steel reference at 350°C as a function of the frame number.

The corresponding grey values are obtained from an integrated area of 60% of the respective sample area. The initial difference in contrast decreases over time, i.e. with the frame number, due to diffusion of H out of the sample. From a fit of the appropriate solution of Fick's equation to the properly normalized and calibrated data an effective diffusion coefficient of H in this steel can be obtained.

A detailed report of the experiments is accepted for publication in Nucl. Inst. Meth. [1].

References

[1] K. Beyer, T. Kannengießer, A. Griesche, and B. Schillinger. Study of hydrogen effusion in austenitic stainless steel by time-resolved in-situ measurements using neutron radiography. *Nucl. Inst. Meth.*, 2010. Accepted for publication.

Dehydration of moulding sand in a simulated casting process examined with neutron radiography

B. Schillinger[1,2], E. Calzada[1,2], C. Eulenkamp[3], G. Jordan[3], and W. W. Schmahl[3]

[1] Forschungsneutronenquelle Heinz Maier-Leibnitz (FRM II), Technische Universität München, D-85748 Garching, Germany
[2] Physik Department E21, Technische Universität München, D-85748 Garching, Germany
[3] Ludwig-Maximilians-Universität München, Department für Geo- und Umweltwissenschaften, Sektion Kristallographie, 80333 München, Germany

Natural bentonites are an important material in the casting industry. Smectites as the main component of bentonites plasticize and stabilize sand moulds. Pore water as well as interlayer water within the smectites are lost as a function of time, location and temperature. Although rehydration of the smectites should be a reversible process, the industrially dehydrated smectites lose their capability to reabsorb water, which limits the number of possible process cycles of the mould material. Understanding of the dehydration process would help to optimize the amount of fresh material to be added, and thus save resources. A simulated metal casting was investigated with neutron radiography at the ANTARES neutron imaging facility of the FRM II.

During the casting process, the interlayer water in smectites is released and the smectites become partially or completely dehydrated. Also the pore water is evaporated, the mold hardens. After the mould is destroyed to extract the casting part, the sand can be processed and partially recycled by adding water, a certain amount of fresh sand and fresh bentonite. Although rehydration of the smectites should be a reversible process, the dehydrated smectites lose their capability to reabsorb water. This limits the number of possible process cycles of the mould material. To study the dehydration behavior of the moulding sand, neutron radiography was employed. A test stand allowed dropping a casting mould filled with moulding sand onto a red-hot copper plate, thus creating a thermal shock in the sand similar to the process of casting liquid metal.

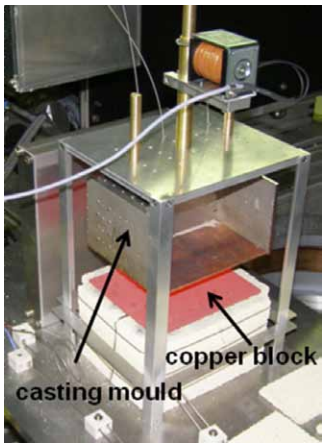

Figure 1: Red-hot copper block with the release system for the casting mould (14 cm in width, 12 cm in depth).

An electrically heated red-hot copper was used to simulate the molten metal. The casting mould was constructed of steel side plates, aluminum front and back-plates (in direction of the neutron beam) and a copper bottom plate. At a temperature of 650°C, the casting mould was dropped down by an electro-mechanical release unit. Thermocouples were placed on defined positions within the moulding sand. The experiment was placed in the ANTARES neutron imaging facility of the FRM II reactor, so the dehydration process could be observed by neutron radiography. Fig. 1 shows the setup with the heated copper block and the casting mould before dropping.

After dropping the mould, a continuous series of 2 second exposures was recorded every 3 seconds. Fig. 2 shows a series of images about 12 seconds apart each. After several seconds, additionally to the initial drying front a second more faint front can be detected. The second front eventually merges with the first front to form again a single vertical dehydration profile. This vertical dehydration gradient eventually remains very stable and moves upwards with time. The separation of the drying fronts may consist of the drying of inter-granular and inter-layer moisture.

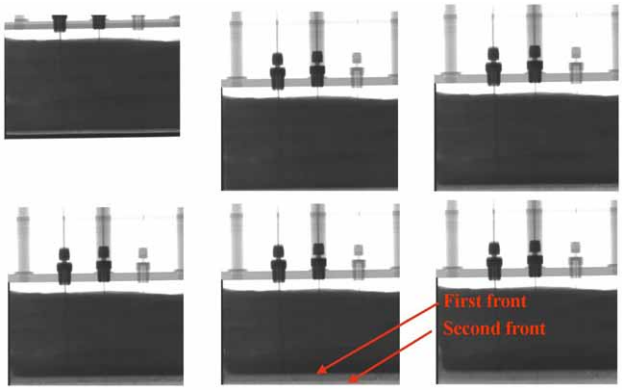

Figure 2: Image sequence of the mould dropped on the hot block. Two drying fronts develop of drying inter-granular and inter-layer moisture.

The experiments revealed a progressive movement of water in the sand and resolved a broad transitional zone from the pristine hydration state of the sand to a fully dehydrated state. At this transitional zone positions can be determined which on one hand relate to the onset of pore water dehydration and on the other hand relate to the completion of interlayer space dehydration. Thus, the experiments allowed us to successfully simulate the shock-heating of the mould material in an industrial casting process. The consequence of the shock-heating is a strongly non-linear temperature-time-position relation convoluted with the diffusion processes.

References

[1] B. Schillinger, E. Calzada, C. Eulenkamp, G. Jordan, and W. W. Schmahl. Dehydration of moulding sand in a simulated casting process examined with neutron radiography. *Nucl. Inst. Meth.*, 2010. Accepted for publication.

Radiography and Partial Tomography of Wood with Thermal Neutrons

K. Osterloh[1], D. Fratzscher[1], A. Schwabe[2], B. Schillinger[3,4], U. Zscherpel[1], and U. Ewert[1]

[1] BAM Bundesanstalt für Materialforschung und -prüfung, 12205 Berlin, Germany
[2] Rathgen Research Laboratory, 14059 Berlin, Germany
[3] Forschungsneutronenquelle Heinz Maier-Leibnitz (FRM II), Technische Universität München, D-85748 Garching, Germany
[4] Physik Department E21, Technische Universität München, D-85748 Garching, Germany

The high neutron attenuation coefficient of hydrogen (48.5 cm^2/g, scattering and absorption) is predestined to emphasise hydrocarbon structures better than X-ray on one hand, but limits the sample thickness on the other hand. Numerous wood samples are of a planar shape with a thickness still allowing the penetration of thermal neutrons in perpendicular, but not in parallel direction. Most tomographic reconstruction algorithms produce artifacts due to missing projections.

Special data treatment suppresses the artifacts and produces incomplete tomographic reconstruction images that show features perpendicular to the covered angular range, but cannot resolve features perpendicular to the missing angular range, i.e. perpendicular to the long side of the sample. In most cases, the obtained information is sufficient for the purpose of the examination.

A single radiography integrates over the attenuation coefficient along the beam path for each pixel of the image and thus loses information about the distribution along the beam path. But since each pixel represents an independent measurement, information perpendicular to the beam path is maintained. By rotating the sample over 180 degrees (for parallel beam, or 360 degrees for cone beam), information is collected for a discrete set of views around the sample, which can be combined into a three-dimensional view by tomographic reconstruction. A special algorithm (to be published) suppresses the artifacts and allows for an incomplete reconstruction where information perpendicular to the missing projections is missing.

A study of this kind was performed at the Antares facility of the FRM II with a neutron beam of $2.6 \times 10^7/cm^2$ s. A planar board made of glulam has been studied to show the glued layers even in a larger sample. Radiographic images were obtained with a fluoroscope consisting of a ZnS(Au,Ag)+LiF scintillation screen and an Andor DW 436 cooled CCD camera delivering 2048 × 2048 pixels. Reconstruction using 1024 × 1024 pixel images was achieved with a proprietary back projection algorithm in the Fourier transformed domain assuming parallel beam geometry. Fig. 1 shows the experimental setup with a wooden board glued from four individual planks.

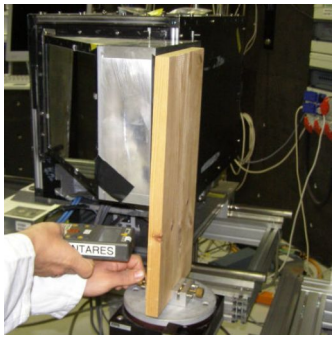

Figure 1: Tomography setup with wooden board with a central glued layer.

Fig. 2 on the top shows the reconstruction of a horizontal cross section of the board with 180° full angular coverage, and only 90° (right). In the 90° reconstruction, the flat surface of the board perpendicular to the small side is no longer properly reconstructed, same as the corners of the board. As can be seen on the annual rings on the sides, structures perpendicular to the long side are beginning to disappear. The large images below are not radiographies but the average of five resp. ten layers inside the three-dimensional reconstructed data set of the wooden board. For this transversal cross section, nearly all information is maintained also in the 90° reconstruction.

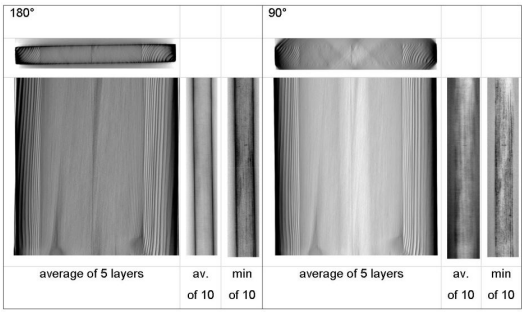

Figure 2: Total tomography (180°) and reconstruction with limited angles (aperture 90° perpendicular to the plane) of the flat board with glued layers. Cross section (transversal, top), central section in flat alignment (left) and along the central glued layer (longitudinal cross section, right, together with a minimum penetration image of 10 layers).

In Fig. 3, the 90 degree reconstruction is compared with a reconstruction using only 60 degrees. The central glue layer between the boards is still well visible, but structures perpendicular to it are about to disappear.

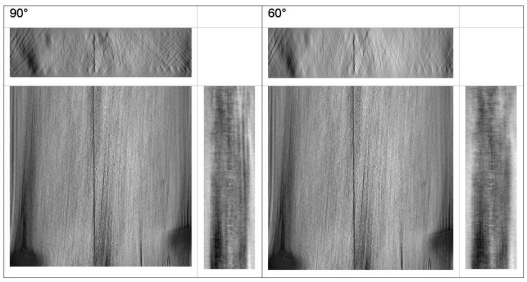

Figure 3: Tomography with limited angles covering an aperture of 90° (left) and 60° (right) perpendicular to the flat plane of the sample board. The glue in the laminar contact area appears to be heterogeneously distributed.

There is no physical and mathematical solution to obtain a complete tomographic reconstruction from incomplete data. But often, an incomplete reconstruction from the available data is sufficient to obtain the information that is required in an experiment. The new algorithm will be published in the future and will be implemented at the neutron radiography facilities ANTARES and NECTAR at FRM II.

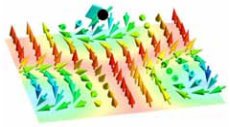

Chapter 5

Instrument Development

Vibrating Coil Magnetometer for milli-Kelvin Temperatures

Stefan Legl[1], Christian Pfleiderer[1], and Karl Krämer[2]

[1] *Physik Department E21, Technische Universität München, D-85748 Garching, Germany*
[2] *Department of Chemistry, University of Bern, CH-3012 Bern, Switzerland*

The magnetization is perhaps the most important thermodynamic property of condensed matter systems. It is a deep probe not just of ferromagnetic materials, but also of systems with complex configurations of the magnetic moments. However, a strikingly small number of experimental studies have been reported at dilution refrigerator temperatures, because of the rather severe requirements of magnetization studies at ultra-low temperatures, notably the need for measurement techniques that offer high mechanical stability under strongly reduced cooling power while avoiding parasitic signal pick-up. We report the design of a vibrating coil magnetometer that offers efficient and reliable magnetization measurements down to milli-Kelvin temperatures [1].

It has long been appreciated that induction techniques based on the harmonic motion of a sample with respect to a set of detection coils may be the simplest, fastest and most reliable method to measure the magnetization. Two implementations exist of this basic idea: In the vibrating sample magnetometer (VSM) the position of the detection coils is fixed and the sample oscillates. This is contrasted by the vibrating coil magnetometer (VCM) in which the position of the sample is fixed and the detection coils oscillate.

However, the performance of vibrating sample magnetometers, in which the sample oscillates, are severely limited by mechanical vibrations and eddy current heating (for previous work see Refs. [2, 3, 4]). The VCM design we have developed avoids this problem. Fig. 1 shows a drawing of the VCM setup as combined with our Oxford TL-400 top-loading dilution refrigerator with a superconducting sample magnet about 400 mm below the mixing chamber. In the studies described here we used a conventional 7 T solenoid; however, the VCM may also be combined with a transverse field or vector magnet without any changes. The VCM unit is attached to the inner vacuum chamber; it is hence completely thermally decoupled from the mixing chamber and sample holder. It is composed of three parts, the vibration drive (i), a transmission system (ii) and the detection coils (iii).

The vibration drive is akin to a loudspeaker. The harmonic vibration is generated by means of a 1000-turn superconducting coil and transmitted to the detection coils by means of a thin-walled carbon-fibre tube. The system composed of vibration coil, transmission tube and detection coils is suspended by two identical circular leaf springs, ensuring a perfectly harmonic motion parallel to the vertical axis of the system. The detection coils are mounted on the lower end of the carbon-fibre tube as shown in Fig. 1.

For our studies a two-coil setup, symmetrically placed around the sample, proved to be perfectly sufficient. However, the VCM described here is completely flexible for use of more complex detection coil geometries. Each detection coil consists of 600 turns of 54 µm copper wire wound on a Delrin coil former. Signal contributions due to the surrounding materials of the dilution unit and sample holder were minimized by strictly using non-magnetic materials. Typical excitation currents of the VCM system up to 1 mA generate a vibration amplitude up to 1 mm at an operating frequency of 37 Hz.

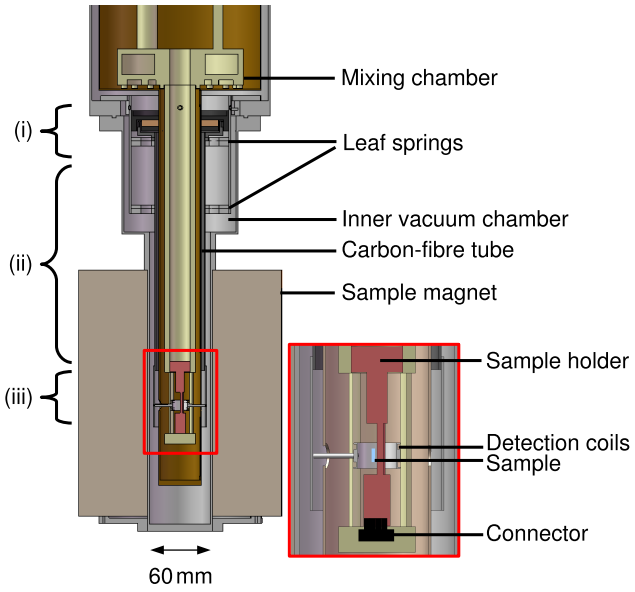

Figure 1: Schematic drawing of the vibrating coil magnetometer as implemented on a top loading dilution refrigerator.

To test the performance of the VCM we have measured the magnetization of the dipolar Ising ferromagnet $LiHoF_4$ (see page 15 in this issue). For the large signal of $LiHoF_4$ a sensitivity of 10^{-3} emu was achieved. In addition, the VCM signal may be amplified by toroidal low temperature transformers, where we readily achieved a sensitivity of 10^{-4} emu and further improvements seem possible.

In conclusion, we have developed a vibrating coil magnetometer for routine studies down to milli-Kelvin temperatures. The combination of the VCM with the top loading dilution refrigerator allows extremely efficient sample changes within a few hours. We believe that the excellent stability of the VCM system and its ease of use will pave the way to resolving a large number of prominent challenges in applied and fundamental physics.

References

[1] S. Legl, C. Pfleiderer, and K. Krämer. *Rev. Sci. Instr.*, 81:043911, 2010.
[2] D. O. Smith. *Rev. Sci. Instr.*, 27:261, 1956.
[3] N. Manivannan, S. Arumugam, S. Kasthurirengan, and N. B. Anand. *Meas. Sci. Technol.*, 19:125801, 2008.
[4] M. Ishizuka, K. Amaya, and S. Endo. *Rev. Sci. Instrum.*, 66:3307, 1995.

Cryogen-free demagnetization refrigerator for milli-Kelvin temperatures

Alexander Regnat[1], **Christian Franz**[1], **and Christian Pfleiderer**[1]

[1] *Physik Department E21, Technische Universität München, D-85748 Garching, Germany*

We have commissioned a cryogen-free demagnetization refrigerator, model DMS-1000 by Dryogenic Ltd (Fig. 1). The system is based on a pulse tube cooler with a nominal cooling power of 1 W, that serves to precool a sample-stick as wells as two superconducting magnets (a 12 T sample magnet and a 7 T magnet for the demagnetization of a paramagnetic salt). When demagnetizing a pill of ferric ammonium alum (FAA) from an initial starting temperature of $\sim$ 5.5 K routinely temperatures around 100 mK may be reached. In its present configuration this system allows reliable measurements of the electric resistivity at temperatures down to 100 mK and applied magnetic fields up to 9 T. As an additional feature, we have also adapted the system for measuremen with Bridgman anvil cells for high pressure resistivity st dies up to 200 kbar in the same temperature and fie range.

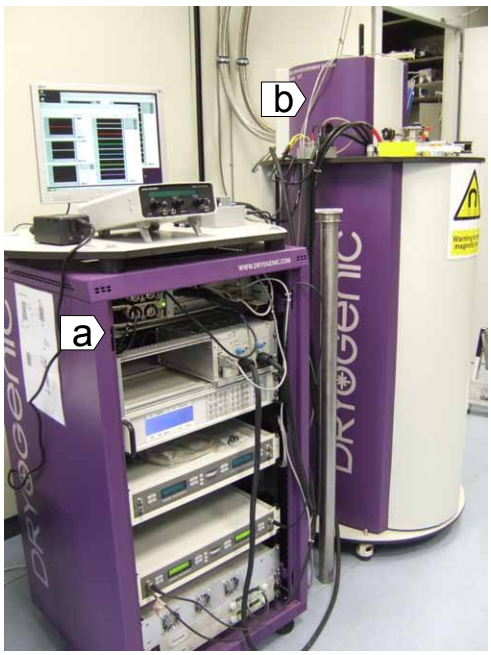

Figure 1: Dryogenic measurement system. (a) Measureme rack and (b) cryostat.

First measurements were carried out on polycrystal ne and single crystal samples of chromium diboride CrB [1] under pressures up to approximately 80 kbar (Fig. [2]. At ambient pressure CrB_2 is an itinerant antiferrom gnet with a transition temperature $T_N \approx 88$ K [3], whe T_N is reflected by a distinct kink in the resistivity. At lo temperatures the resistivity follows the quadratic temperature dependence of a weakly spin polarized Fermi liquid state.

Unfortunately the cryogen-free refrigerator as supplied displayed a large number of technical flaws that had to be resolved first. For instance, the resistivity data was very noisy due to the use of a multiplexer and parts of the operating software had to be corrected (the maximum field value accessible in automated measurements is still limited to 9 T due to a software problem that could not be identified). Perhaps most importantly, the original Cryomech pulse tube cooler recently failed after an operating time of only 13.000 hours and had to be replaced by a reliable model from Sumitomo. Despite of these problems our cryogen-free refrigerator has been running around the clock for the better part of a year, offering a fast option for exploratory measurements on new materials.

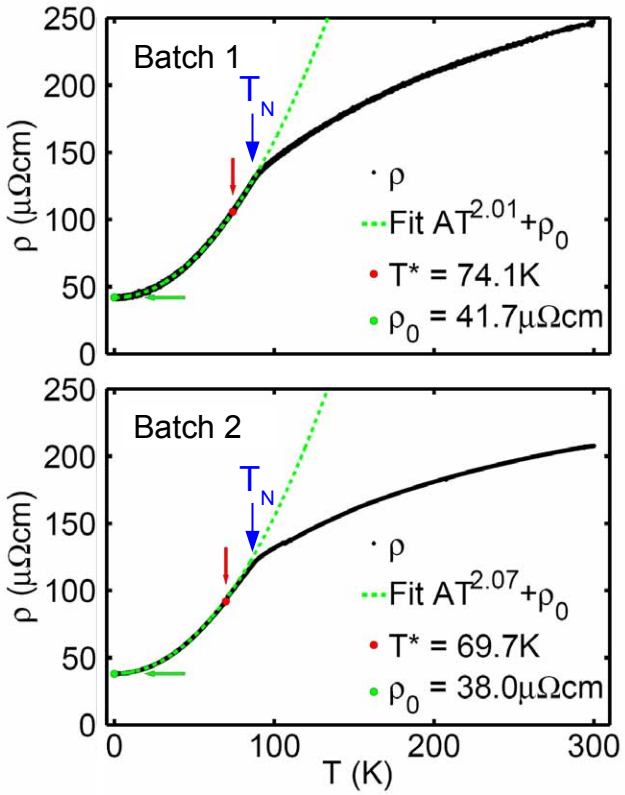

Figure 2: Resistivity of polycrystalline (Batch 1) and single crystal (Batch 2) CrB_2 samples as a function of temperature at zero pressure, denoted as batch 1 and 2, respectively. T_N marks the antiferromagnetic Néel transition and T^* the temperature of the largest slope of $\rho(T)$. In the ordered phase the resistivity obeys a T^2 dependence (green dashed line). Data were recorded down to approximately 100 K.

References

[1] J. Boeuf. PhD thesis, Universiät (TH) Karlsruhe, 2003.

[2] A. Regnat. Diploma thesis, Technische Universität München, 2010.

[3] R. G. Barnes and R. B. Creel. Chromium-like antiferromagnetic behavior of CrB_2. *Phys. Lett. A*, 29, 1969.

UHV-compatible rod casting furnaces for single crystal growth

Andreas Bauer[1], Andreas Neubauer[1], Wolfgang Münzer[1], Barbara Russ[1], and Christian Pfleiderer[1]

[1] *Physik Department E21, Technische Universität München, D-85748 Garching, Germany*

High-quality single crystals are one of the most important prerequisite for major advances in condensed matter physics. For growing single crystals of highest purity achievable it is crucial to avoid contaminations in every step of the crystal growth process. Besides the impurities left in commercially available metal elements, in most cases their affinity to oxygen, nitrogen and carbon are the most important source of contaminations. In order to meet these criteria of high purity we have refurbished an image furnace to be all-metal-sealed for ultra-high vacuum compatible conditions [1]. To prepare the starting rods for optical float zoning under the same stringent conditions we have set up a UHV compatible drop-furnace [2] (Fig. 1) and a UHV system with a horizontal cold-boat (Fig. 2).

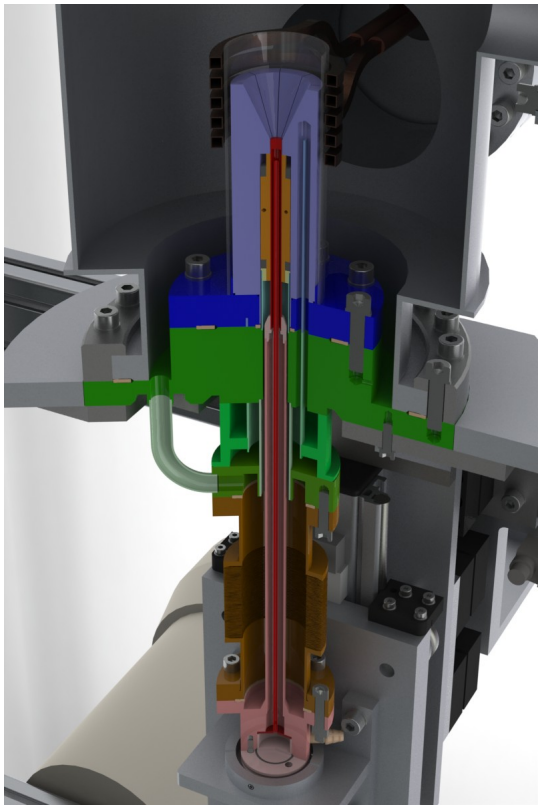

Figure 1: Cut-away view of our UHV-compatible drop furnace.

The drop furnace is based on a Huykin type cold crucible (shown in blue shading), in which the samples may be melted through radio frequency (RF) induction heating. As the entire setup is all-metal sealed it may be baked out. For compounds with high vapor pressure the UHV represents a precondition for the use of a high-purity argon atmosphere which may be applied at pressures up to 3 bar.

The drop-furnace was first set up by A. Neubauer using standard Viton O-rings [3]. It was then adapted to UHV-compatible conditions W. Münzer, who constructed a vacuum chamber bellows system [4]. Finally, the Huykin crucible and support flange (shown in green shading) were replaced to by all-metal sealed components [5]. The crucible is made of copper (light blue) while the connection to the support flange providing cooling water (dark blue) consists of stainless steel. Both parts were high temperature vacuum soldered onto each other. This way only three standard CF copper sealing have to be replaced when (de)mounting the sample and a baking temperatures exceeding 200 °C is ensured.

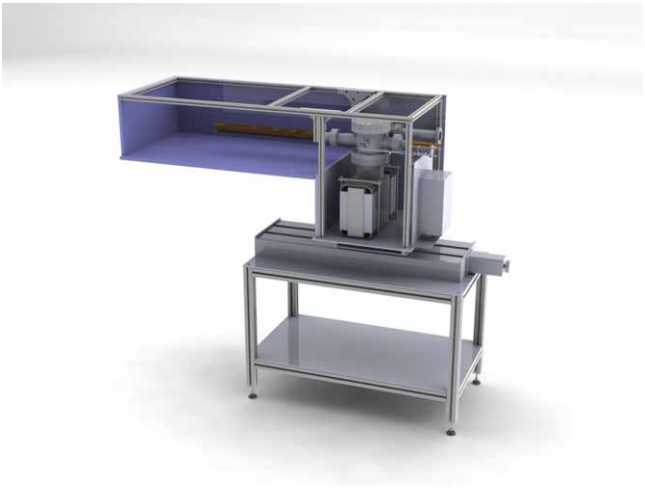

Figure 2: Schematic overview of the our all-metal sealed horizontal RF heated cold-boat system including baking tent.

Moreover, a UHV system with a horizontal water cooled cold-boat and bespoke heating tent was set up (see Fig. 2) [5], which allows to reach an ultimate pressures better than 10^{-10} mbar. This versatile system may be used for the preparation of irregularly shaped rods for float-zoning, as well as sintering, prereacting delicate compounds, joining broken feed rods, or for annealing polycrystalline or single crystal samples. For handling highly reactive starting materials and to reduce contamination when preparing polycrystalline material the cold boat system will be combined with a high purity glove box in the near future.

References

[1] A. Neubauer, J. Bœuf, A. Bauer, B. Russ, H. von Löhneysen, and C. Pfleiderer. *Rev. Sci. Instr.*, 82:013902, 2011.
[2] A. Neubauer, A. Bauer, W. Münzer, B. Russ, and C. Pfleiderer. to be published, 2011.
[3] A. Neubauer. PhD thesis, Technische Universität München, 2010.
[4] W. Münzer. Diploma thesis, Technische Universität München, 2008.
[5] A. Bauer. Diploma thesis, Technische Universität München, 2009.

MIEZE on MIRA: Measuring at sub-μeV resolution

Georg Brandl[1,2], Robert Georgii[1,2], Reinhard Schwikowski[1,2], Christian Pfleiderer[1], and Peter Böni[1]

[1] Physik Department E21, Technische Universität München, D-85748 Garching, Germany
[2] Forschungsneutronenquelle Heinz Maier-Leibnitz (FRM II), Technische Universität München, D-85748 Garching, Germany

The MIEZE (Modulation of IntEnsity by Zero Effort) technique [1] is a variant of neutron spin echo where all beam manipulation is done before the sample, and spin phase oscillations are converted to an intensity modulation. This allows measuring quasi-elastic scattering at the high energy resolution of spin echo without magnetically shielding the sample region, or even with magnetic fields applied in the sample.

In 2010, the MIEZE development at MIRA has reached the stage where we can offer this option as a standard user option for quasi-elastic small angle scattering with a maximum spin echo time of about 1 ns. The whole setup is now fully motorized as shown in Fig. 1. This offers the possibility to scan the small angle scattering pattern and put the detector at a defined position in the plane perpendicular to the beam. In addition, a new position sensitive CASCADE detector [2] will be available shortly, allowing recording MIEZE data over a range of q values simultaneously. Furthermore measuring at different frequency ratios, resulting in different MIEZE points on the axis along the beam, can now be fully automatized. The control software offers simple commands for switching between the different MIEZE times, which help the user to run his experiment in a fully automatic way. A special library for visualization and treatment of MIEZE data collected at MIRA has been implemented and allows a very quick on-line evaluation of a running MIEZE experiment.

Figure 1: The MIEZE setup at MIRA. The π-flipper coils are contained within the μ-metal box on the left hand side, followed by the polarisation analyser (blue box) and the sample inside a magnet. On the right the detector on its x,y,z-support is shown.

Measurements on MnSi

As a first measurement with the improved MIEZE setup, we chose to investigate the linewidth of the magnetic phases of the helimagnet MnSi [3, 4]. Here, both the helical ordering at zero magnetic field and the skyrmion lattice discovered in the A phase, described in more detail on page 6 in this issue, present opportunities for quasi-elastic neutron scattering.

Fig. 2 (a) shows typical data in the helimagnetic state (B = 0) of the intermediate scattering function $S(q,\tau)/S(q,0)$ as measured by MIEZE for various temperatures. For the correction of the instrumental resolution, the linewidth is normalized to data measured at the lowest temperature T = 3 K, where the magnetic structure is supposed to be static. The resulting line widths as a function of temperature are shown in Fig. 2 (c). While the measured linewidth is resolution limited below T_c, there is broadening above T_c, which is in agreement with data measured using the NRSE technique at the instrument RESEDA.

The measured Γ in the A phase of MnSi at B = 0.18 T (shown in Fig. 2 (b)) is similar to the one in the helical phase. This demonstrates that on the one hand there is no loss of resolution involved when measuring under applied magnetic fields, and on the other hand the magnetic structure in the A phase is as static as that in the helical phase.

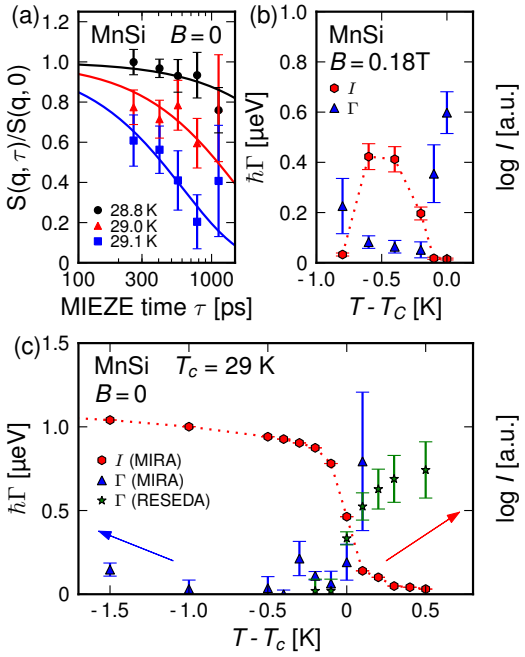

Figure 2: (a) Typical normalised intermediate scattering functions $S(q,\tau)$ in the helimagnetic state of MnSi at various temperatures. (b) Line width Γ in the A phase of MnSi at B = 0.18 T. The total scattering intensity is shown as solid hexagons, MIEZE data as solid triangles. (c) Line width Γ of the magnetic order in MnSi at B = 0. The data are normalised to the line width at T = 3 K. For comparison, NRSE data from the instrument RESEDA are shown as stars.

References

[1] R. Gähler, R. Golub, and T. Keller. Neutron resonance spin echo–a new tool for high resolution spectroscopy. *Physica B*, 180-181:899–902, 1992.
[2] C. Schmidt and M. Klein. *Neutron News*, 17:12–15, 2006.
[3] R. Georgii, G. Brandl, N. Arend, W. Häußler, A. Tischendorf, C. Pfleiderer, P. Böni, and J. Lal. *Appl. Phys. Lett.*, 98:073505, 2011.
[4] G. Brandl. First measurements of the linewidth in magnetic phases of MnSi using MIEZE. Diploma thesis, Technische Universität München, 2010.

Brilliant Polarized Neutron Beams using Halo Isomers in Stable Nuclei

D. Habs[1], M. Gross[1], P. G. Thirolf[1], and P. Böni[2]

[1] *Fakultät für Physik, Ludwig Maximilians Universität, München, D-85748 Garching, Germany*
[2] *Physik Department E21, Technische Universität München, D-85748 Garching, Germany*

Presently, neutron beams for neutron scattering are produced at large-scale facilities like reactors or spallation sources by the moderation of high energy neutrons. Recently, it was suggested using inertial fusion to boost the neutron flux by two orders of magnitude [1]. However, moderators and shielding result in very large sources with a diameter of $\simeq$ 10 m representing a large nuclear inventory and neutron beams with large cross sections, which do not match the small size of typical samples. In contrast to neutron sources, the brilliance of x-ray sources is more than 20 orders of magnitude higher and will increase soon by several orders of magnitude with the commissioning of free electron lasers.

There are essentially two reasons why the brilliance of present day neutron sources is limited, namely i) cooling of the fuel element or the spallation target and ii) the moderation process of the neutrons leading to a strong reduction of the brilliance. These limitations can be overcome if the neutron production process would yield directed beams emerging from a tiny volume without moderation.

We suggest the following two step production scheme (Fig. 1) [2]: A neutron halo isomer is excited in a target with a diameter of approximately 0.1 mm by means of a brilliant γ-beam of 6–8 MeV. The halo state is a longer-lived nuclear state, where one neutron of the nucleus is excited into a weakly bound state extending far out of the nuclear core. The halo neutron is finally released by a second intense polarized laser or photon beam producing a brilliant polarized neutron beam that emerges into a small solid angle parallel to the vector of the electric field (Fig. 2).

Using a γ-beam with 10^{13} quanta/s of 7 MeV and a bandwidth of 7 keV, approximately 10^8 isomers/s can be produced in a spot with a diameter of $\simeq$ 0.1 mm. The p-wave neutrons are emitted with a $(100\,\text{mrad})^2$ opening angle and a bandwidth better than 0.1%. Thus, a peak brilliance of $\simeq 10^{11}$[(mm mrad)^2 0.1% BW s] (Fig. 3) can be achieved that is more than 5 orders of magnitude larger than at a future modern pulsed source [2].

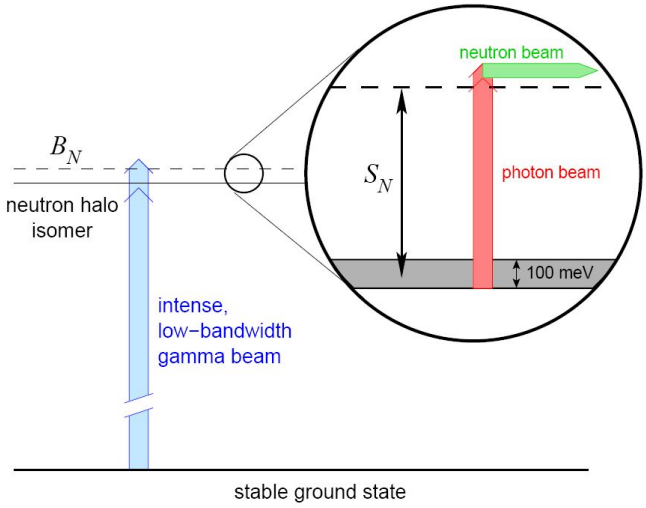

Figure 1: An intense γ-beam shown in blue excites a neutron halo isomer with a neutron separation energy S_N below the binding energy of the neutron. In a second step, a photon beam of low energy shown in red releases the halo neutrons.

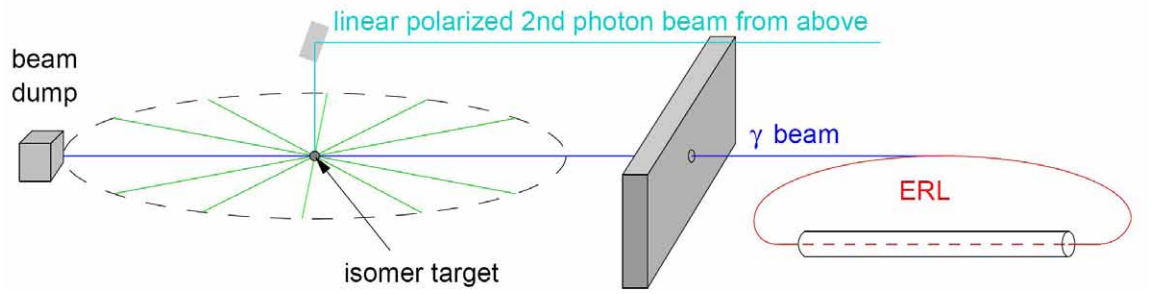

Figure 2: The halo neutron of the isomer target is released by a 2nd photon beam from above. The polarization of the photon beam injects the neutrons into the selected neutron guide.

The strongly directed neutron beams will feed elliptic or parabolic neutron guides [3] that transport the neutrons to various beam lines for neutron scattering (Fig. 4). Since the *E*-field of the second photon beam oscillates in opposite directions, two beam lines are fed at the same time. Because of the small size of the target, neutron beams from halo nuclei will be small and therefore particularly useful for the investigation of small samples and samples under extreme conditions. Rough estimates show that the halo neutron source will even be competitive for samples with a size of approximately 10 mm $\times$ 10 mm. Of course by increasing the γ-flux, the gains may be further increased by orders of magnitude [2].

References

[1] A. Taylor et al. A Route to the Brightest Possible Neutron Source? *Science*, 315:1092, 2007.
[2] D. Habs, M. Gross, P. G. Thirolf, and P. Böni. Neutron halo isomers in stable nuclei and their possible application for the production of low energy, pulsed, polarized neutron beams of high intensity and high brilliance. *Appl. Phys. B*, accepted for publication.
[3] P. Böni. New concepts for neutron instrumentation. *Nucl. Inst. and Meth. A*, 586:1, 2008.

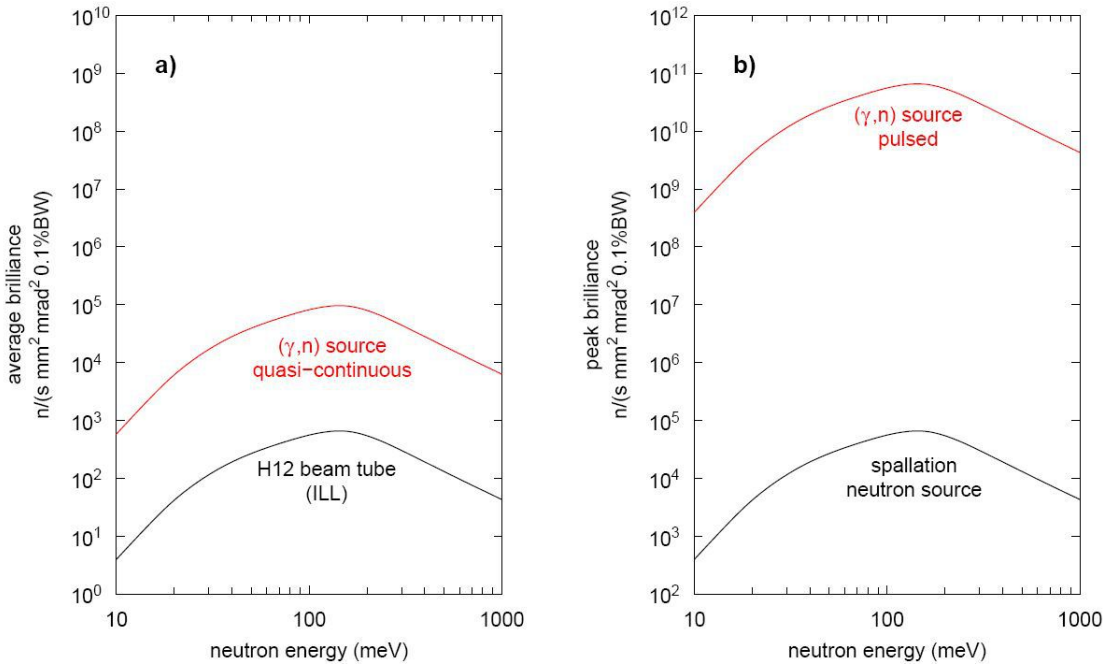

Figure 3: Average (a) and peak (b) brilliance of a continuous and pulsed neutron source, respectively, as a function of neutron energy. For the peak brilliance of the spallation source we increased the brilliance of the ILL by a factor of 100. The detailed dependence of the brilliance depends on the design of the neutron guides.

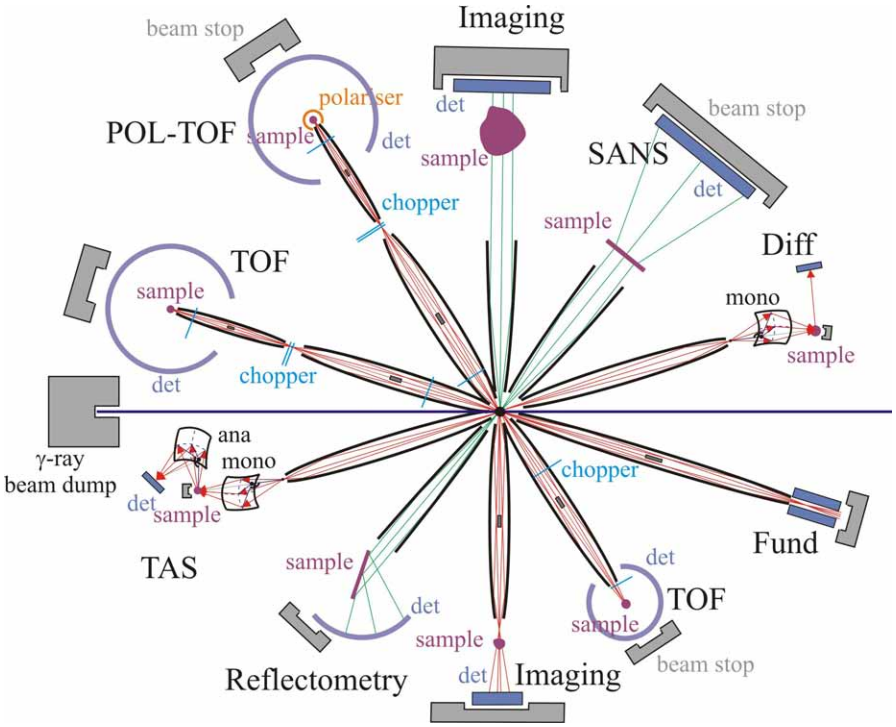

Figure 4: Experimental setup of a brilliant pulsed micro-neutron beam facility. The brilliant γ-ray shown in dark blue hits the neutron converter target producing the halo isomers.

Optimisation of Elliptic Neutron Guides for Triple-axis Spectroscopy

Marc Janoschek[1,2], Peter Böni[2], and Markus Braden[1]

[1] *II. Physikalisches Institut, Universität zu Köln, D-50937 Köln, Germany*
[2] *Physik Department E21, Technische Universität München, D-85748 Garching, Germany*

Recently, it was shown by means of Monte-Carlo simulations that by using an elliptic guide a flux gain of the order of 5 can be achieved compared to a conventional $m = 2$ guide [1]. The elliptic geometry reduces the number of reflections in the guide to essentially one which decreases the losses in the guide. Later it was experimentally demonstrated that the concept can be used to focus the neutrons on tiny samples inside a pressure cell [2]. We have carried out Monte-Carlo simulations to evaluate the use of such elliptic neutron guides for a new triple-axis spectrometer (TAS) that will be built at the end position of the cold guide NL-1 in the neutron guide hall of the research reactor FRM II in Munich, Germany.

For our simulations we used the Monte-Carlo neutron ray-tracing package McStas. The complete guide NL-1 including the cold-source of FRM II was modeled by means of the standard components of McStas. The boundary conditions for our simulations are given by a gap (G) in the guide of 400 mm length where the monochromator of the up-stream instrument N-REX$^+$ is situated and approximately 8 m of distance between this gap and the position of the monochromator of the TAS (M) (cf. Fig. 1).

We considered the two different implementations of an elliptic guide section between (G) and (M) that are illustrated in Fig. 1, where in both cases only horizontal focusing of the beam was employed. The first model (A) corresponds to a straight guide section with an elliptically tapered nose pointing towards (M) and is equivalent to the implementation of reference [3] (s. Fig. 1(a)) whereas the second variant (B) employs a full elliptic section (s. Fig. 1(b)). For both models a slit was placed at the position of the focal spot of the elliptic section that serves as a virtual source (VS) for a double focusing monochromator. In order to benchmark our results we additionally performed a simulation with a further variant (C) consisting of a conventional straight guide combined with a virtual source (s. Fig. 1(c)).

The comparison of both models showed that model (B) is superior to model (A) in several key aspects, namely intensity (≈50% more flux), focusing performance and beam divergence. The reasons for the better performance are mainly, (i) in model (B) less reflections are necessary to transport the neutrons through the neutron guide, and (ii) the entrance side of model (B) can be setup to reduce losses due to the gap in the neutron guide at the position of the previous instrument. This is explained in full detail in our publication[4] and here we focus on the results of model (B).

In Fig. 2 the simulated performance of a complete TAS setup based on model (B) is illustrated (for the details of the TAS s. [4]). The provided energy resolution and respective intensities have been obtained by performing constant-Q-scans (k_f fixed) on a virtual, cylindrical vanadium sample of 3 cm height and 6 mm diameter. As benchmark we have used model (C) in two limiting cases: (C1) the virtual source slit was set to D_{VS} = 30 mm and Rowland (symmetric) focusing of the monochromator was applied (high resolution), and (C2) the virtual source aperture was removed ($D_{VS} = \infty$) and the focusing was optimized for highest intensity.

As can be seen from Figs. 2(a) and (b) model (B1) with loutw = 0.3 m allows that for low values of final wave vectors k_f identical intensities as for the (high intensity) setup (C2) are achieved while at the same time identical energy resolution as for the high resolution setup (C1) can be realized. For k_f larger than 1.25 Å^{-1} the intensity is only slightly lower than for (C2) but still significantly higher than for (C1).

In summary, our results demonstrate that an elliptic guide section at the end of a conventional guide can be used to at least maintain the total neutron flux onto the sample, while significantly improving the energy resolution of the spectrometer. A more detailed description can be found in [4].

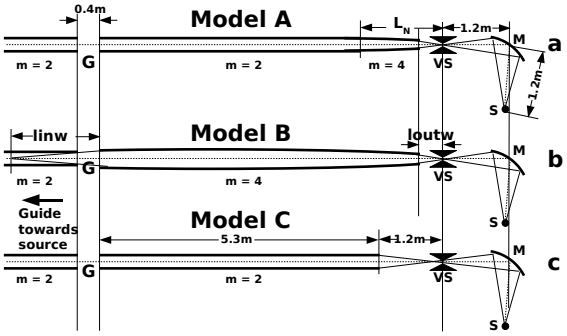

Figure 1: The different guide system setups that were compared via McStas simulations are illustrated. (a) Conventional guide with an elliptic tapered nose. (b) Complete elliptic guide. (c) Conventional straight guide for comparison.

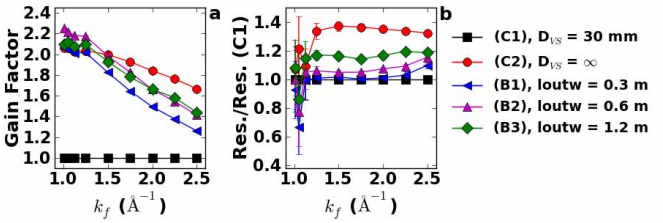

Figure 2: The intensity gain (a) and the resolution (b) at the sample position of different configurations of model (B) is compared to model (C1) (black squares), where the virtual source aperture was set to D_{VS} = 30 mm. loutw is the focal length of the elliptic section.

References

[1] C. Schanzer, P. Böni, U. Filges, and T. Hils. *Nucl. Inst. Meth. A*, 259:63, 2004.
[2] P. G. Niklowitz, C. Pfleiderer, S. Mühlbauer, P. Böni, T. Keller, P. Link, A. de Visser, J. A. Wilson, M. Votja, and J. A. Mydosh. *Physica B*, 404:2955, 2009.
[3] M. Boehm, S. Roux, A. Hiess, and J. Kulda. *J. Magn. Magn. Mater.*, 310:e965, 2007.
[4] M. Janoschek, P. Böni, and M. Braden. *Nucl. Inst. Meth. A*, 613:119, 2010.

Polarizing and focusing design of the KOMPASS spectrometer

Alexander Christoph Komarek[1,2], Andreas Ostermann[3], Peter Böni[2], and Markus Braden[1]

[1] *II. Physikalisches Institut, Universität zu Köln, Zülpicher Str. 77, D-50937 Köln, Germany*
[2] *Physik Department E21, Technische Universität München, D-85748 Garching, Germany*
[3] *Forschungsneutronenquelle Heinz Maier-Leibnitz (FRM II), Technische Universität München, D-85748 Garching, Germany*

The KOMPASS spectrometer is a new triple-axis spectrometer which will be built at the end position of the cold neutron guide NL1 at the FRM II. The main purpose of this instrument is the study of magnetic excitations with polarization analysis. In order to optimize the polarization of the neutron beam as well as neutron flux and resolution, new polarizing and focusing concepts have been contrived and optimized by elaborate Monte-Carlo ray-tracing simulations. By the invention of a novel triple-V cavity polarizer it was possible to attain exorbitant high degrees of polarization close to 100% together with rather high values of neutron transmission. Next, the neutron flux could be enhanced drastically by an optimized parabolic neutron focusing concept. Further, it was possible to enhance the neutron flux by a monochromator design optimized for the short distances of KOMPASS.

The Triple-V Polarizing Cavity

After simulating several polarizers, a new concept of a triple-V polarizing cavity turned out to yield surprisingly high values for polarization and transmission. This new polarizer consists of a consecutive series of three V-cavities and is subdivided into four channels which are situated within the focusing guide. The polarizing and focusing features are decoupled by a 90 degree rotation of the V-cavities around the beam axis. Fig. 1 shows the superior properties of the triple-V cavity compared to an equivalent setup with a double-V cavity.

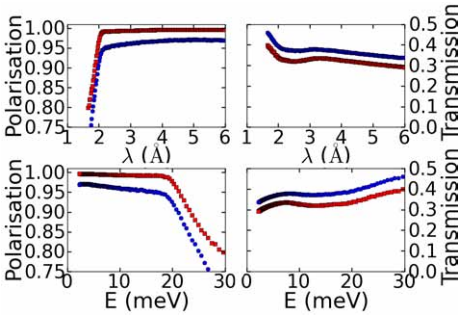

Figure 1: Polarization and transmission of triple-V-cavity (red squares) versus double-V-cavity (blue circles).

The Parabolic Focusing

In Ref. [1] an elliptic focusing concept was presented. We calculated different competing setups and found that a parabolic guide is superior to it: 1st, the intensity at the sample position is distinctly higher, see Fig. 2 (a-b); 2nd, the energy-resolution is remarkably better, see Fig. 2 (c-d); and 3rd, also the peak profile in transverse direction to **Q** does not show the multiple-peak structure of the elliptic concept, see Fig. 2 (e). The physical reason for the superior properties of the parabolic concept is that the parabolic guide focuses neutrons with small (zero) divergence from the whole entrance window into the focal point whereas the elliptic guide focuses neutrons with high divergence from the outer parts of the entrance window into its focal point. But at these distances from the reactor the intensity of neutrons with higher divergence are already significantly diminished.

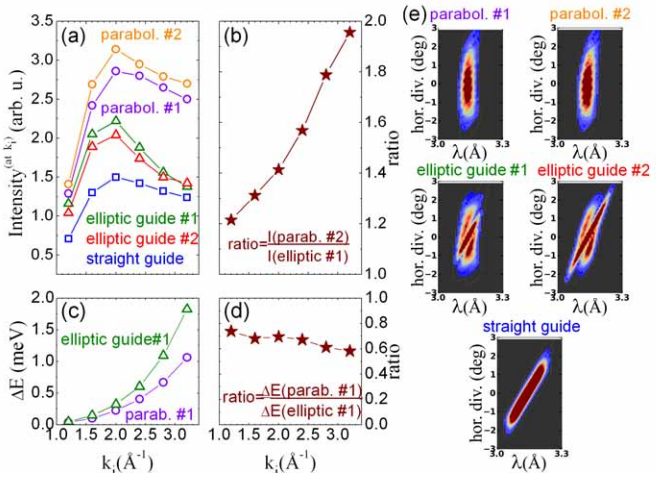

Figure 2: (a-b) Intensity as a function of of k_i for different parabolic configurations (#1/#2: with/without last nose) compared to elliptic and straight guides. (b-c) Energy resolution. (e) Intensity as a function of wavelength and divergence at $k_i = 2$ Å^{-1}.

The Double Focusing Monochromator

Finally, we were able to enhance the intensity further by additional ∼33% (on top) due to an optimized double focusing monochromator concept with smaller crystal size; see Fig. 3.

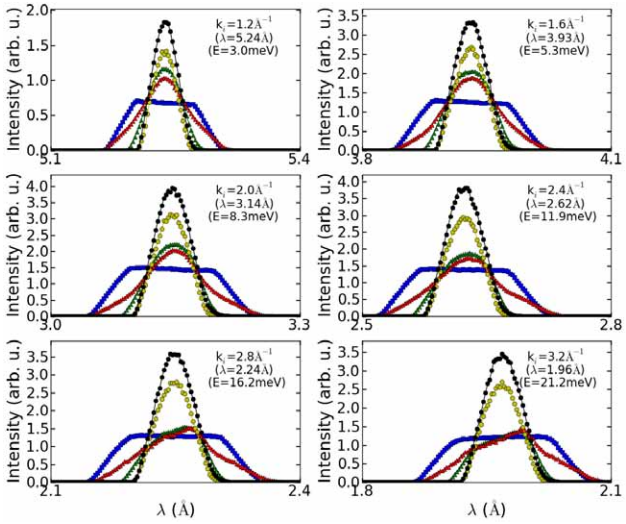

Figure 3: Intensity as a function of wavelength for different setups and values of k_i. Blue: straight guide; green/red: elliptic guides #1 and #2 corresponding to [1]; yellow: parabolic guide #2; black: parabolic guide #2 with optimized monochromator.

References

[1] M. Janoschek et al. *Nucl. Inst. Meth. A*, 613:119, 2010.

Shielding of Elliptic Guides with Direct Sight to the Moderator

Peter Böni[1], Florian Grünauer[2], and Christian Schanzer[3]

[1] *Physik Department E21, Technische Universität München, D-85748 Garching, Germany*
[2] *Physics Consulting, Herzog-Otto-Weg 17, D-85604 Zorneding, Germany*
[3] *SwissNeutronics, Neutron Optical Components, Brühlstrasse 28, CH-5313 Klingnau, Switzerland*

With the invention of elliptic guides, the neutron flux can be increased significantly even without sacrificing resolution [1]. In addition, the phase space homogeneity of the delivered neutrons is improved. We have performed Monte-Carlo simulations using the program package MCNP5 to calculate the shielding requirements for an elliptic guide geometry [2] assuming for the initial guide sections elements composed of super-polished Al-substrates [3].

Contour plots of the dose rate (DR) for neutron and γ-radiation of a curved guide using the approximate dimensions of the TASP-guide at SINQ [1] are shown in Fig. 1. Outside the direct line of sight, the DRs are massively reduced. It is the fast neutron group $E > 0.1$ MeV that is mostly responsible for the DR. These neutrons are emitted by the moderator and enter the guide. After the line of sight, they are moderated and scattered by the guide walls and the shielding thus leading to a fast decrease of the DR. The guided neutrons are not relevant for the DR of the neutrons. Similarly, the DR for the γ-radiation drops also significantly upstream of the line of sight. The γs are mostly produced by the interaction of the neutrons with the guide coating.

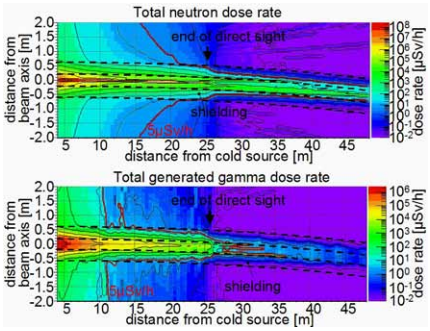

Figure 1: Contour plot of the total dose rate (DR) for neutrons (top) and γ-radiation (bottom) of a curved guide. Outside the direct line of sight of 25.6 m, the radiation levels drop quickly to below 1 μSv/h. The outer radius of the heavy concrete shielding is 0.6 m (broken black line).

Fig. 2 shows the contours of the DR for the neutron and γ-radiation for the elliptic guide. The comparison with the DR of the curved guide shows that the background is higher in the second half of the guide section. Obviously, the beam catcher does not help to reduce the background significantly: Most of the fast neutrons from the moderator pass the beam catcher and hit the guide structure downstream of it.

Similarly as for the curved guide, it is only the DR of the fast neutrons $E > 0.1$ MeV and of the γ-radiation in the energy window $E > 0.5$ MeV, which contribute significantly to the background. The background caused by the guided cold and thermal neutrons is irrelevant. The simulations show that the background as produced by the elliptic guide is well within the acceptable limits of a few μSv/h.

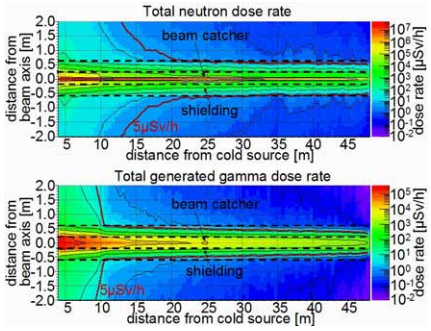

Figure 2: Contour plot of the total dose rate (DR) for neutrons (top) and γ-radiation (bottom) of an elliptic guide. The outer radius of the heavy concrete shielding is 0.6 m. Its outer contour is indicated by broken lines in black. The dark red contour indicates the DR-level of 5 μSv/h.

Of most concern are the fast neutrons hitting directly the sample in the focal point of the elliptic guide. The simulations demonstrate that the DR is only enhanced by a factor of 15 when compared with a curved guide. Considering, that the useful neutron flux is increased by approximately a factor of four or more by the elliptic design, the increase of the DR is irrelevant.

Elliptic guides have many advantages. One is that they deliver neutrons with a homogeneous and compact phase space. As shown in Fig. 3, the divergence of the neutrons can be tuned by the index *m* of the coating and by the ellipticity of the guide. Therefore, for a given divergence the *m*-value of the elliptic guide can be reduced when compared with a conventional guide.

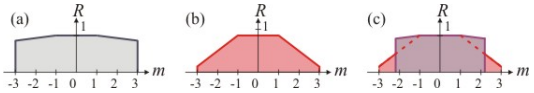

Figure 3: Reflectivity losses for an elliptic guide (a) and a conventional guide (b). The losses of a conventional guide are much larger due to the many reflections when compared with an elliptic guide, where the neutrons are reflected essentially once. (c) shows the reflectivity curve of an elliptic guide with a reduced divergence leading to a more compact phase space.

We have shown that the elliptic design for neutron guides does not lead to a problem with increased radiation at the sample position despite the direct line of sight to the moderator. With respect to the aging of neutron guides, elliptic guides are favorable too because the number of reflection of neutron is dramatically reduced. A further advantage of elliptic guides is the ease of adjusting the beam size and the divergence depending on the needs of the experiment [4].

References

[1] C. Schanzer, P. Böni, U. Filges, and T. Hils. *Nucl. Inst. Meth. A*, 529:63, 2004.
[2] P. Böni, F. Grünauer, and C. Schanzer. *Nucl. Inst. Meth. A*, 624:162–167, 2010.
[3] C. Schanzer, P. Böni, and M. Schneider. *J. Phys.: Conf. Series*, 251:012082, 2010.
[4] P. Böni. *Nucl. Inst. Meth. A*, 586:1, 2008.

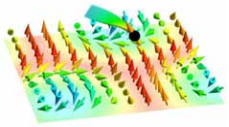

Chapter 6

Activities 2009/2010

Lectures, Courses and Seminars

A. Bauer	Tutor “Mathematische Methoden der Chemie I” (WS 2008/09)
	Tutor “Physik für Lebensmittelchemiker” (SS 2009)
	Tutor “Experimentalphysik 4” (SS 2001)
	Tutor “Experimentalphysik für Chemieingenieure und Restauratoren”
P. Böni	Lecture “Experimentalphysik I für Geodäsie und Geoinformation” (WS 2008/09; WS 2009/10)
	Exercises “Experimentalphysik I für Geodäsie und Geoinformation” (WS 2008/09; WS 2009/10)
	Lecture “Experimentalphysik II für Geodäsie und Geoinformation” (SS 2009; SS 2010)
	Exercises “Experimentalphysik II für Geodäsie und Geoinformation” (SS 2009; SS 2010)
	Lecture “Physics with Neutrons I” (WS 2010/11)
	Exercises “Physics with Neutrons I” (WS 2010/11)
	Seminar “Neutronen in Forschung und Industrie”, together with Prof. W. Petry, Prof. K. Schreckenbach and Dr. W. Häussler
	Seminar “Experimentelle Methoden in der Festkörperphysik” together with Prof. C. Pfleiderer and Dr. C. Hugenschmidt
	Seminar “Methoden und Experimente in der Neutronenstreuung” together with C. Morkel
	Solid State Colloquium of the Transregio TRR 80
R. Georgii	Lab course “Fortgeschrittenenpraktikum für Physiker” (at FRM II) (2009 and 2010)
	Organization 4th FRM II Workshop on Neutron Scattering in Rothenfels (2009)
W. Häußler	Seminar “Neutronen in Forschung und Industrie” together with P. Böni and W. Petry (2009 and 2010)
C. Hugenschmidt	Lecture “Physik mit Positronen I / II”
	Seminar “Experimentelle Methoden der Festköperphysik”, together with C. Pfleiderer and P. Böni
	Lab course “F-Praktikum Positronen-Annihilation”
F. Jonietz	Tutor “Experimentalphysik I” (WS 2008/09)
	Tutor “Experimentalphysik II” (SS 2009)
P. Pikart	Lab course “F-Praktikum Positronen-Annihilation”
	Lab course “Elektronikpraktikum” (WS 2009/10, SS 2010)
C. Pfleiderer	Lecture “Electronic Correlations and Magnetism 1” (WS 2008/09; WS 2009/10; WS 2010/11)
	Lecture “Electronic Correlations and Magnetism 2” (SS 2009; SS 2010)
	Lecture “Introduction to Crystal Growth” (SS 2009)
	Seminar “Vielteilchenphänomene und Streumethoden”, together with R. Hackl and W. Zwerger (SS 2009; SS 2010)
	Lecture “Physik stark korrelierter Elektronensysteme” (WS 2008/09)
	Seminar “Elektronische Korrelationen”, together with R. Hackl (WS 2009/10)
	Lecture “Experimental Physics for Chemical Engineering” (WS 2010/11)
	Seminar “Experimental Methods in Condensed Matter Physics”, together with C. Hugenschmidt and P. Böni

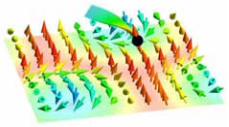

C. Piochacz	Lab course “F-Praktikum Positronen-Annihilation”
R. Ritz	Lab course “Physikalisches Grundlagenpraktium für Bachelor” (SS 2010) Tutor “Introduction to Solid State Physics”
B. Schillinger	Lab course “Elektronikpraktikum”
M. Schulz	Lab course “Elektronikpraktikum”
M. Reiner	Lab course “Physikpraktikum für Maschinenbauer” (SS 2010) Tutor “Physik mit Positronen I” (WS 2010/11)
M. Wagner	Tutor “Experimentalphysik 4” (SS 2010) Tutor “Experimentalphysik für Chemie-Ingenieurwesen und Restauratoren” (WS 2010/11)

Seminar “Neutronen in Industrie und Forschung” 2009

Date	Speaker	Title
Jan 12	G. Brandl	Introduction to Multiferroics and their study with neutrons
Jan 19	Dr. Y. Su	Neutron scattering on iron-arsenic-based superconductor compounds
Jan 26	C. Pioczaz	The beam enhancement devices at NEPOMUC for the Munich scanning positron microscope
Feb 9	Prof. T. Nylander	Neutron Reflectometry to Investigate the Delivery of Lipids and DNA to Interfaces
Feb 16	S. Gottlieb-Schönmeyer	Cu-Yb – a superstructural detective story
Feb 23	U. Wasmuth	Time- and space-resolved Residual-Stress-Analysis of Composite Castings
Apr 20	Dr. P. Štěpánek	Hierarchical structure of self-organized microemulsions investigated by SAXS, SANS and USANS
May 11	Dr. J. Wuttke	Ein Jahr Nutzerbetrieb am neuen Rückstreuspektrometer SPHERES
May 18	L. Canella	The PGAA Facility at FRM II
Jun 8	R. Hengstler	Fuel Development for Nuclear Research and Power Reactors
Jun 22	Dr. E. Faulhaber	Untersuchung der magnetischen Eigenschaften von $CeCu_2(Si_{1-x}Ge_x)_2$ mittels Neutronenstreuung
Jun 29	Prof. K. Rätzke	Free volume and positron annihilation in polymeric membranes and epoxides: selected applications
Jul 6	Dr. V. Hinkov	The spin-excitation spectrum in the normal and superconducting state of an iron-arsenide superconductor
Jul 13	P.-M. Lemoin	Fuel Development for the New Jules Horowitz Research Reactor
Jul 20	N. Munnikes	A NRSE-TAS study of phonon anomalies in conventional superconductors
Sep 21	Dr. P. G. Niklowitz	The “hidden order” in URu_2Si_2 studied by Larmor diffraction under pressure
Oct 19	Prof. Dr. M. Braden	Magnetism in layered ruthenates: from spin-triplet superconductivity to a Mott-insulator
Oct 26	Prof. Dr. Th. Hellweg	Dynamics of Bicontinuous Microemulsions and Lipid Vesicles
Nov 2	M. Jungwirth	Bestimmung des Gamma-Spektrums in einem intensiven Spaltneutronenstrahl
Nov 9	Prof. Dr. A. Zheludev	Magnetism of non-magnetic quantum magnets
Nov 16	Prof. Dr. O. Paris	Nanomaterials in the new light: Scattering experiments with synchrotron radiation and neutrons
Nov 23	Priv.-Doz. Dr. H. Schmidt	Neutronenreflektometrie zum Studium atomarer Diffusionsvorgänge auf der (Sub-)Nanometerskala
Nov 30	Dr. R. Mole	Neutron and EPR investigation of exchange interactions in cobalt dimers
Dec 7	Dr. W. Schweika	Spin Correlations in Frustrated Magnets
Dec 14	Dr. O. Holderer	Membrane Fluctuations in “classical” and supercritical microemulsions probed with neutron spin-echo spectroscopy

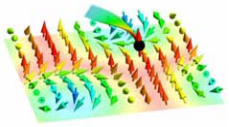

Seminar “Neutronen in Industrie und Forschung” 2010

Date	Speaker	Title
Jan 11	Prof. T. Soldner	Measurement of correlations in neutron decay. The PERC project
Jan 18	Dr. S. Petit	Spin lattice coupling in multiferroic $RMnO_3$
Jan 25	Dr. P. P. Deen	Exotic magnetic order studied by neutron polarization analysis
Feb 8	Dr. B. Nafradi	Low Temperature Spin Dynamics in a Haldane-spin Chain IPA-$CuCl_3$
Feb 22	Dr. W. Klein	The structural anomaly of zinc: Temperature dependent structure investigations of elemental zinc
Apr 26	Dr. M. Deppe	$CePd_{1-x}Rh_x$: From ferromagnetism to a quantum Griffiths phase
May 3	Prof. M. Kenzelmann	Coupled superconducting and magnetic order in CeCoIn5
May 10	Dr. C. Grünzweig	Visualization of magnetic domains and magnetization processes in bulk materials by neutron dark-field imaging
May 17	T. Mittermeier	Einführung in die Larmor Diffraktion
May 31	Prof. H. M. Ronnow	Low-dimensional quantum magnetism – neutrons in the quasi-particle zoo
Jun 7	F. Lux	Positronenphysik am FRM II
Jun 14	Prof. Dr. G. Badurek	Quantenphysikalische Experimente mit polarisierten Neutronen
Jun 21	Dr. M. Weik	Protein and hydration-water dynamics as assessed by neutron scattering and complementary biophysical methods
Jun 28	Prof. Dr. P. Fierlinger	The Search for the Neutron Electric Dipole Moment
Jul 5	Dr. J.-F. Moulin	Reflectomery and GISANS at REFSANS
Jul 12	Prof. K. Schreckenbach	Neutron Lifetime Measurement with the UCN trap-in-trap MAMBO II
Jul 19	Dr. C. Linsmeier	Die erste Wand von Fusionsreaktoren – eine Herausforderung für Materialentwicklung und -charakterisierung
Sep 13	Dr. Z. Revay	Das PGAA Instrument in Budapest und dessen Weiterentwicklung
Oct 25	Prof. M. T. Rekveldt	The role of the neutron in cosmology
Nov 8	Dr. T. Unruh	From neutron guides and choppers to molecular liquids and membranes – 9 years at FRM II: a review
Nov 15	Dr. J. Repper	High Resolution Neutron diffraction for materials investigations
Nov 22	Prof. F. Mezei	ESS neutron beams: new challenges and unprecedented opportunities
Nov 29	Dr. F. Piegsa	Polarised Neutrons and Nuclei in Radiography and Laue Diffraction
Dec 6	Dr. K. Habicht	The art of neutron scattering instrumentation – basic tools for basic concepts
Dec 13	Prof. Dr. P. Fierlinger	Physics opportunities with ultra-cold neutrons at the FRM II
Dec 20	Dr. W. Sprengel	Atomic Defects in Ultrafine-Grained Metals: Direct and Specific Studies for their Characterization and of their Kinetics

Publications 2009/2010

[1] T. Adams, S. Mühlbauer, A. Neubauer, W. Münzer, F. Jonietz, R. Georgii, B. Pedersen, P. Böni, A. Rosch, and C. Pfleiderer. Skyrmion Lattice Domains in $Fe_{1-x}Co_xSi$. *Journal of Physics: Conference Series*, 200(3):032001, 2010.

[2] S. T. Astner, R. A. Bundschuh, A. J. Beer, S. I. Ziegler, B. J. Krause, M. Schwaiger, M. Molls, A. L. Grosu, and M. Essler. Assessment of Tumor Volumes in Skull Base Glomus Tumors Using Gluc-Lys[^{18}F]-TOCA Positron Emission Tomography. *International Journal of Radiation Oncology, Biology, Physics*, 73(4):1135–1140, 2009.

[3] A. Bauer, A. Neubauer, C. Franz, W. Münzer, M. Garst, and C. Pfleiderer. Quantum Phase Transitions in Single-Crystal $Mn_{1-x}Fe_xSi$ and $Mn_{1-x}Co_xSi$: Crystal Growth, Magnetization, AC Susceptibility and Specific Heat. *Physical Review B*, 82(6):064404, 2010. Recommended as Editor's Choice.

[4] P. Böni, F. Grünauer, and C. Schanzer. Elliptic guides using super-polished metal substrates: Shielding issues. *Proceedings of ICANS-XIX*, ISSN 1019-6447:IP073, 2010.

[5] P. Böni, F. Grünauer, and C. Schanzer. Shielding of Elliptic Guides with Direct Sight to the Moderator. *Nuclear Instruments and Methods in Physics Research, Section A*, 624:162–167, 2010.

[6] P. Böni and K. Lefmann. Neutron Optics and Monte Carlo Simulations in NMI3. *Neutron News*, 20:26–29, 2009.

[7] P. Böni, W. Münzer, and A. Ostermann. Instrumentation with Polarized Neutrons. *Physica B: Condensed Matter*, 404:2620–2623, 2009.

[8] R. S. Brusa, S. Mariazzi, L. Ravelli, P. Mazzoldi, G. Mattei, W. Egger, C. Hugenschmidt, B. Löwe, P. Pikart, C. Macchi, and A. Somoza. Study of defects in implanted silica glass by depth profiling positron annihilation spectroscopy. *Nuclear Instruments and Methods in Physics Research, Section B*, 268:3186–3190, 2010.

[9] R. A. Bundschuh, M. Essler, J. Dinges, C. Berchtenbreiter, J. Mariss, A. Martínez-Möller, G. Delso, M. Hohberg, S. G. Nekolla, D. Schuly, S. I. Ziegler, and M. Schwaiger. Semiautomatic Algorithm for Lymph Node Analysis Corrected for Partial Volume Effects in Combined Positron Emission Tomography-Computed Tomography. *Molecular Imaging*, 9(6):319–328, 2010.

[10] E. Calzada, F. Grünauer, M. Mühlbauer, B. Schillinger, and M. Schulz. New design for the ANTARES-II facility for neutron imaging at FRM II. *Nuclear Instruments and Methods in Physics Research, Section A*, 605(1-2):50–53, 2009.

[11] H. Ceeh, S. Gärtner, C. Hugenschmidt, K. Schreckenbach, D. Schwalm, and P. Thirolf. Status report on the setup for the decay rate measurement of the negative positronium ion. *Journal of Physics: Conference Series*, 262(1):012011, 2010.

[12] J. Cizek, I. Prochazka, O. Melikhova, M. Vlach, N. Zaludova, G. Brauer, W. Anwand, W. Egger, P. Sperr, C. Hugenschmidt, R. Gemma, A. Pundt, and R. Kirchheim. Hydrogen-induced defects in Pd films. *physica status solidi (c)*, 6(11):2364–2366, 2009.

[13] J. P. Clancy, J. P. C. Ruff, S. R. Dunsiger, Y. Zhao, H. A. Dabkowska, J. S. Gardner, Y. Qiu, J. R. D. Copley, T. Jenkins, and B. D. Gaulin. Revisiting static and dynamic spin-ice correlations in $Ho_2Ti_2O_7$ with neutron scattering. *Physical Review B*, 79:014408, 2009.

[14] F. Demmel, S. Howells, C. Morkel, and W.-C. Pilgrim. Slow dynamics in liquid metals as seen by QENS. *Zeitschrift für Physikalische Chemie*, 224:83–99, 2010.

[15] W. J. Duncan, O. P. Welzel, D. Moroni-Klementowicz, C. Albrecht, P. G. Niklowitz, D. Grüner, M. Brando, A. Neubauer, C. Pfleiderer, N. Kikugawa, A. P. Mackenzie, and F. M. Grosche. Quantum phase transitions in $NbFe_2$ and $Ca_3Ru_2O_7$. *physica status solidi (b)*, 247:544–548, 2010.

[16] S. R. Dunsiger, J. P. Carlo, T. Goko, G. Nieuwenhuys, T. Prokscha, A. Suter, E. Morenzoni, D. Chiba, Y. Nishitani, T. Tanikawa, F. Matsukura, H. Ohno, J. Ohe, S. Maekawa, and Y. J. Uemura. Spatially homogeneous ferromagnetism of (Ga, Mn)As. *Nature Materials*, 9:299, 2010.

[17] G. Festa, C. Andreani, M. P. De Pascale, R. Senesi, G. Vitali, S. Porcinai, A. M. Giusti, R. Schulze, L. Canella, P. Kudejova, M. Mühlbauer, B. Schillinger, and Ancient Charm Collaboration. A non destructive stratigraphic and radiographic neutron study of Lorenzo Ghiberti's reliefs from Paradise and North doors of Florence Baptistery. *Journal of Applied Physics*, 106:074909, 2009.

[18] R. Frahm, D. Lützenkirchen-Hecht, M. Jentschel, W. Urban, J. Krempel, and K. Schreckenbach. Positron-Electron Pair Creation Near Threshold. *AIP Conference Proceedings*, 1090:554–558, 2009.

[19] R. Frahm, D. Lützenkirchen-Hecht, M. Jentschel, W. Urban, J. Krempel, and K. Schreckenbach. The Miracle of the Electron-Positron Pair Production Threshold. *Synchrotron Radiation News*, 22:31–38, 2009.

[20] C. Franz, C. Pfleiderer, A. Neubauer, M. Schulz, B. Pedersen, and P. Böni. Magnetization of $Pd_{1-x}Ni_x$ near quantum criticality. *Journal of Physics: Conference Series*, 200(1):012036, 2010.

[21] A. Frei, E. Gutsmiedl, C. Morkel, A. R. Müller, S. Paul, S. Rols, H. Schober, and T. Unruh. Understanding of ultra-cold neutron production in solid deuterium. *Europhysics Letters*, 92:62001, 2010.

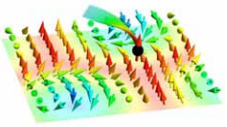

[22] A. Frei, E. Gutsmiedl, C. Morkel, A. R. Müller, S. Paul, M. Urban, H. Schober, S. Rols, T. Unruh, and M. Hölzel. Density of states in solid deuterium: Inelastic neutron scattering study. *Physical Review B*, 80:64301, 9 2009.

[23] A. Frei, K. Schreckenbach, B. Franke, F.J. Hartmann, T. Huber, R. Picker, S. Paul, and P. Geltenbort. Transmission Measurements of Guides for Ultra-Cold Neutrons using UCN Capture Aktivation Analysis of Vanadium. *Nuclear Instruments and Methods in Physics Research, Section A*, 612:349–353, 2009.

[24] S. Giemsa and P. Böni. Positioning unit. Patent Application, Aktenzeichen 10 2009 056 271.0, 2010.

[25] K. Habicht, M. Enderle, B. Fåk, K. Hradil, P. Böni, and T. Keller. Neutron resonance spin echo spectroscopy on split modes. *Journal of Physics: Conference Series*, 211:012028, 2010.

[26] K. Hain, C. Hugenschmidt, P. Pikart, and P. Böni. Spatially resolved positron annihilation spectroscopy on friction stir weld induced defects. *Science and Technology of Advanced Materials*, 11(2):025001, 2010.

[27] F. Hameed, B. Schillinger, A. Rohatsch, M. Zawishky, and H. Rauch. Investigations of stone consolidants by neutron imaging. *Nuclear Instruments and Methods in Physics Research, Section A*, 605(1-2):150–153, 2009.

[28] K. Hermann, B. J. Krause, R. A. Bundschuh, T. Dechow, and M. Schwaiger. Monitoring Response to Therapeutic Interventions in Patients With Cancer. *Seminars in Nuclear Medicine*, 39(3):210–232, 2009.

[29] R. Huber, P. Klemm, S. Neusser, B. Botters, A. Wittmann, M. Weiler, S. T. B. Goennenwein, C. Heyn, M. Schneider, P. Böni, and D. Grundler. Advanced techniques for all-electrical spectroscopy on spin caloric phenomena. *Solid State Communications*, 150:492–495, 2010.

[30] C. Hugenschmidt. *The Applications of Research Reactors*, volume in press, chapter X: Positron Source. International Atomic Energy Agency, 2009.

[31] C. Hugenschmidt. *International School of Physics "E. Fermi" Course CLXXIV: Physics with many positrons*, chapter Positron Sources and Positron Beams. IOS press Amsterdam, 2010.

[32] C. Hugenschmidt, J. Mayer, and K. Schreckenbach. High-resolution Auger-electron spectroscopy induced by positron annihilation on Fe, Ni, Cu, Zn, Pd, and Au. *Journal of Physics: Conference Series*, 225(1):012015, 2010.

[33] C. Hugenschmidt, P. Pikart, and K. Schreckenbach. Coincident Doppler-broadening spectroscopy of Si, amorphous SiO_2, and alpha-quartz using mono-energetic positrons. *physica status solidi (c)*, 6(11):2459–2461, 2009.

[34] C. Hugenschmidt, N. Qi, M. Stadlbauer, and K. Schreckenbach. Correlation of mechanical stress and Doppler broadening of the positron annihilation line in Al and Al alloys. *Physical Review B*, 80(22):224203, 2009.

[35] V. Hutanu, M. Janoschek, M. Meven, P. Böni, and G. Heger. MuPAD: Test at the hot single-crystal diffractometer HEiDi at FRM II. *Nuclear Instruments and Methods in Physics Research, Section A*, 612:155–160, 2009.

[36] M. Janoschek, F. Bernlochner, S. Dunsiger, C. Pfleiderer, P. Böni, B. Roessli, P. Link, and A. Rosch. Helimagnon bands as universal excitations of chiral magnets. *Physical Review B*, 81:214436, 2010.

[37] M. Janoschek, P. Böni, and M. Braden. Optimisation of elliptic neutron guides for triple-axis spectroscopy. *Nuclear Instruments and Methods in Physics Research, Section A*, 613:119, 2010.

[38] M. Janoschek, P. Fischer, J. Schefer, B. Roessli, V. Pomjakushin, M. Meven, V. Petricek, G. Petrakovskii, and L. Bezmaternikh. Single magnetic chirality in the magnetoelectric $NdFe_3(^{11}BO_3)_4$. *Physical Review B*, 81(9):094429, 2010.

[39] M. Janoschek, F. Jonietz, P. Link, C. Pfleiderer, and P. Böni. Helimagnons in the Skyrmion Lattice of MnSi. *Journal of Physics: Conference Series*, 200:032026, 2010.

[40] F. Jonietz, S. Mühlbauer, C. Pfleiderer, A. Neubauer, W. Münzer, A. Bauer, T. Adams, R. Georgii, P. Böni, R. A. Duine, K. Everschor, M. Garst, and A. Rosch. Spin Transfer Torques in MnSi at Ultralow Current Densities. *Science*, 330(6011):1648–1651, 2010.

[41] W. Kaltner, K. Lorenz, B. Schillinger, A. Jentys, and J. A. Lercher. Using Tomography for Exploring Complex Structured Emission Control Catalysts. *Catalysis Letters*, 134(1-2):24–30, 2010.

[42] N. Kardjilov, A. Hilger, M. Dawson, I. Manke, J. Banhart, M. Strobl, and P. Böni. Neutron tomography using an elliptic focusing guide. *Journal of Applied Physics*, 108:034905, 2010.

[43] D. J. Keeble, R. A. Mackie, W. Egger, B. Löwe, P. Pikart, C. Hugenschmidt, and T. J. Jackson. Identification of vacancy defects in a thin film perovskite oxide. *Physical Review B*, 81(6):064102, 2010.

[44] R. F. Kiefl, M. D. Hossain, B. M. Wojek, S. R. Dunsiger, G. D. Morris, T. Prokscha, Z. Salman, J. Baglo, D. A. Bonn, R. Liang, W. N Hardy, A. Suter, and E. Morenzoni. Direct measurement of the London penetration depth in $YBa_2Cu_3O_{6.92}$ using low-energy μSR. *Physical Review B*, 81:180502, 2010.

[45] D. Lamago, M. Hoesch, M. Krisch, R. Heid, K.-P. Bohnen, P. Böni, and D. Reznik. Measurement of strong phonon softening in Cr with and without Fermi-surface nesting by inelastic x-ray scattering. *Physical Review B*, 82:195121, 2010.

[46] S. Legl, C. Franz, A. Neubauer, C. Pfleiderer, D. Souptel, and G. Behr. Pressure dependence of the magnetization in Pr_5Si_3. *Physica B: Condensed Matter*, 404(19):2887–2889, 2009.

[47] S. Legl, C. Pfleiderer, and K. Krämer. Vibrating Coil Magnetometer for milli-Kelvin Temperatures. *Review of Scientific Instruments*, 81:043911, 2010.

[48] B. Löwe, K. Schreckenbach, and C. Hugenschmidt. Positron remoderation by gas cooling within an electric drift field. *Nuclear Instruments and Methods in Physics Research, Section B*, 268(5):529–532, 2010.

[49] T. Mairoser, A. Schmehl, A. Melville, T. Heeg, L. Canella, P. Böni, J. Schubert W. Zander, D. E. Shai, E. J. Monkman, K. M. Shen, D. G. Schlom, and J. Mannhart. Is there an intrinsic limit to the charge-carrier-induced increase of the Curie temperature of EuO? *Physical Review Letters*, 105:257206, 2010.

[50] A. Martínez-Möller, M. Souvatzoglou, G. Delso, R. A. Bundschuh, C. Chefdhotel, S. I. Ziegler, N. Navab, M. Schwaiger, and S. G. Nekolla. Tissue Classification as a Potential Approach for Attenuation Correction in Whole-Body PET/MRI: Evaluation with PET/CT Data. *J. Nucl. Med.*, 50(4):520–526, 2009.

[51] J. Mayer, C. Hugenschmidt, and K. Schreckenbach. Direct observation of the surface segregation of Cu in Pd by time-resolved positron-annihilation-induced Auger electron spectroscopy. *Physical Review Letters*, 105(20):207401, 2010.

[52] J. Mayer, C. Hugenschmidt, and K. Schreckenbach. High resolution positron annihilation induced Auger electron spectroscopy of the Cu $M_{2,3}VV$-transition and of Cu sub-monolayers on Pd and Fe. *Surface Science*, 604:1772–1777, 2010.

[53] J. Mayer, K. Schreckenbach, and C. Hugenschmidt. Recent development of the PAES set up at NEPOMUC. *physica status solidi (c)*, 6(11):2468–2470, 2009.

[54] S. Mühlbauer, B. Binz, F. Jonietz, C. Pfleiderer, A. Rosch, A. Neubauer, R. Georgii, and P. Böni. Skyrmion lattice in a chiral magnet. *Science*, 323(5916):915–919, 2009.

[55] S. Mühlbauer, C. Pfleiderer, P. Böni, E. M. Forgan, E. H. Brandt, A. Wiedenmann, and U. Keiderling. Intrinsic Bulk Vortex Dynamics Revealed by Time Resolved Small Angle Neutron Scattering. *Physica B: Condensed Matter*, 404:3231, 2009.

[56] S. Mühlbauer, C. Pfleiderer, P. Böni, E. M. Forgan, M. Laver, U. Keiderling, G. Behr, and D. Fort. Morphology of the Superconducting Vortex Lattice in Ultrapure Niobium. *Physical Review Letters*, 102(13):136408, 2009.

[57] W. Münzer, A. Neubauer, T. Adams, S. Mühlbauer, C. Franz, F. Jonietz, R. Georgii, P. Böni, B. Pedersen, M. Schmidt, A. Rosch, and C. Pfleiderer. Skyrmion lattice in the doped semiconductor $Fe_{1-x}Co_xSi$. *Physical Review B*, 81(4):041203, 2010.

[58] A. Neubauer, C. Pfleiderer, B. Binz, A. Rosch, R. Ritz, P. G. Niklowitz, and P. Böni. Topological Hall Effect in the A Phase of MnSi. *Physical Review Letters*, 102(18):186602, 2009.

[59] A. Neubauer, C. Pfleiderer, R. Ritz, P. G. Niklowitz, and P. Böni. Hall effect and magnetoresistance in MnSi. *Physica B: Condensed Matter*, 404(19):3163–3166, 2009.

[60] P. G. Niklowitz, C. Pfleiderer, T. Keller, M. Vojta, Y.-K. Huang, and J. Mydosh. Parasitic small-moment-antiferromagnetism and non-linear coupling of hidden order and antiferromagnetism in URu_2Si_2 observed by Larmor diffraction. *Physical Review Letters*, 104:106406, 2010.

[61] P. G. Niklowitz, C. Pfleiderer, S. Mühlbauer, P. Böni, T. Keller, P. Link, J. A. Wilson, M. Vojta, and J. A. Mydosh. New Angles on the Border of Antiferromagnetism in NiS_2 and URu_2Si_2. *Physica B: Condensed Matter*, 404:2955, 2009.

[62] B. Oberdorfer, E.-M. Steyskal, W. Sprengel, W. Puff, P. Pikart, C. Hugenschmidt, M. Zehetbauer, R. Pippan, and R. Würschum. In situ probing of fast defect annealing in Cu and Ni with a high-intensity positron beam. *Physical Review Letters*, 105(14):146101, 2010.

[63] K. Osterloh, M. Jechow, D. Fratzscher, N. Wrobel, U. Zscherpel, U. Ewert, T. BÃ¼cherl, B. Schillinger, A. Schwabe, A. Hasenstab, P. Weiss, C. Weiss, and T. Tannert. Durchstrahlungsverfahren – ein komplexer Einblick in Objekte, ohne sie zu zerlegen. *METALLA*, 3:52–54, 2010.

[64] S. R. Parnell, E. Babcock, K. Nanighoff, M. W. A. Skoda, S. Boag, S. Masalovich, R. Georgii, and J. M. Wild. Study of spin-exchange optically pumped ^{3}He cells with high polarisation and long lifetimes. *Nuclear Instruments and Methods in Physics Research, Section A*, 598(3):774–778, 2009.

[65] J. Perlich, V. Körstgens, E. Metwalli, L. Schulz, R. Georgii, and P. Müller-Buschbaum. Solvent content in thin spin-coated polystyrene homopolymer films. *Macromolecules*, 42:337–344, 2009.

[66] C. Pfleiderer. Superconducting phases of f-electron compounds. *Reviews of Modern Physics*, 81:1551, 2009. Contribution upon request of the editor.

[67] C. Pfleiderer. Magnetismus mit Drehsinn. *Physik Journal*, page 25, November 2010.

[68] C. Pfleiderer, T. Adams, A. Bauer, W. Biberacher, B. Binz, F. Birkelbach, P. Böni, C. Franz, R. Georgii, M. Janoschek, F. Jonietz, T. Keller, R. Ritz, S. Mühlbauer, W. Münzer, A. Neubauer, B. Pedersen, and A. Rosch. Skyrmion lattices in metallic and semiconducting B20 transition metal compounds. *Journal of Physics: Condensed Matter*, 22(16):164207, 2010.

[69] C. Pfleiderer, P. Böni, C. Franz, T. Keller, A. Neubauer, P. Niklowitz, P. Schmakat, M. Schulz, Y.-K. Huang, J. Mydosh, M. Vojta, W. Duncan, F. Grosche, M. Brando, M. Deppe, C. Geibel, F. Steglich, A. Krimmel, and A. Loidl. Search for Electronic Phase Separation at Quantum Phase Transitions. *Journal of Low Temperature Physics*, 161:167–181, 2010.

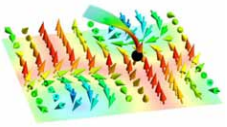

[70] C. Pfleiderer, A. Neubauer, S. Mühlbauer, F. Jonietz, M. Janoschek, S. Legl, R. Ritz, W. Münzer, C. Franz, P. G. Niklowitz, T. Keller, R. Georgii, P. Böni, B. Binz, A. Rosch, U. K. Rössler, and A. N. Bogdanov. Quantum order in the chiral magnet MnSi. *Journal of Physics: Condensed Matter*, 21(16):164215, 2009.

[71] C. Pfleiderer and A. Rosch. Condensed-matter physics - Single skyrmions spotted. *Nature*, 465:880–881, 2010.

[72] A. Pichlmaier, V. Varlamov, K. Schreckenbach, and P. Geltenbort. Neutron lifetime measurement with the UCN trap-in-trap MAMBO II. *Physics Letters B*, 693(3):221–226, 2010.

[73] P. Pikart, C. Hugenschmidt, and K. Schreckenbach. Doppler-broadening (DB) measurement of ionic liquids using a monoenergetic positron beam. *physica status solidi (c)*, 6(11):2487–2489, 2009.

[74] R. Ritz, S. Mühlbauer, C. Pfleiderer, T. Keller, J. White, M. Laver, E.M. Forgan, R. Cubitt, C. Dewhurst, P.G. Niklowitz, A. Prokofiev, and E. Bauer. Distribution of Lattice Constants in $CePt_3Si$ Observed by Larmor Diffraction and SANS. *Journal of Physics: Conference Series*, 200:012165, 2010.

[75] J. Rodriguez, A. A Aczel, J. P. Carlo, S. R. Dunsiger, G. J. Macdougall, P. L. Russo, A. T. Savici, Y. J. Uemura, C. R. Wiebe, and G. M. Luke. Study of the Ground State Properties of $LiHo_xY_{1-x}F_4$ Using Muon Spin Relaxation. *Physical Review Letters*, 105:107203, 2010.

[76] C. Schanzer, P. Böni, and M. Schneider. High Performance Supermirrors on Metallic Substrates. *Journal of Physics: Conference Series*, 251:012082, 2010.

[77] B. Schillinger. Various neutron imaging methods at the FRM II reactor source and potential features at a spallation source installation. *Nuclear Instruments and Methods in Physics Research, Section A*, 600:28–31, 2009.

[78] B. Schillinger, P. Böni, C. Breunig, E. Calzada, C. Leroy, M. Mühlbauer, and M. Schulz. A neutron optical periscope used for neutron imaging. *Nuclear Instruments and Methods in Physics Research, Section A*, 605(1-2):40–42, 2009.

[79] A. Schmehl, V. Vaithyanathan, A. Herrnberger, S. Thiel, C. Richter, T. Heeg, M. Röckerath, L. F. Kourkoutis, S. Mühlbauer, P. Böni, D. A. Muller, Y. Barash, J. Schubert, J. Mannhart, and D. G. Schlom. Comment on "Half-metallicity in europium oxide conductively matched with silicon". *Physical Review B*, 610:237301, 2009.

[80] M. Schneider, J. Stahn, and P. Böni. Focusing Cold Neutrons: Performance of a Laterally Graded and Parabolically Bent Multilayer. *Nuclear Instruments and Methods in Physics Research, Section A*, 610:530–533, 2009.

[81] K. Schreckenbach, C. Hugenschmidt, B. Löwe, J. Maier, P. Pikart, C. Piochacz, and M. Stadlbauer. Performance of the (n,γ)-based positron beam facility NEPOMUC. *AIP Conference Proceedings*, 1090(1):549–553, 2009.

[82] L. Schulz, W. Schirmacher, A. Omran, V. R. Shah, P. Böni, W. Petry, and P. Müller-Buschbaum. Elastic torsion effects in magnetic nanoparticle diblock-copolymer structures. *Journal of Physics: Condensed Matter*, 22:346008, 2010.

[83] M. Schulz, P. Böni, E. Calzada, M. Mühlbauer, A. Neubauer, and B. Schillinger. A polarizing neutron periscope for neutron imaging. *Nuclear Instruments and Methods in Physics Research, Section A*, 605(1-2):43–46, 2009.

[84] M. Schulz, P. Böni, E. Calzada, M. Mühlbauer, and B. Schillinger. Energy-dependent neutron imaging with a double crystal monochromator at the ANTARES facility at FRM II. *Nuclear Instruments and Methods in Physics Research, Section A*, 605(1-2):33 – 35, 2009.

[85] M. Schulz, P. Böni, C. Franz, A. Neubauer, E. Calzada, M. Mühlbauer, B. Schillinger, C. Pfleiderer, A. Hilger, and N. Kardjilov. Comparison of Polarizers for Neutron Radiography. *Journal of Physics: Conference Series*, 251(1):012068, 2010.

[86] M. Schulz, A. Neubauer, S. Masalovich, M. Mühlbauer, E. Calzada, B. Schillinger, C. Pfleiderer, and P. Böni. Towards a Tomographic Reconstruction of Neutron Depolarization Data. *Journal of Physics: Conference Series*, 211(1):012025, 2010.

[87] M. Schulz, A. Neubauer, M. Mühlbauer, E. Calzada, B. Schillinger, C. Pfleiderer, and P. Böni. Polarized neutron radiography with a periscope. *Journal of Physics: Conference Series*, 200(11):112009, 2010.

[88] N. Semioshkina, I. Fiedler, B. Schillinger, A. Ulanovsky, V. Potapov, O. Ivanov, F. M. Wagner, and U. Gerstmann. Comparison of three non-destructive methods to measure Sr-90 in human tooth samples. In *Radiation Measurements, Special Issue*. Elsevier, 2010.

[89] M. S. Skidmore, R. M. Ambrosi, D. Vernon, E. Calzada, G. K. Benedix, T. Bücherl, and B. Schillinger. Prompt gamma-ray activation analysis of Martian analogues at the Forschungsneutronenquelle Heinz Maier-Leibnitz neutron reactor and the verification of a Monte Carlo planetary radiation environment model. *Nuclear Instruments and Methods in Physics Research, Section A*, 607:421–431, 2009.

[90] T. Soldner, V. Nesvizhevsky, C. Plonka-Spehr, K. Protasov, K. Schreckenbach, and O. Zimmer, editors. *Proceedings of the International Workshop on Particle Physics with Slow Neutrons*, volume 611 of *Nuclear Instruments and Methods in Physics Research, Section A*, 2009.

[91] A. Strzelec, D. Foster, H. Bilheux, C. Daw, C. Rutland, B. Schillinger, and M. Schulz. Neutron Imaging of Diesel Particulate Filters. *SAE international*, pages 2009–01–2735, 2009.

Conference, Workshop and Seminar Contributions 2009/2010

[1] T. Adams, A. Bauer, S. Mühlbauer, C. Franz, F. Jonietz, W. Münzer, A. Neubauer, R. Georgii, A. Rosch, and C. Pfleiderer. Evolution of the Skyrmion Lattice in $Mn_{1-x}Fe_xSi$. Poster. *International Conference on Magnetism (ICM), Karlsruhe, Germany, July 2009.*

[2] T. Adams, A. Bauer, A. Neubauer, C. Franz, P. Böni, C. Pfleiderer, S. Mühlbauer, R. Georgii, and B. Pedersen. Quantum Phase Transitions in $Mn_{1-x}Fe_xSi$ and $Mn_{1-x}Co_xSi$: II. Small Angle Neutron Scattering. Talk. *Frühjahrstagung der Deutschen Physikalischen Gesellschaft, Regensburg, Germany, March 2010.*

[3] T. Adams, S. Mühlbauer, A. Bauer, A. Neubauer, C. Franz, R. Georgii, and C. Pfleiderer. Skyrmion Lattice in $Mn_{1-x}Fe_xSi$ and $Mn_{1-x}Co_xSi$. Poster. *Deutsche Tagung für Forschung mit Synchrotronstrahlung, Neutronen und Ionenstrahlen an Grossgeräten (SNI 2010), Berlin, Germany, February 2010.*

[4] T. Adams, S. Mühlbauer, A. Bauer, A. Neubauer, C. Franz, R. Georgii, and C. Pfleiderer. Skyrmion Lattice in $Mn_{1-x}Fe_xSi$ and $Mn_{1-x}Co_xSi$. Poster. *Hercules Specialized Course 12: Synchrotron Radiation and Neutron for Extreme Conditions Studies, Grenoble, France, October 2010.*

[5] T. Adams, S. Mühlbauer, W. Münzer, A. Neubauer, F. Jonietz, C. Franz, R. Georgii, P. Böni, A. Rosch, and C. Pfleiderer. Skyrmion Lattice in a Doped Semiconductor. Poster. *FRM II User Meeting, Garching, Germany, May 2009.*

[6] T. Adams, C. Pfleiderer, S. Mühlbauer, A. Neubauer, W. Münzer, F. Jonietz, C. Franz, M. Janoschek, A. Bauer, F. Birkelbach, R. Ritz, S. Legl, P. Niklowitz, B. Pedersen, P. Link, R. Georgii, and P. Böni. Skyrmion Lattice in a Doped Semiconductor. Talk. *Frühjahrstagung der Deutschen Physikalischen Gesellschaft, Dresden, Germany, March 2009.*

[7] T. Adams, C. Pfleiderer, S. Mühlbauer, A. Neubauer, W. Münzer, F. Jonietz, C. Franz, M. Janoschek, A. Bauer, F. Birkelbach, R. Ritz, S. Legl, P. Niklowitz, B. Pedersen, P. Link, R. Georgii, and P. Böni. Skyrmion Lattice in a Doped Semiconductor. Talk. *4th FRM II Workshop on Neutron Scattering, Rothenfels, Germany, June 2009.*

[8] T. Adams, J. Repper, M. Rahn, P. Böni, C. Pfleiderer, S. Dunsiger, and R. Georgii. Neutron scattering in Mn_3Si with elliptic neutron guides. Poster. *TRR80 Retreat Meeting, October 2010.*

[9] T. Adams, J. Repper, M. Rahn, P. Böni, C. Pfleiderer, S. Dunsiger, and R. Georgii. Neutron scattering in Mn_3Si with elliptic neutron guides. Poster. *FRM II User Meeting, Garching, Germany, October 2010.*

[10] M. Althammer, M. Wagner, A. Brandlmaier, M. Weiler, S. Geprägs, R. Gross, and S. T. B. Gönnenwein. Angle-dependent magnetotransport in Nickel thin films. Poster. *Frühjahrstagung der Deutschen Physikalischen Gesellschaft, Regensburg, Germany, March 2009.*

[11] A. Bauer and T. Adams. MnSi – Introduction. Talk. *Workshop on MnSi, Garching, Germany, May 2010.*

[12] A. Bauer, T. Adams, C. Franz, S. Mühlbauer, F. Jonietz, A. Neubauer, W. Münzer, R. Georgii, and C. Pfleiderer. Doping dependence of the skyrmion lattice in $Mn_{1-x}Fe_xSi$ and $Mn_{1-x}Co_xSi$. Talk. *4th FRM II Workshop on Neutron Scattering, Rothenfels, Germany, June 2009.*

[13] A. Bauer, T. Adams, C. Franz, A. Neubauer, S. Mühlbauer, M. Garst, and C. Pfleiderer. Quantum Phase Transitions in $Mn_{1-x}Fe_xSi$ and $Mn_{1-x}Co_xSi$: (Crystal Growth), Magnetization and Specific Heat. Talk. *Workshop on MnSi, Garching, Germany, May 2010.*

[14] A. Bauer, T. Adams, C. Franz, A. Neubauer, S. Mühlbauer, M. Garst, and C. Pfleiderer. Quantum Phase Transitions in $Mn_{1-x}Fe_xSi$ and $Mn_{1-x}Co_xSi$: I. Crystal Growth, Magnetization and Specific Heat. Talk. *Frühjahrstagung der Deutschen Physikalischen Gesellschaft, Regensburg, Germany, March 2010.*

[15] A. Bauer, T. Adams, C. Franz, A. Neubauer, S. Mühlbauer, F. Jonietz, W. Münzer, R. Georgii, and C. Pfleiderer. Single Crystal Growth of $Mn_{1-x}Fe_xSi$ and $Mn_{1-x}Co_xSi$. Talk. *DGKK-Arbeitskreis-Treffen "Intermetallische und oxidische Systeme mit Spin- und Ladungskorrelationen", Karlsruhe, Germany, October 2009.*

[16] A. Bauer, T. Adams, C. Franz, A. Neubauer, S. Mühlbauer, F. Jonietz, W. Münzer, R. Georgii, and C. Pfleiderer. Skyrmion Lattices in B20 Transition Metal Compounds. Talk. *Workshop on High Pressure Techniques, Garching, Germany, December 2009.*

[17] A. Bauer, T. Adams, C. Franz, A. Neubauer, S. Mühlbauer, F. Jonietz, W. Münzer, R. Georgii, and C. Pfleiderer. Quantum phase transitions in $Mn_{1-x}Fe_xSi$ and $Mn_{1-x}Co_xSi$. Talk. *DGKK Deutsche Kristallzüchtungstagung, Freiburg, Germany, March 2010.*

[18] A. Bauer, T. Adams, S. Mühlbauer, C. Franz, F. Jonietz, W. Münzer, A. Neubauer, R. Georgii, A. Rosch, and C. Pfleiderer. Evolution of the Skyrmion Lattice in $Mn_{1-x}Co_xSi$. Poster. *International Conference on Magnetism (ICM), Karlsruhe, Germany, July 2009.*

[19] A. Bauer, C. Franz, T. Adams, K. Mittermüller, D. Mallinger, S. Gottlieb-Schönmeyer, A. Regnat, A. Neubauer, M. Garst, and C. Pfleiderer. Single Crystal Growth of Intermetallic Compounds at TUM. Talk. *DGKK-Arbeitskreis-Treffen "Intermetallische und oxidische Systeme mit Spin- und Ladungskorrelationen", München, Germany, October 2010.*

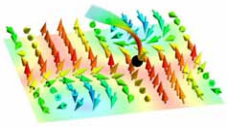

[20] A. Bauer, K. Mittermüller, A. Regnat, S. Gottlieb-Schönmeyer, and C. Pfleiderer. Static UHV Electrotransport and Preparation of itinerant AFMs. Poster. *TRR80-Retreat Meating, Freising, Germany, October 2010.*

[21] P. Böni. Funktionalität von Bulk und Nanostrukturen. Talk. *Begutachtung des Transregioantrags TRR 80, DFG, Augsburg, Germany, September 2009.*

[22] P. Böni. Phason Modes in Cr. Talk. *4th FRM II Workshop on Neutron Scattering, Burg Rothenfels am Main, Germany, June 2009.*

[23] P. Böni. Die Neutronenquelle FRM II - Brilliant und einmalig. Talk. *Transregio Kick-Off Meeting, Institut für Physik, Universität Augsburg, Germany, March 2010.*

[24] P. Böni. Introduction to Neutron Scattering. Invited Talk. *TRR 80, Focused Lectures of the Integrated Graduate School, Garching, Germany, June 2010.*

[25] P. Böni. Magnetische Wirbel in Mangansilizium: Neutronenstreuung am FRM II. Talk. *TUMlive Videokonferenz Deutsches Museum, Munich, Germany, January 2010.*

[26] P. Böni. Neutronenstrahlen: Eine Sonde zur Messung von dynamischen Prozessen in stark korrelierten Elektronensystemen. Invited Talk. *Physik Kolloquium, Augsburg, Germany, May 2010.*

[27] P. Böni, F. Grünauer, and C. Schanzer. Stability and Shielding Issues of Elliptic Guides. Talk. *Workshop on Neutron Delivery Systems, Institut Laue-Langevin, Grenoble, France, July 2009.*

[28] P. Böni, F. Grünauer, and C. Schanzer. Elliptic Guides Using Super-Polished Metal Substrates: Shielding Issues. Talk. *International Conference on Advanced Neutron Sources (ICANS-XIX), Grindelwald, Switzerland, March 2010.*

[29] P. Böni, D. Lamago, D. Reznik, K.-P. Bohnen, M. Hoesch, M. Krisch, and R. Heid. Phonon Softening in Cr with and without Fermi Surface Nesting. Talk. *Deutsche Tagung für Forschung mit Synchrotronstrahlung, Neutronen und Ionenstrahlen an Grossgeräten (SNI 2010), Berlin, Germany, February 2010.*

[30] P. Böni, S. Mühlbauer, B. Binz, F. Jonietz, C. Pfleiderer, M. Janoschek, P. Link, A. Rosch, A. Neubauer, and R. Georgii. Skyrmion Lattice in MnSi. Talk. *XIV International Conference on Small-Angle Scattering SAS-2009, September 2009.*

[31] P. Böni and R. Valicu. Advanced Focusing Techniques. Talk. *NMI3/FP7 Launch Meeting, Villigen PSI, Switzerland, March 2009.*

[32] P. Böni and R. Valicu. High Flux Reflectometry and Energy Analysis. Talk. *NMI3/FP7 Launch Meeting, Villigen PSI, Switzerland, March 2009.*

[33] G. Brandl. Miau and Wow: MIEZE studies in MnSi. Talk. *Workshop on High Pressure Techniques, Garching, Germany, December 2009.*

[34] G. Brandl, R. Georgii, C. Pfleiderer, and P. Böni. Dynamics in the B-T Phase Diagram of MnSi measured with MIEZE. Talk. *Frühjahrstagung der Deutschen Physikalischen Gesellschaft, Regensburg, Germany, March 2010.*

[35] S. R. Dunsiger. Investigation of Ferromagnetic Semiconductors through Depth Resolved Spin Resonance Techniques. Talk. *Super-PIRE / REIMEI / MWN joint Kickoff Meeting, Knoxville, Tennessee, October 2010.*

[36] S. R. Dunsiger. Investigation of Ferromagnetic Semiconductors through Depth Resolved Spin Resonance Techniques. Talk. *2. TUM Nanomagnetik Workshop, Technische Universität München, Garching, Germany, January 2010.*

[37] C. Franz, R. Ritz, S.Legl, A. Neubauer, C. Pleiderer, and M. Schulz. Ferromagnetic quantum phase transition on $Pd_{1-x}Ni_x$. Talk. *Frühjahrstagung der Deutschen Physikalischen Gesellschaft, Dresden, Germany, March 2009.*

[38] C. Franz, M. Schulz, A. Neuabauer, C. Pleiderer, and P. Böni. Nature of the quantum phase transition in $Pd_{1-x}Ni_x$. Talk. *Forschergruppentreffen der DFG, Karlsruhe, Germany, June 2009.*

[39] C. Franz, M. Schulz, A. Neubauer, P. Böni, and R. Ritz. Ferromagnetic quantum phase transition in $Pd_{1-x}Ni_x$. Poster. *FRM II User Meeting, Munich, Germany, May 2009.*

[40] C. Franz, M. Schulz, A. Neubauer, P. Böni, and R. Ritz. Ferromagnetic quantum phase transition in $Pd_{1-x}Ni_x$. Poster. *International Conference on Magnetism (ICM), Karlsruhe, Germany, July 2009.*

[41] C. Franz, M. Schulz, A. Neubauer, C. Pfleiderer, and P. Böni. Investigation of the quantum critical behaviour of $Pd_{1-x}Ni_x$: A challenge to crystal growth. Talk. *Deutsche Kristallzüchtertagung, Karlsruhe, Germany, July 2009.*

[42] C. Franz, M. Schulz, A. Neubauer, C. Pfleiderer, and P. Böni. Neutron depolarization and magnetization at the ferromagnetic quantum phase transition of $Pd_{1-x}Ni_x$. Talk. *4th FRM II Workshop on Neutron Scattering, Rothenfels, Germany, June 2009.*

[43] R. Georgii. MIEZE measurements in the B-T phase diagram of MnSi. Invited Talk. *Institute seminar of the Argonne National Lab, Chicago, USA, October 2009.*

[44] R. Georgii. MIEZE in a box: The Skyrmions in MnSi and the polymer F127. Talk. *Conference on Polarized Neutrons Condensed Matter Investigations, Delft, The Netherlands, July 2010.*

[45] R. Georgii, G. Brandl, and P. Böni. MIEZE measurements at MIRA. Poster. *Conference on Polarized Neutrons and Synchrotron X-rays for Magnetism, Bonn, Germany, August 2009.*

[46] R. Georgii, W. Häussler, P. Böni, G. Brandl, and R. Schwikowski. MIEZE - First results and perspectives. Talk. *International Conference on Neutron Scattering (ICNS), Knoxville, USA, May 2009.*

[47] C. Hugenschmidt. Coincidence Doppler-Broadening Spectroscopy for Element Selective Studies. Invited Lecture. *ISPS - International School on Positron Studies, Kolkata, India, January 2009.*

[48] C. Hugenschmidt. Experiments at the High-Intensity Positron Source NEPOMUC: Applications for Bulk and Surface Studies. Invited Talk. *International Coincidence Workshop, Max-Planck Society, Ringberg, Germany, December 2009.*

[49] C. Hugenschmidt. High Selective Surface Studies Using the Low-Energy Positron Beam at NEPOMUC. Invited Talk. *Institut für Materialwissenschaft, Universität Kiel, October 2009.*

[50] C. Hugenschmidt. Intense Positron Beams for Application in Surface and Materials Science. Invited Talk. *ASR 2009 - Advanced Science Research Symposium 2009: Positron, Muon and other exotic particle beams for materials and atomic sciences, Tokai, Japan, November 2009.*

[51] C. Hugenschmidt. Metals and Oxides Studied by Coincident Doppler-Broadening Spectroscopy. Invited Talk. *The XV International Conference on Positron Annihilation (ICPA-15), Kolkata, India, January 2009.*

[52] C. Hugenschmidt. Positron Sources and Positron Beams. Invited Talk. *International School of Physics Enrico Fermi: Physics with many Positrons, Varenna, Italy, July 2009.*

[53] C. Hugenschmidt. From the Surface to the Bulk: Application of Low-Energy Positron Beams of Highest Intensity. Invited Talk. *TRR Seminar, Experimental Physics, University Augsburg, Germany, June 2010.*

[54] C. Hugenschmidt. The Low-Energy High-Intensity Positron Beam at NEPOMUC and Novel Positron Beam Applications. Invited Talk. *Institute Seminar, ANSTO, Sydney, Australia, August 2010.*

[55] C. Hugenschmidt. The Status of the Positron Beam Facility NEPOMUC and (Coincident) Doppler Broadening Spectroscopy on Metallic Systems. Plenary Talk. *12th International Workshop on Slow Positron Beam Techniques for Solids and Surfaces, SLOPOS-12, Magnetic Island, Australia, August 2010.*

[56] M. Janoschek. Goldstone modes in helical magnets. Talk. *International Conference on Magnetism (ICM), Karlsruhe, Germany, July 2009.*

[57] M. Janoschek. Goldstone modes in helical magnets. Talk. *Frühjahrstagung der Deutschen Physikalischen Gesellschaft, Dresden, Germany, March 2009.*

[58] M. Janoschek. Goldstone modes in helical magnets. Talk. *Korrelationstage, Dresden, Germany, March 2009.*

[59] M. Janoschek. Goldstone modes in helical magnets. Poster. *International Conference on Neutron Scattering, Knoxville, USA, May 2009.*

[60] M. Janoschek. Optimisation of elliptic neutron guides for triple axis spectroscopy. Talk. Conference on *Neutron Delivery Systems, Grenoble, France, June 2009.*

[61] M. Janoschek. Polarized neutron studies of the helimagnet MnSi. Talk. *Conference on Polarized Neutrons and Synchrotron X-rays for Magnetism, Bonn, Germany, August 2009.*

[62] S. Legl. Magnetisation of the Dipolar Ising-Magnet $LiHoF_4$. Poster. *Workshop on Quantum Criticality and Novel Phases, Dresden, Germany, August 2009.*

[63] S. Legl. Vibrating Coil Magnetometer for the Use Inside a Dilution Refrigerator. Talk. *Workshop on High Pressure Techniques, Garching, Germany, August 2009.*

[64] T. Mairoser, A. Schmehl, J. Mannhart, A. Melville, T. Heeg, D. G. Schlom, P. Böni, L. Canella, and J. Schubert. Curie temperature of electron-doped EuO - is there an intrinsic limit? Talk. *16th International Workshop on Oxide Electronics, Tarragon, Spain, October 2009.*

[65] T. Mairoser, A. Schmehl, J. Mannhart, A. Melville, T. Heeg, D. G. Schlom, P. Böni, L. Canella, and J. Schubert. Correlation between Curie temperature and carrier density of electron-doped EuO - is there an intrinsic limit on T_c? Talk. *Frühjahrstagung der Deutschen Physikalischen Gesellschaft, Regensburg, Germany, March 2010.*

[66] J. Mannhart, A. Schmehl, S. Thiel, S. Dunsiger, and P. Böni. Heterostructures of functional oxides - characterization needs and new developments. Invited Talk. *Joint Users' Meeting PSI: JUMP'09, Villigen PSI, Switzerland, October 2009.*

[67] J. Mayer, C. Hugenschmidt, and K. Schreckenbach. High resolution positron annihilation induced Auger electron spectroscopy on copper. Poster. *Frühjahrstagung der Deutschen Physikalischen Gesellschaft, Dresden, Germany, March 2009.*

[68] J. Mayer, C. Hugenschmidt, and K. Schreckenbach. Latest development of the PAES-facility at NEPOMUC. Poster. *The XV International Conference on Positron Annihilation (ICPA-15), Kolkata, India, January 2009.*

[69] J. Mayer, C. Hugenschmidt, and K. Schreckenbach. Recent developments of the PAES setup at NEPOMUC. Talk. *4th FRM II Workshop on Neutron Scattering, Rothenfels, Germany, June 2009.*

[70] S. Mühlbauer. Skymion lattice in a chiral magnet. Talk. *Frühjahrstagung der Deutschen Physikalischen Gesellschaft, Dresden, Germany, February 2009.*

[71] S. Mühlbauer. Skymion lattice in a chiral magnet. Talk. *FRM II User Meeting, Garching, Germany, May 2009.*

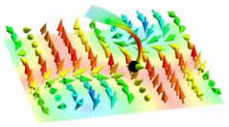

[72] S. Mühlbauer. Skyrmion lattice in a chiral magnet. Poster. *International Conference on Neutron Scattering (ICNS), Knoxville, USA, May 2009.*

[73] S. Mühlbauer. Time resolved stroboscopic small angle neutron scattering on the vortex lattice in niobium. Talk. *Frühjahrstagung der Deutschen Physikalischen Gesellschaft, Dresden, Germany, February 2009.*

[74] S. Mühlbauer. Time resolved stroboscopic small angle neutron scattering on the vortex lattice in niobium. Talk. *4th FRM II Workshop on Neutron Scattering, Rothenfels, Germany, June 2009.*

[75] S. Mühlbauer. Time resolved stroboscopic small angle neutron scattering on the vortex lattice in niobium. Talk. *Studying Kinetics with Neutrons: SANS and Reflectometry, SKIN 2009, Institut Laue-Langevin, Grenoble, France, September 2009.*

[76] S. Mühlbauer. Time resolved stroboscopic small angle neutron scattering on the vortex lattice in niobium. Talk. *JUMP, SINQ user meeting, Paul Scherrer Insitut, Villingen, Switzerland, September 2009.*

[77] S. Mühlbauer. Time resolved stroboscopic small angle neutron scattering on the vortex lattice in niobium. Talk. *JUM, BER II user meeting, Helmholtz Zentrum Berlin, Germany, November 2009.*

[78] S. Mühlbauer. Time resolved stroboscopic small angle neutron scattering on the vortex lattice in niobium. Poster. *International Conference on Magnetism (ICM), Karlsruhe, Germany, July 2009.*

[79] S. Mühlbauer. Vortices in superconducting niobium and skyrmion lattices in chiral magnets investigated by small angle neutron scattering. Invited Talk. *Paul Scherrer Institut, Villingen, Switzerland, August 2009.*

[80] A. Neubauer, C. Franz, W. Münzer, A. Bauer, B. Russ, C. Pfleiderer, G. Behr, and A. Erb. Einkristallzüchtung an der TUM (E21). Talk. *DGKK-Arbeitskreis-Treffen "Intermetallische und, oxidische Systeme mit Spin- und Ladungskorrelationen", Karlsruhe, Germany, October 2009.*

[81] A. Neubauer, C. Franz, W. Münzer, A. Bauer, B. Russ, C. Pfleiderer, M. Schulz, S. Masalovich, G. Behr, N. Wizent, A. Erb, K. Hradil, and C. Felser. Neutron spin depolarisation under pressure - Ni_3Al & Magnetic and transport properties of Fe_2TiSn under pressure. Talk. *Workshop on High Pressure Techniques, Garching, Germany, December 2009.*

[82] A. Neubauer, S. Mühlbauer, T. Adams, F. Jonietz, C. Franz, W. Münzer, A. Bauer, C. Pfleiderer, A. Rosch, R. Georgii, B. Pedersen, and P. Böni. Partial magnetic order in $Fe_{1-x}Co_xSi$. Poster. *International Conference on Magnetism (ICM), Karlsruhe, Germany, July 2009.*

[83] A. Neubauer and C. Pfleiderer. Border of itinerant local-moment ferromagnetism in a Heusler compound - Fe_2TiSn. Talk. *4th FRM II Workshop on Neutron Scattering, Rothenfels, Germany, June 2009.*

[84] A. Neubauer, M. Schulz, C. Pfleiderer, and G. Behr. Fe_2TiSn: Floating zone crystal growth and tomographic polarized neutron analyses. Poster. *DGKK Jahrestagung 2009, Dresden, Germany, March 2009.*

[85] A. Neubauer, M. Schulz, C. Pfleiderer, P. Böni, K. Hradil, and G. Behr. Single crystal Fe_2TiSn under high pressure and magnetic field. Talk. *Frühjahrstagung der Deutschen Physikalischen Gesellschaft, Regensburg, Germany, March 2010.*

[86] A. Neubauer, M. Schulz, C. Pfleiderer, P. Böni, A. Köhler, Nadja Wizentz, and G. Behr. Crystal growth and polarized neutron radiography of Fe_2TiSn (and Ni_3Al). Talk. *Frühjahrstagung der Deutschen Physikalischen Gesellschaft, Dresden, Germany, March 2009.*

[87] A. Ostermann and P. Böni. Monte-Carlo Simulations of a Double V-cavity Transmission Polarizer. Talk. *Workshop on Neutron Delivery Systems, Institut Laue-Langevin, Grenoble, France, July 2009.*

[88] C. Pfleiderer. Complex Novel Forms of Electronic Order. Invited Talk. *4th FRM II Workshop on Neutron Scattering, Rothenfels, Germany, June 2009.*

[89] C. Pfleiderer. Festkörperphysik mit Twist. Talk. *Tag der offenen Tür der Technischen Universität München, Garching, Germany, October 2009.*

[90] C. Pfleiderer. Larmor Diffraction: A Neutron Resonance Spin-Echo (NRSE) Technique. Talk. *Workshop on High Pressure Techniques, Garching, Germany, December 2009.*

[91] C. Pfleiderer. Phase Segregation at Ferromagnetic Quantum Phase Transitions. Talk. *DFG-Forschergruppe FOR 960: Quantum Phase Transitions, Karlsruhe, Germany, November 2009.*

[92] C. Pfleiderer. Skyrmion Lattices in Chiral Magnets. Talk. *Korrelationstage 2009, Max Planck Institut für komplexe Systeme, Dresden, Germany, March 2009.*

[93] C. Pfleiderer. Skyrmion Lattices in Chiral Magnets. Talk. *Condensed Matter Physics Seminar, University of Cambridge, UK, February 2009.*

[94] C. Pfleiderer. Skyrmion Lattices in Magnetic Metals and Magnetic Semiconductors. Talk. *Condensed Matter Physics Seminars, University of Oxford, UK, November 2009.*

[95] C. Pfleiderer. Skyrmion Lattices in Magnetic Metals and Magnetic Semiconductors. Invited Talk. *International Conference on Magnetism (ICM), Karlsruhe, Germany, July 2009.*

[96] C. Pfleiderer. Skyrmion Lattices in Magnetic Metals and Magnetic Semiconductors. Invited Talk. *Workshop on Topological Order, Max Planck Institut für komplexe Systeme, Dresden, Germany, July 2009.*

[97] C. Pfleiderer. Spin Torque Effects in the Skyrmion Lattice of a Chiral Magnet. Talk. *1. TUM Nanomagnetik Workshop, Technische Universität München, Garching, Germany, February 2009.*

[98] C. Pfleiderer. Topological Magnetism: The Mixed State of Magnetic Materials. Invited Talk. *Conference on Quantum Criticality and Novel Phases Dresden, Germany, August 2009.*

[99] C. Pfleiderer. Topological Solitons in Superconductors and Chiral Magnets. Invited Talk. *3rd International Symposium on Functional Matter, Technische Universität Wien, Vienna, Austria, November 2009.*

[100] C. Pfleiderer. Topological Solitons in Superconductors and Chiral Magnets. Invited Talk. *Fermions 2009, Universitätszentrum Obergurgl, Austria, October 2009.*

[101] C. Pfleiderer. Topological Solitons in Superconductors and Chiral Magnets. Invited Talk. *Orbital-2009, Helmholtz-Zentrum Berlin, Germany, October 2009.*

[102] C. Pfleiderer. Complex Spin Textures in Non-Centrosymmetric Materials. Invited Talk. *449. W. & E. Heraeus Seminar "Rashba and related spin-orbit effects in metals", Bad Honnef, Germany, January 2010.*

[103] C. Pfleiderer. Condensed Matter Particle Physics. Talk. *Zürich Physics Colloquium, ETH Zürich, Switzerland, November 2010.*

[104] C. Pfleiderer. Condensed Matter Particle Physics. Talk. *TRR80 Retreat Meeting, Freising, Germany, October 2010.*

[105] C. Pfleiderer. Exploring Quantum Phase Transitions with Polarized Neutrons. Invited Talk. *Kick-off Conference on Pressure Effects in Materials, ICMR, University of California, Santa Barbara, USA, August 2010.*

[106] C. Pfleiderer. Larmor Diffraction in URu_2Si_2 under Pressure. Invited Talk. *Workshop on the Dual Nature of f-Electrons, Max Planck Institut für komplexe Systeme, Dresden, Germany, May 2010.*

[107] C. Pfleiderer. Larmor Diffraction URu_2Si_2. Talk. *Karlsruher Institut for Technology, Karlsruhe, Germany, January 2010.*

[108] C. Pfleiderer. Proposal of a Topological Hall Sensor. Talk. *2. TUM Nanomagnetik-Workshop, Technische Universität München, Garching, Germany, January 2010.*

[109] C. Pfleiderer. Radiography with Polarized Neutrons of Ferromagnetic Quantum Phase Transitions. Talk. *Deutsche Tagung für Forschung mit Synchrotronstrahlung, Neutronen und Ionenstrahlen an Großgeräten (SNI 2010), Berlin, Germany, February 2010.*

[110] C. Pfleiderer. Skyrmion lattices in metals and doped semiconductors. Invited Talk. *Frühjahrstagung der Deutschen Physikalischen Gesellschaft, Regensburg, Germany, March 2010.*

[111] C. Pfleiderer. Spin Dynamics and Spin Freezing at Quantum Phase Transitions. Talk. *Review of the DFG Research Unit FOR 960 (Quantum Phase Transitions) Karlsruhe Institut for Technology, Germany, April 2010.*

[112] C. Pfleiderer. Spin-Transfer Torques at Ultra-low Current Densities. Invited Talk. *Super-PIRE Kick-off Meeting, Knoxville, USA, October 2010.*

[113] C. Pfleiderer. Spin-Transfer Torques at Ultra-low Current Densities. Invited Talk. *JCNS Workshop on Modern Trends and Perspectives in Neutron Scattering: Magnetism and Correlated Electron Systems, Bernried, Germany, October 2010.*

[114] C. Pfleiderer. Spin-Transfer Torques at Ultra-low Current Densities. Talk. *SpinAge 2010, Watsonville, USA, August 2010.*

[115] C. Pfleiderer. Spin Transfer Torques in MnSi at Ultra-low Current Densities. Invited Talk. *Physical Phenomena at High Magnetic Fields VII, Florida State University, Tallahassee, December 2010.*

[116] C. Pfleiderer. Versatile Neutron Scattering Techniques with Ultra-high Resolution. Invited Talk. *Jahrestagung der Österreichischen Physikalischen Gesellschaft, Universität Salzburg, Austria, September 2010.*

[117] C. Pfleiderer. Vibrating coil magnetometry of quantum criticality in $LiHoF_4$. Talk. *Frühjahrstagung der Deutschen Physikalischen Gesellschaft, Regensburg, Germany, March 2010.*

[118] C. Pfleiderer. Von der Korrelation zu ungewöhnlichen topologischen Eigenschaften. Talk. *Universität zu Köln, Germany, January 2010.*

[119] P. Pikart, C. Hugenschmidt, and K. Schreckenbach. Doppler-broadening (DB) measurement of ionic liquids using a monoenergetic positron beam. Talk. *The XV International Conference on Positron Annihilation (ICPA-15), Kolkata, India, January 2009.*

[120] P. Pikart, C. Hugenschmidt, and K. Schreckenbach. Doppler-broadening (DB) measurement of ionic liquids using a monoenergetic positron beam. Talk. *Frühjahrstagung der Deutschen Physikalischen Gesellschaft, Dresden, Germany, March 2009.*

[121] P. Pikart, C. Hugenschmidt, and K. Schreckenbach. Coincident Doppler Broadening measurement on embedded thin layers of different materials with a positron beam of variable energy. Talk. *Frühjahrstagung der Deutschen Physikalischen Gesellschaft, Regensburg, Germany, March 2010.*

[122] P. Pikart, C. Hugenschmidt, and K. Schreckenbach. Coincident Doppler Broadening measurement on embedded thin layers of different materials with a positron beam of variable energy. Talk. *Deutsche Tagung für Forschung mit Synchrotronstrahlung, Neutronen und Ionenstrahlen an Großgeräten (SNI 2010), Berlin, Germany, February 2010.*

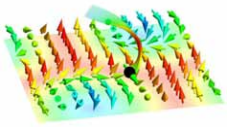

[123] P. Pikart, C. Hugenschmidt, and K. Schreckenbach. Spectroscopy with a high intensity, reactor based beam of monoenergetic positrons - Measurements on thin metallic layers. Invited Talk. *International Workshop on Advanced Positron Beam Technology for Material Science, Algiers, Algeria, March 2010.*

[124] C. Piochacz and C. Hugenschmidt. Defect spectroscopy with low energy positrons at NEPOMUC. Talk. *Fusion Energy Materials Science (FEMaS) Meeting, Athen, Greek, January 2010.*

[125] C. Piochacz and C. Hugenschmidt. The experimental determination of the phase space distribution of a positron beam. Poster. *12th International Workshop on Slow Positron Beam Techniques SLOPOS-12, Magnetic Island, Australia, August 2010.*

[126] C. Piochacz, G. Kögel, and G. Dollinger. Das Münchner Scanning Positron Microscope und dessen Implementierung am FRM II. Poster. *Deutsche Tagung für Forschung mit Synchrotronstrahlung, Neutronen und Ionenstrahlen an Großgeräten (SNI2010), Berlin, Germany, February 2010.*

[127] C. Piochacz, G. Kögel, W. Egger, C. Hugenschmidt, K. Schreckenbach, P. Sperr, and G. Dollinger. The beam enhancement devices at NEPOMUC for the Munich scanning positron microscope. Poster. *The XV International Conference on Positron Annihilation (ICPA-15), Kolkata, India, January 2009.*

[128] C. Piochacz, G. Kögel, W. Egger, C. Hugenschmidt, K. Schreckenbach, P. Sperr, and G. Dollinger. The beam enhancement and pulsing devices at NEPOMUC for the munich scanning positron microscope. Poster. *12th International Workshop on Slow Positron Beam Techniques SLOPOS-12, Magnetic Island, Australia, August 2010.*

[129] C. Piochacz, G. Kögel, W. Egger, C. Hugenschmidt, K. Schreckenbach, P. Sperr, and G. Dollinger. The status of the beam enhancement and pulsing devices at NEPOMUC for the munich scanning positron microscope. Poster. *12th International Workshop on Slow Positron Beam Techniques SLOPOS-12, Magnetic Island, Australia, August 2010.*

[130] M. Reiner. Depth resolved Doppler broadening spectroscopy in thin metallic films. Talk. *39th Polish Seminar on Positron Annihilation, Kazimierz Dln., Poland, June 2010.*

[131] R. Ritz, S. Mühlbauer, C. Pfleiderer, T. Keller, J. White, M. Laver, E. M. Forgan, R. Cubitt, C. Dewhurst, P. G. Niklowitz, A. Prokofiev, and E. Bauer. Distribution of Lattice Constants in $CePt_3Si$ Observed by Larmor Diffraction and SANS. Poster. *International Conference on Magnetism (ICM), Karlsruhe, Germany, July 2009.*

[132] R. Ritz, C. Pfleiderer, T. Keller, A. D. Huxley, D. Sokolov, P. G. Niklowitz, A. Prokofiev, and E. Bauer. Larmor Diffraction in Antiferromagnetic and Ferromagnetic Superconductors. Talk. *FRM2 User Meeting, Munich, Germany, May 2009.*

[133] R. Ritz, C. Pfleiderer, T. Keller, A. D. Huxley, D. Sokolov, P. G. Niklowitz, A. Prokofiev, and E. Bauer. Neutron Larmor Diffraction in Antiferromagnetic and Ferromagnetic Superconductors. Talk. *Workshop of the DFG Research Unit FOR 960 Quantum Phase Transitions, Karlsruhe, Germany, June 2009.*

[134] R. Ritz, C. Pfleiderer, T. Keller, A. D. Huxley, D. Sokolov, P. G. Niklowitz, A. Prokofiev, and E. Bauer. Neutron Larmor Diffraction in Antiferromagnetic and Ferromagnetic Superconductors. Talk. *4th FRM II Workshop on Neutron Scattering, Rothenfels, Germany, June 2009.*

[135] R. Ritz, C. Pfleiderer, A. Neubauer, P. G. Niklowitz, and P. Böni. Pressure Dependence of the Magnetotransport Properties of MnSi. Talk. *Frühjahrstagung der Deutschen Physikalischen Gesellschaft, Dresden, Germany, March 2009.*

[136] R. Ritz, D. Sokolov, T. Keller, A. D. Huxley, and C. Pfleiderer. Larmor Diffraction in the Ferromagnetic Superconductor UGe_2. Talk. *Frühjahrstagung der Deutschen Physikalischen Gesellschaft, Regensburg, Germany, March 2010.*

[137] R. Ritz, D. Sokolov, T. Keller, A. D. Huxley, and C. Pfleiderer. Larmor Diffraction Studies on the Ferromagnetic Superconductor UGe_2. Poster. *Dual Nature of f-Electrons, The Third International Workshop, Dresden, Germany, May 2010.*

[138] R. Ritz, D. Sokolov, T. Keller, A. D. Huxley, and C. Pfleiderer. Larmor Diffraction Studies on the Ferromagnetic Superconductor UGe_2. Poster. *Summer School on Condensed Matter Research: Magnetic phenomena, Zuoz, Switzerland, August 2010.*

[139] R. Ritz, D. Sokolov, T. Keller, A. D. Huxley, and C. Pfleiderer. Larmor Diffraction Studies on the Ferromagnetic Superconductor UGe_2. Poster. *FRM II User Meeting, Munich, Germany, October 2010.*

[140] K. Schreckenbach. Positron annihilation spectroscopy for the study of materials. Talk. *FEMas Workshop, Lisbon, Portugal, January 2009.*

[141] K. Schreckenbach. Positron physics in our galaxy and in the laboratory. Talk. *Kepler Kolloquium, Tübingen, Germany, January 2009.*

[142] K. Schreckenbach. Positronenphysik im Universum und Labor. Talk. *MLL Kolloquium, Garching, Germany, February 2009.*

[143] K. Schreckenbach. Transmission measurements of UCN guides using UCN neutron capture activation of vanadium. Talk. *7th UCN Workshop, St. Petersburg, Russia, June 2009.*

[144] K. Schreckenbach. Neutron lifetime measurement with the UCN trap-in-trap MAMBO II. Talk. *Seminars Physik Department E18 and FRM II, Garching, Germany, June 2010.*

[145] R. Valicu and P. Böni. Monte Carlo Simulations for Focusing Elliptical Guides. Talk. *NMI3/FP7 Launch Meeting, Villigen PSI, Switzerland, March 2009.*

[146] R. Valicu and P. Böni. Wolter type telescopes. Talk. *NMI3/FP7 Launch Meeting, Villigen PSI, Switzerland, March 2009.*

[147] R. Valicu, P. Böni, and G. Borchert. Monte Carlo Simulation for Focusing Elliptical Guides. Talk. *Workshop on Neutron Delivery Systems, Institut Laue-Langevin, Grenoble, France, July 2009.*

[148] R. Valicu, P. Böni, J. Stahn, U. Filges, T. Panzner, Y. Bodenthin, M. Schneider, and C. Schanzer. Monte Carlo simulation for adaptive optics. Talk. *International Workshop on Neutron Optics 2010 (NOP2010), Alpe d'Huez, France, March 2010.*

[149] R. Valicu, G. G. Simeoni, and P. Böni. Development of a new focusing neutron guide for TOFTOF. Talk. *International Workshop on Neutron Optics 2010 (NOP2010), Alpe d'Huez, France, March 2010.*

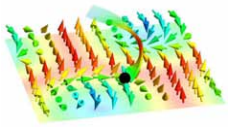

Services to the Community

P. Böni

- Reviewer of experimental proposals, GKSS, Geesthacht, Germany.
- TUM-Beirat for the FRM-II, Garching, Germany.
- Coordinator of Work Package on Neutron Optics, Joint Research Project JRA3: NMI3 FP6.
- Member of the International Programme Committee of the European Workshop on Neutron Optics NOP2010, Alpe d'Huez, France.
- Member of the International Advisory Committee of the Workshop on Polarized Neutrons in Condensed Matter Investigations PNCMI2010, Delft, Netherlands.
- Member of the Program Committee of the Workshop on Neutron Delivery Systems, Institut Laue-Langevin, Grenoble, France.
- Member of the Program Committee of the International Conference on Neutron Scattering ICNS-2009.
- Vice-Chairman of the ESS Scientific Advisory Committee (ESS-SAC) of the European Spallation Source.
- Chairman of the ESS Scientific Advisory Committee for Instrumentation (ESS-iSAC) of the European Spallation Source.
- Associate Coordinator of the Transregio TRR 80.

C. Pfleiderer

- Vertrauensdozent der Studienstiftung des deutschen Volkes.
- Komittee für Forschung mit Neutronen (KFN): elected member and deputy chairman.
- Jülich Centre for Neutron Science (JCNS): member of beam time panel.
- Paul-Scherrer Institut (PSI): member of beam time panel.
- European Spallation Source: Member of Scientific Advisory Council.
- Chairman of the Integrated Graduate School of DFG-TRR 80.
- Münchner Physik Kolloquium, Coordinator (TUM).
- Weihnachtsvorlesung (2009 & 2010), Schirmherr.
- Member of the Fachbereichsrat of the Physik-Department.
- Member of the Fachmentorat MSc (Condensed Matter Physics).
- Member of the BSc Prüfungsausschuss.

K. Schreckenbach

- Chairman of the Subcommittee College 3, Institute Laue Langevin, Grenoble, France.
- Member of the Scientific Counsil of the ILL, Grenoble, France.

R. Georgii

- Member of the Instrument development team (IDT) for MISANS@SNS.
- Member of the review panel for single investigators and small groups (SISGR) of the Department of Energy DOE.

W. Häußler

- Member of the Comittee A, LLB Tables Rondes, France (2009 and 2010).

C. Hugenschmidt

- Member of the International Advisory Committee for Positron Annihilation (since January 2009).
- Representative of Kommittee für Forschung mit nuklearen Sonden und Ionen - KFSI (since April 2009).
- Member of the Scientific Advisory Committee for the Radiation Source ELBE (since July 2009).

M. Janoschek

- Committee responsible for the program of the session "Advanced Techniques at PSI Large Facilities" within the PSI User Meeting.

G. Brandl

- Member of the Instrument development team (IDT) for MISANS@SNS.

Accomplished Habilitation Theses

Christoph Hugenschmidt	Novel Applications Using the High Intensity Low-Energy Positron Beam at NEPOMUC.

Accomplished PhD Theses

Stefan Legl	Entwicklung eines Spulen-Vibrationsmagentometers zur Untersuchung korrelierter Elektronensysteme bei ultra-tiefen Temperaturen.
Jakob Mayer	High energy resolution and first time-dependent positron annihilation induced Auger electron spectroscopy.
Sebastian Mühlbauer	Vortex Lattices in Superconducting Niobium and Skyrmion Lattices in Chiral MnSi: An Investigation by Neutron Scattering.
Christian Piochacz	Generation of a High-Brightness Pulsed Positron Beam for the Munich Scanning Positron Microscope.
Michael Schulz	Radiography with Polarized Neutrons.

Accomplished Master's Theses

Tim Adams	Skyrmionengitter und partielle Ordnung in B20 Übergangsmetallverbindungen.
Andreas Bauer	Quantenphasenübergänge und Skyrmion-Gitter in $Mn_{1-x}Fe_xSi$ und $Mn_{1-x}Co_xSi$.
Georg Brandl	First measurements of the linewidth in magnetic phases of MnSi using MIEZE.
Hubert Ceeh[1]	Produktion und Lebensdauermessung des negativ geladenen Positroniumions.
Wolfgang Münzer	Einkristallzüchtung und magnetische Eigenschaften von MnSi und $Fe_{1-x}Co_xSi$.
Alexander Regnat	Hochdruckexperimente am itineranten Antiferromagneten Chromdiborid.
Mathias Sandhofer	First Measurements of the linewidth of MnSi near T_c by neutron spin echo.
Alexander Tischendorf	Spin echo measurements of magnetic fluctuations in helical $Mn_{1-x}Fe_xSi$.
Katja Zechmeister	Evaluierung neuer Detektoren für die kombinierte PET/MR-Bildgebung, basierend auf SiPM und schnellen Szintillationskristallen.

[1] awarded with a student prize at the 12th International Workshop on Slow Positron Beam Techniques, Magnetic Island, Australia

Zulassungsarbeiten für Lehramt

Felicitas Birkelbach	Aufbau eines Drehmomentmagnetometers.
Michael Scheungraber	Einführung in die physikalischen Grundlagen ausgewählter Analyseverfahren mit Neutronen und deren Nutzung in der Gemäldetiefenanalyse.

Accomplished Bachelor's Theses

Alfonso Chacón Roldán	Design of a uniaxial pressure experiment for neutron scattering.
Benedikt Friedl	Temperature dependent Doppler broadening spectroscopy.
Karin Hain	Spatially Resolved Positron Annihilation Spectroscopy on Weld Induced Defects.
Daniel Rudolph (FH Enschede, Netherlands)	Development of a three axis option on MIRA.
Michael Wiedemann	FEM simulation and experimental verification of the magnetic field of a Spin-Echo coil.

Semestral Theses

Tatjana Stölzl (Hochschule München)	Aufbau eines Motorteststandes für MIRA.

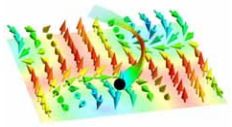

Facharbeiten an Gymnasien

Korbinian Eller (Gymnasium Dachau)	Nutzung von Neutronen in der Wissenschaft.

E21 Members

Phone/Fax: +49-89-289- PH: Physics Department, FRM: FRM II grounds, RCM: Radiochemistry

Name	Phone	Fax	Room	E-Mail
Adams Tim, Dipl. Phys.	-12515	-14724	PH 1, 2373	tim.adams@frm2.tum.de
Bauer Andreas, Dipl. Phys.	-12512	-14724	PH 1, 2367	andreas.bauer@frm2.tum.de
Böni Peter, Prof. Dr.	-14711	-14713	PH 1, 2213	peter.boeni@frm2.tum.de
Brandl Georg, diploma student	-10754	-14620	FRM, UYA 0345	georg.brandl@frm2.tum.de
Bundschuh Ralph, Dipl. Phys.	+49-89-4140-4570	+49-89-4140-4938	Klinik für Nuklearmedizin	ralph.bundschuh@ph.tum.de
Ceeh Hubert, diploma student	-14568	-14620	FRM, UYL 0235	hubert.ceeh@frm2.tum.de
Chacon Alfonso, master student	-12512	-14724	PH 1, 2367	alfonso.chacon@frm2.tum.de
Dollinger Christoph, student	-14515	-14724	PH 1, 2341	christoph.dollinger@frm2.tum.de
Dunsiger Sarah, Dr.	-14722	-14724	PH 1, 2207	sarah.dunsiger@frm2.tum.de
Franz Christian, Dipl. Phys.	-14515	-14724	PH 1, 2341	christian.franz@frm2.tum.de
Giemsa Stefan, mechanician	-14737	-14724	PH 1, 2341	stefan.giemsa@frm2.tum.de
Gottlieb-Schönmeyer Saskia, Dr.	-12476	-14724	PH 1, 2201	sgottlie@frm2.tum.de
Halder Marco, diploma student	-14515	-14724	PH 1, 2367	marco.halder@frm2.tum.de
Hohberg Melanie, Dipl. Phys.	+49-89-4140-6457	+49-89-4140-4938	Klinik für Nuklearmedizin	melanie.hohberg@tum.de
Jones Sylvia, secretary	-14712	-14713	PH 1, 2211	sylvia.jones@frm2.tum.de
Jonietz Florian, Dipl. Phys.	-12512	-14724	PH 1, 2367	florian.jonietz@frm2.tum.de
Korntner Ralf, diploma student	-14515	-14724	PH 1, 2341	ralf.korntner@frm2.tum.de
Krey Christopher, diploma student	-12515	-14724	PH 1, 2373	christopher.krey@frm2.tum.de
Kreuzpaintner Wolfgang, Dr.	-14740	-14724	PH 1, 2207	wolfgang.kreuzpaintner@frm2.tum.de
Lochner Katharina, diploma student	-14737	-14724	PH 1, 2341	katharina.lochner@frm2.tum.de
Mallinger Dorothea, diploma student	-12476	-14724	PH 1, 2201	dorothea.mallinger@frm2.tum.de
Mantwill Andreas, mechanician	-14887	–	–	–
Mittermüller Kilian, diploma student	-14737	-14724	PH 1, 2341	kilian.mittermueller@frm2.tum.de
Morkel Christoph, PD Dr.	-12157	-14724	PH 1, 2214	christoph.morkel@frm2.tum.de
Mühlbauer Martin, Dipl. Phys.	-12106	-14997	FRM, UYA 0367	martin.muehlbauer@frm2.tum.de
Mühlberg Astrid, secretary from 01/01/2011	-14712	-14713	PH 1, 2211	astrid.muehlberg@frm2.tum.de
Neubauer Andreas, Dipl. Phys.	-12512	-14724	PH 1, 2367	andreas.neubauer@frm2.tum.de
Othman Osama, Dipl. Phys.	-14641	-14724	FRM, UYA 0367	osama.othman@frm2.tum.de
Pikart Philip, Dipl. Phys.	-12161	-14620	FRM, UYL 10	philip.pikart@frm2.tum.de
Pfleiderer Christian, Prof. Dr.	-14712	-14713	PH 1, 2205	christian.pfleiderer@frm2.tum.de
Piochacz Christian, Dr.	-12179	-14620	FRM, UYL 12	christian.piochacz@frm2.tum.de
Rahn Marein, student	-14737	-14724	PH 1, 2341	marein.rahn@frm2.tum.de

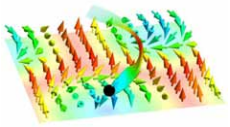

Phone/Fax: +49-89-289- PH 1: Physics Department, FRM: FRM II grounds, RCM: Radiochemistry

Regnat Alexander, diploma student	-14515	-14724	PH 1, 2341	alexander.regnat@frm2.tum.de
Reiner Markus, diploma student	-14568	-14620	FRM, UYL 0235	markus.reiner@frm2.tum.de
Reingen Gabriel, mechanician	-12656	–	PH 1, 1321	–
Ritz Robert, Dipl. Phys.	-12515	-14724	PH 1, 2373	robert.ritz@frm2.tum.de
Rohrmoser Benjamin, Dipl. Phys.	-13951	-14347	RCM, 107	benjamin.rohrmoser@radiochemie.de
Russ Barbara, Dipl. Ing.	-14717	-14724	PH 1, 2203	barbara.russ@frm2.tum.de
Schmakat Philipp, diploma student	-12106	-14724	FRM, UYA 0343	philipp.schmakat@frm2.tum.de
Schörner Karsten, Dipl. Phys.	+49-89-6364-8593	+49-89-6364-6192	Siemens AG	karsten.schoerner.ext@siemens.de
Schulz Michael, Dipl. Phys.	-14718	-13776	FRM, UYA 0343	michael.schulz@frm2.tum.de
Schulz Tomek, diploma student	-14515	-14724	PH 1, 2341	tomek.schulz@frm2.tum.de
Tischendorf Alexander, diploma student	-14737	-14724	FRM, UYA 0345	alexander.tischendorf@frm2.tum.de
Valicu Roxana, Dipl. Phys.	-14677	-14997	FRM, UYA 120	roxana.valicu@frm2.tum.de
Wagner Michael, Dipl. Phys.	-14515	-14724	PH 1, 2341	michael.wagner@frm2.tum.de
Weber Josef-Andreas, Dipl. Phys.	-14568	-14620	FRM, UYL 0235	josef-andreas.weber@frm2.tum.de
Wiedemann Birgit, Dipl. Phys.	-14725	-14724	PH 1, 2214	birgit.wiedemann@frm2.tum.de
Zechmeister Katja, Dipl. Phys.	+49-89-4140-4569	+49-89-4140-4938	Klinik für Nuklearmedizin	katja.zechmeister@tum.de

Associated Members at FRM II

Phone/Fax: +49-89-289- FRM: FRM II grounds

Name	Phone	Fax	Room	E-Mail
Calzada Elbio, Dipl. Ing.	-14611	-14997	FRM, UYA 0342	elbio.calzada@frm2.tum.de
Georgii Robert, Dr.	-14986	-14989	FRM, UYH 0336	robert.georgii@frm2.tum.de
Häußler Wolfgang, Dr.	-14921	-14989	FRM, UYC	wolfgang.haeussler@frm2.tum.de
Hugenschmidt Christoph, Dr.	-14609	-14620	FRM, UYL 9	christoph.hugenschmidt@frm2.tum.de
Repper Julia, Dr.	-14668	-14989	FRM, UYH 0345	julia.repper@frm2.tum.de
Schillinger Burkhard, Dr.	-12185	-13776	FRM, UYA 0341	burkhard.schillinger@frm2.tum.de
Schwikowski Reinhard, technician	-14915	-14995	FRM, UYH 0336	reinhard.schwikowski@frm2.tum.de
Wipp Michael, technician	-10751	-14989	FRM, UYC 018	michael.wipp@frm2.tum.de

Emeriti

Phone/Fax: +49-89-289- PH 1: Physics Department, FRM: FRM II grounds

Name	Phone	Fax	Room	E-Mail
Böning Klaus, Prof. Dr. emerit.	-12150	-12191	FRM, UBA 0325	klaus.boening@frm2.tum.de
Gläser Wolfgang, Prof. Dr. emerit.	-12183	-14724	PH 1, 2281	wglaeser@ph.tum.de
Schreckenbach Klaus, Prof. Dr. emerit.	-12183	-14724	PH 1, 2281	klaus.schreckenbach@frm2.tum.de

Longterm Guests and Alumni

Phone/Fax: +49-89-289- FRM: FRM II grounds

Name	Phone	Room / Inst.	E-Mail
Chabior Michael, Dipl. Phys.	+49-89-3635-1042	Siemens AG, München	michael.chabior.ext@siemens.de
Gähler Roland, Dr. habil.	+33-4-7620-7189	ILL, Grenoble	gahler@ill.fr
Janoschek Marc, Dr.	–	Maple Group, UCSD, San Diego, USA	mjanoschek@physics.ucsd.edu
Keller Thomas, Dr.	-12164	FRM, UYC 106, Garching	thomas.keller@frm2.tum.de
Legl Stefan, Dr.	+49-89-984437	Ter Meer, Steinmeister & Partner GbR, München	legl@termeer.de
Mühlbauer Sebastian, Dr.	+41-44-633-91-35	ETH Zürich, Zürich	muehlbas@phys.ethz.ch
Niklowitz Philipp, Dr.	+44-1784-44-3499	Royal Holloway, London	philipp.niklowitz@rhul.ac.uk
Stadlbauer Martin, Dr.	–	MTU Aero Engines, München	martin.stadlbauer@mtu.de
Vollmer Nico, Dr.	+49-9131-1893018	Fuel Europe Engineering Materials, Erlangen	nico.wieschalla@areva.com

Short-term Scientific Visitors

Name	Institute	Duration of stay
Hering Eduardo	CBPF, Rio de Janeiro, Brasil	Nov – Dec 2009
Merz Tyler	Ohio State University, USA	Jul – Sep 2009
Ramos Sheilla	CBPF, Rio de Janeiro, Brasil	Nov – Dec 2009
Wilson Caspar[1]	King's College, London, UK	Jun – Aug 2009

[1] DAAD-RISE: http://www.daad.de/rise/

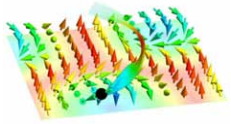

Guided Tours at FRM II

The FRM II is open for everybody to come and visit the scientific and experimental facilities (Experimental Hall and Neutron Guide Hall). Therefore, Guided Tours are organized by a specially established division, the “Besucherdienst”, and conducted by the scientists and the technical personnel of FRM-II.

In 2009/2010, the members of E21 guided approx. 300 officially registered tours and several others at various occasions, thus contributing a significant amount of time and personal effort to help making the neutron source FRM-II a publicly transparent and accepted research facility.

Third Party Funding

We gratefully acknowledge financial support from

- Deutsche Forschungsgemeinschaft (DFG)
- Bundesministerium für Bildung und Forschung (BMBF)
- European Community: COST-P16 Program
- European Community: NMI3 Program
- Bavaria California Technology Center (BaCaTeC)
- Deutscher Akademischer Austauschdienst (DAAD)
- Swiss National Science Foundation (SNF)

We also acknowledge beam time at:

- Forschungsneutronenquelle Heinz Maier-Leibnitz (FRM II)
- Helmholtz-Zentrum Berlin (BENSC)
- European Synchrotron Radiation Facility (ESRF), France
- Institut Laue-Langevin (ILL), France
- Paul-Scherrer-Institut (PSI), Switzerland
- Oak Ridge National Laboratory (ORNL), USA

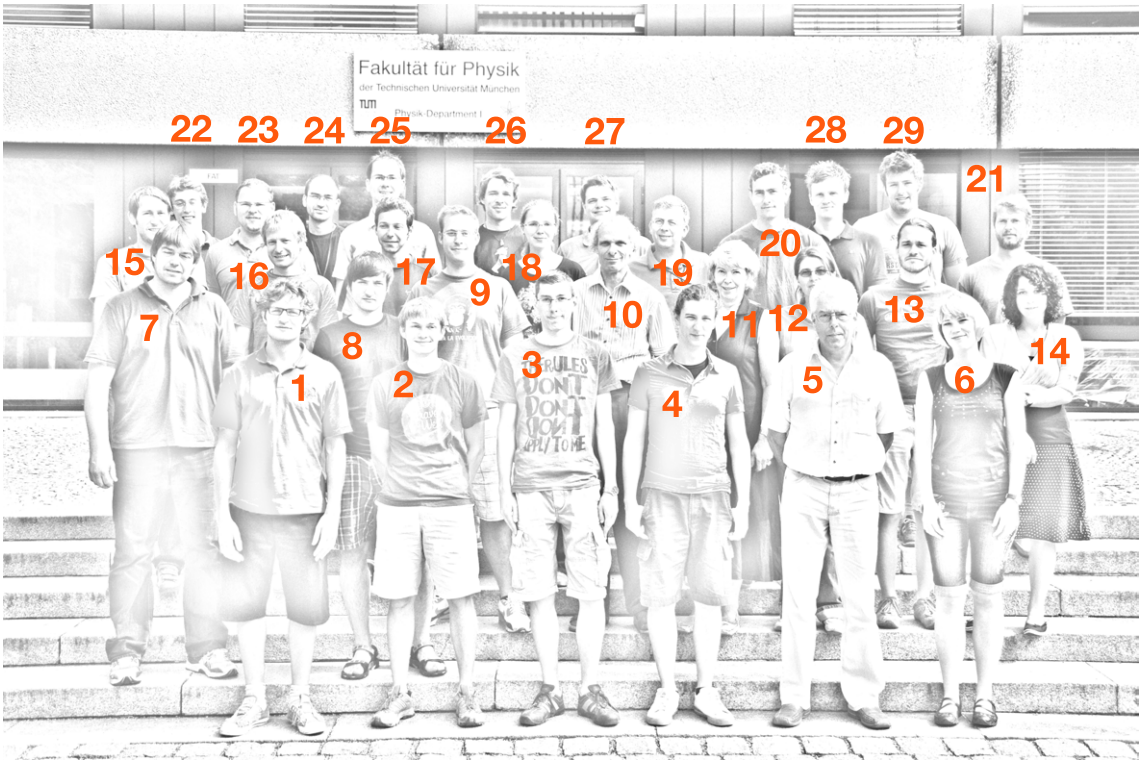

1	K. Mittermüller	9	R. Ritz	17	C. Franz	25	P. Pikart
2	A. Regnat	10	P. Böni	18	J. Repper	26	J. Mayer
3	M. Ebert	11	B. Russ	19	R. Georgii	27	G. Brandl
4	M. Wagner	12	R. Valicu	20	T. Adams	28	T. Schulz
5	R. Schwikowski	13	A. Bauer	21	W. Häußler	29	H. Ceeh
6	S. Gottlieb-Schönmeyer	14	D. Mallinger	22	B. Friedl		
7	C. Pfleiderer	15	A. Neubauer	23	C. Piochacz		
8	C. Krey	16	M. Schulz	24	F. Jonietz		

Missing: R. Bundschuh, E. Calzada, A. Chacon, C. Dollinger, S. Dunsiger, S. Giemsa, M. Halder, M. Hohberg, C. Hugenschmidt, R. Korntner, W. Kreuzpaintner, K. Lochner, A. Mantwill, C. Morkel, M. Mühlbauer, O. Othman, M. Reiner, G. Reingen, B. Rohrmoser, B. Schillinger, P. Schmakat, K. Schörner, A. Tischendorf, R. Valicu, J.-A. Weber, B. Wiedemann, M. Wipp, K. Zechmeister